NOTE TO USERS

This reproduction is the best copy available.

UMI®

DISSERTATION

MOLECULAR RECOGNITION BY THE TRANSCRIPTIONAL ACTIVATOR AP-1

Submitted by
Kathleen M. Campbell
Department of Biochemistry and Molecular Biology

In partial fulfillment of the requirements for the
Degree of Doctorate of Philosophy
Colorado State University
Fort Collins, Colorado
Spring 2002

COLORADO STATE UNIVERSITY

February 19, 2002

WE HEREBY RECOMMEND THAT THE DISSERTATION PREPARED UNDER OUR SUPERVISION BY KATHLEEN M. CAMPBELL ENTITLED

MOLECULAR RECOGNITION BY THE TRANSCRIPTIONAL ACTIVATOR AP-1

BE ACCEPTED AS FULFILLING IN PART REQUIREMENTS FOR THE DEGREE OF DOCTORATE OF PHILOSOPHY.

Committee on Graduate Work

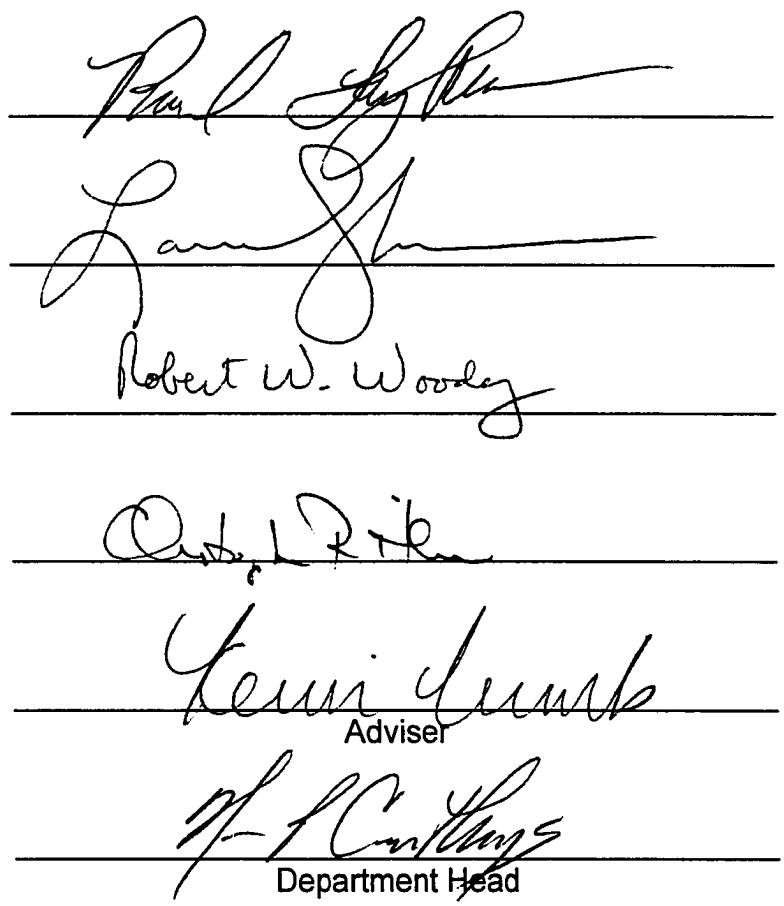

Adviser

Department Head

ABSTRACT OF DISSERTATION

Molecular Recognition by the Transcriptional Activator AP-1

Members of the Jun family of mitogen-inducible transcriptional activators homodimerize or heterodimerize with the Fos or ATF/CREB activators to form the transcriptional regulator AP-1. AP-1 activates transcription of genes involved in a diverse range of biological processes, including cell proliferation, differentiation, neuronal development, and apoptosis. This thesis addresses the structural and biochemical basis of AP-1 function.

Fos and Jun heterodimerize, and Jun homodimerizes, via the leucine zipper coiled coil. Fos does not form a stable homodimer due to unfavorable interhelical electrostatic interactions in the Fos homodimeric coiled coil. Fos contains two lysine residues at positions that are buried in a dimeric coiled coil. Sedimentation equilibrium, circular dichroism and fluorescence indicate that substitution of one of these lysine residues with norleucine results in a very stable homotetramer with native-like properties, indicating that the electrostatic mechanism of Fos destabilization can be overcome by an oligomerization switch that is mediated by a buried polar residue. This finding was extended to protein design and used to impart dimerization specificity and native-like properties in a designed heterodimeric coiled coil.

c-Fos contains a C-terminal activation domain that binds TBP (TATA-Binding Protein). Using a combination of circular dichroism, nuclear magnetic resonance, and hydrodynamic techniques, the C-terminal activation domain of human c-Fos was shown to be functional for transcriptional activation yet unfolded. Studies of the complex formed between C-terminal activation domain of Fos and TBP were hindered by the limited solubility of TBP. However, using analytical ultracentrifugation and immunoprecipitation techniques, TBP was shown to be predominately monomeric at physiological concentrations. This finding challenges the notion that DNA binding by TBP is regulated by TBP dimerization.

c-Jun contains an N-terminal activation domain, which was also shown to be largely unfolded. Circular dichroism suggests that the Jun activation domain undergoes a folding transition upon binding the KIX domain of CBP (CREB-Binding Protein). A combination of circular dichroism and NMR reveals a novel mode of recognition of the KIX domain by c-Jun, and suggests a structural basis for combinatorial recruitment of CBP by multiple transcriptional activators.

Kathleen M. Campbell
Department of Biochemistry
and Molecular Biology
Colorado State University
Fort Collins, Colorado 80523
Spring 2002

Acknowledgements

I would like to thank my advisor, Dr. Kevin Lumb. Without his encouragement I never would have had the confidence to start graduate school. He has also been extremely supportive throughout the graduate process. He has been an excellent teacher and has put a lot of effort into helping me. He has taught me a great deal and it has been a pleasure to work with him.

I would like to thank my committee members, Dr. Paul Laybourn, Dr. Christopher Rithner, Dr. Laurie Stargell and Dr. Robert Woody for their time and helpful suggestions. A special thanks to Dr. Christopher Rithner for his patience and help with the NMR.

I would like to thank Drs. Paul J. Laybourn and Andrea R. Terrell for their collaborative contributions to the c-Fos studies and Drs. Laurie A. Stargell and Ryan T. Ranallo for their collaboration on the TBP studies.

I would like to thank Dr. Alan J. Kennan and the members of his laboratory for assistance with peptide synthesis and the use of their CD.

I would like to thank Drs. Robert and A-Young Woody and the members of their laboratory for all of their help and the use of their CD.

I would like to thank the members of the Lumb laboratory past and present. I would like to thank Josh Adkins, whose help and friendship I really appreciate; Ewa Bienkiewicz, who I enjoyed working with and who taught me NMR processing; Santano Mestas, who was fun to work with and who bought me lots of chocolate; Andrew Vendel, who was a constant source of entertainment and a fun lab partner; Yu Wei, who was very helpful and a pleasure to work with;

Teresa Groesch and Shannon Flaugh, who were great lab partners; and Aaron Sholders, for all of his hard work on the Fos leucine-zipper studies.

I would like to thank my parents, including my in-laws, for all of their support and encouragement. In particular, I would like to thank my mother for encouraging my interest in science at a young age.

I am deeply indebted to my family. I would like to thank Chad, for all of his support, love and encouragement. I could not have done it without him. The daily inquires about when I would graduate were also very inspiring. Lastly, I would like to thank Megan for bringing me much joy.

Table of Contents

Chapter 1

Gene Expression

1.1. GENE EXPRESSION

Protein-encoding genes typically contain core-promoters, which are recognized by the general transcription factors, and gene-specific DNA elements, which are recognized by regulatory factors (Orphanides *et al.*, 1996). These genes are transcribed by RNA polymerase II (Pol II), a large protein complex with at least twelve different evolutionarily conserved subunits (Roeder, 1996). Pol II transcription initiation requires the general transcription factors TFIID, TFIIB, TFIIE, TFIIF, and TFIIH (Roeder, 1996).

The pre-initiation complex forms either by stepwise assembly on DNA or is a pre-formed holoenzyme, which is recruited to DNA by TFIID (Burley & Roeder, 1996; Lemon & Tjian, 2000). However it remains unclear if the holoenzyme exists *in vivo* (Burley & Roeder, 1996). In either case, the first step in transcription initiation after chromatin remodeling is the sequence-specific binding of TFIID to the promoter (Orphanides *et al.*, 1996; Roeder, 1996). TFIID is a multi-subunit protein composed of the TATA-binding protein (TBP) and TBP-associated factors (TAFS). In the stepwise assembly model, following TFIID binding, TFIIA and TFIIB sequentially bind the DNA and stabilize the TFIID-DNA complex. TFIID then recruits the preformed Pol II-TFIIF complex. TFIIE recognizes and binds to this complex and then recruits TFIIH, which is the final factor included in the pre-initiation complex (Orphanides *et al.*, 1996; Roeder, 1996).

Promoter clearance is initiated by TFIIH, which phosphorylates the C-terminal domain of Pol II and contains helicase activity, which facilitates melting of the DNA. Transcription is then initiated, and Pol II and TFIIF are found in the elongating complex (Orphanides *et al.*, 1996; Roeder, 1996).

Although assembly of Pol II and associated general transcription factors at the promoter is sufficient for transcription at basal levels *in vitro*, transcription at elevated levels, requires DNA-binding proteins called transcriptional activators and their binding partners, the co-activators (Orphanides *et al.*, 1996; Näär *et al.*, 2001). Transcriptional regulation by activators occurs largely through the recruitment of Pol II and the general transcription factors to the promoter (Orphanides *et al.*, 1996; Näär *et al.*, 2001). The DNA-binding domains of transcriptional activators bind specific enhancer regions of promoters and impart specificity of gene expression. Each gene has a different combination of tightly clustered enhancer sequences and unique combinations of transcriptional activators bind a given promoter along with DNA-bending proteins such as HMG and LEF-1. This activation complex is called an enhanceosome (Carey, 1998). The cluster of activators bind cooperatively to the DNA and can synergistically recruit the general transcription factors to the promoter. Since activators are expressed and modified in response to different signals, formation of the enhanceosome will only occur when all of the appropriate physiological signals are coordinated. This allows for precise and sensitive control of gene expression (Carey, 1998; Lemon & Tjian, 2000).

In addition to the general transcription factors, transcriptional activators also recruit co-activators and co-repressors. Coactivators, such as p300/CBP, pCAF, Src-1, ACTR, and $TAF_{II}250$, are important binding partners to transcriptional activators, and contribute to transcription by acting as bridging molecules and by acetylating or de-acetylating (corepressors) histones (Utley *et al.*, 1998; Näär *et al.*, 2001). Histone acetylation is likely to contribute to transcription regulation by remodeling chromatin to an active form.

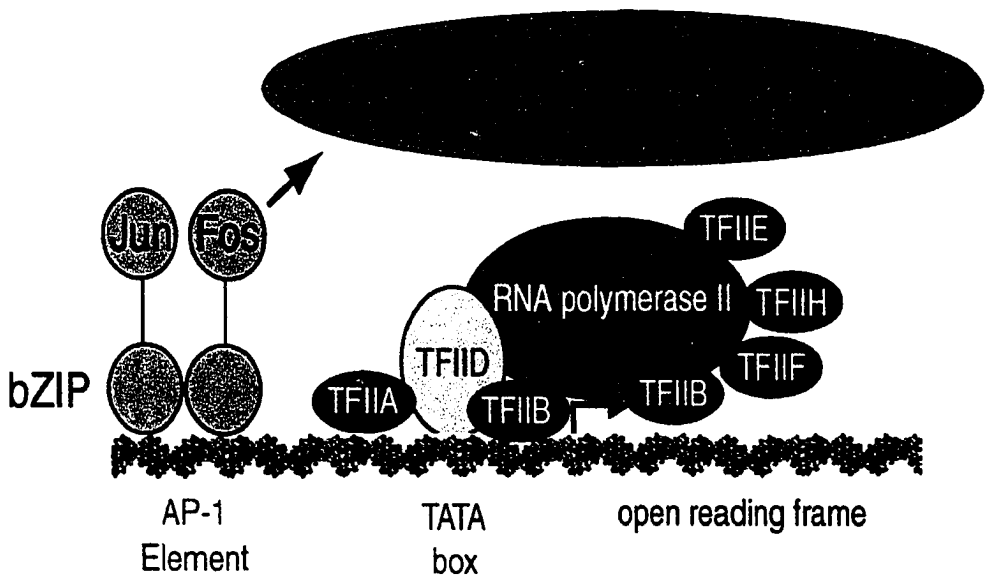

Figure 1.1. Schematic representation of the pre-initiation complex and an example activator (c-Fos/c-Jun) and coactivator (CBP).

1.1.A. Modular Structure of Transcriptional Activators

Transcriptional activators contain a DNA-binding domain and one or more activation domains (Triezenberg, 1995). The DNA-binding and activation domains are functionally independent, in that heterologous DNA-binding domains

can be fused to activation domains without affecting activation as long as DNA binding is maintained (Ptashne, 1988).

Many activation domains are essentially unfolded. Such intrinsic disorder has been observed for VP16, GCN4, human NF-κB, human gluticorticoid receptor, yeast heat-shock factor, p53, c-Myc and KID (kinase-inducible domain of CREB). (Donaldson & Capone, 1992; O'Hare & Williams, 1992; Van Hoy *et al.*, 1992; Schmitz *et al.*, 1994; Chang *et al.*, 1995; Dahlman-Wright *et al.*, 1995; Cho *et al.*, 1996; McEwan *et al.*, 1996; Radhakrishnan *et al.*, 1997; Lee *et al.*, 2000).

1.1.B. Molecular Recognition by Disordered Activation Domains

Molecular recognition has traditionally been considered to result from interactions between preordered structures. Transcriptional activators, and other unfolded yet functional proteins (Plaxco & Gross, 1997; Frankel & Smith, 1998; Wright & Dyson, 1999) question the notion that well-ordered structures are a prerequisite for recognition specificity. One hypothesis is that activators bind to their targets nonspecifically (Sigler, 1988). However, recent structural studies by NMR and X-ray crystallography, provide direct evidence for induced-folding of activation domains upon binding their targets. NMR studies using the transferred nuclear Overhauser effect (NOE) show that a peptide corresponding to a region of the VP16 activation domain adopts a helical structure on binding $TAF_{II}31$ (Uesugi *et al.*, 1997). The X-ray crystal structure of a peptide derived from the p53 activation domain bound to MDM2 shows that the p53 peptide also adopts a

helical structure in the complex (Kussie *et al.*, 1996). The NMR structure of the KIX domain of CBP, bound to the kinase-inducible activation domain of CREB (KID) (Radhakrishnan *et al.*, 1997), revealed that the KID domain is largely disordered in isolation, but folds into a pair of orthogonal helices upon binding to KIX (Figure 1.2).

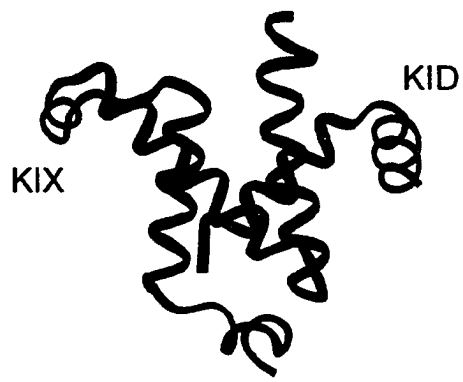

Figure 1.2. NMR structure of the KIX domain of CBP bound to the pKID domain of CREB (Radhakrishnan *et al.*, 1997).

An intrinsic lack of protein structure can be advantageous. Structural flexibility likely allows the protein to bind to a number of different targets (Wright & Dyson, 1999). It also allows for more precise control over specificity. Since the entropic penalty for binding is so high, the role of phosphorylation or precise interactions with other components of the transcriptional machinery can greatly affect the enthalpy and therefore the specificity of binding (Spolar & Record, 1994; Wright & Dyson, 1999). Unfolded proteins might also be more prone to proteolysis than globular proteins, which allows the cells to tightly regulate the cellular concentration of these important regulatory proteins (Wright & Dyson, 1999).

Finally, intrinsic disorder may confer a kinetic advantage to binding in some cases (Shoemaker *et al.*, 2001; Bienkiewicz *et al.*, 2002).

1.1.C. The AP-1 Family of Transcriptional Activators

AP-1 (Activating Protein-1) activates transcription of genes involved in a diverse range of biological processes, including cell transformation, proliferation, differentiation, migration and apoptosis (Karin *et al.*, 1997; Bohmann, 1999). Therefore, the *jun* and *fos* genes have strong oncogenic potential and deregulation of their expression has marked effects on cell growth and differentiation (Ransone & Verma, 1990; Curran & Vogt, 1992; Bohmann, 1999). The AP-1 family of transcriptional activators consist of Jun (v-Jun, c-Jun, JunB, JunD), Fos (v-Fos, c-Fos, Fra1, Fra2, FosB and ΔFosB) and ATF (ATF2, ATF3/LRF1, B-ATF). These proteins have intermittent regions of sequence conservation and each contains a basic region-leucine zipper (bZIP) DNA-binding and dimerization domain and one or more activation domains (Figure 1.3). The Jun and ATF proteins homodimerize or heterodimerize with other members of the AP-1 family (Figure 1.3). Fos proteins cannot homodimerize but instead heterodimerize with members of the Jun or ATF families (Kerppolla & Curran, 1991; Karin *et al.*, 1997). Fos and Jun have also been shown to heterodimerize with related bZIP proteins of the Maf and NF-E2 families (Chinenov & Kerppola, 2001). Therefore, many different combinations of AP-1 proteins are possible, each with a different regulatory property (Bohmann, 1999). AP-1 also interacts with many other transcription factors and activators

(Chinenov & Kerppola, 2001), including NFAT and Smad, which act synergistically with AP-1 by concomitantly binding composite enhancer sites.

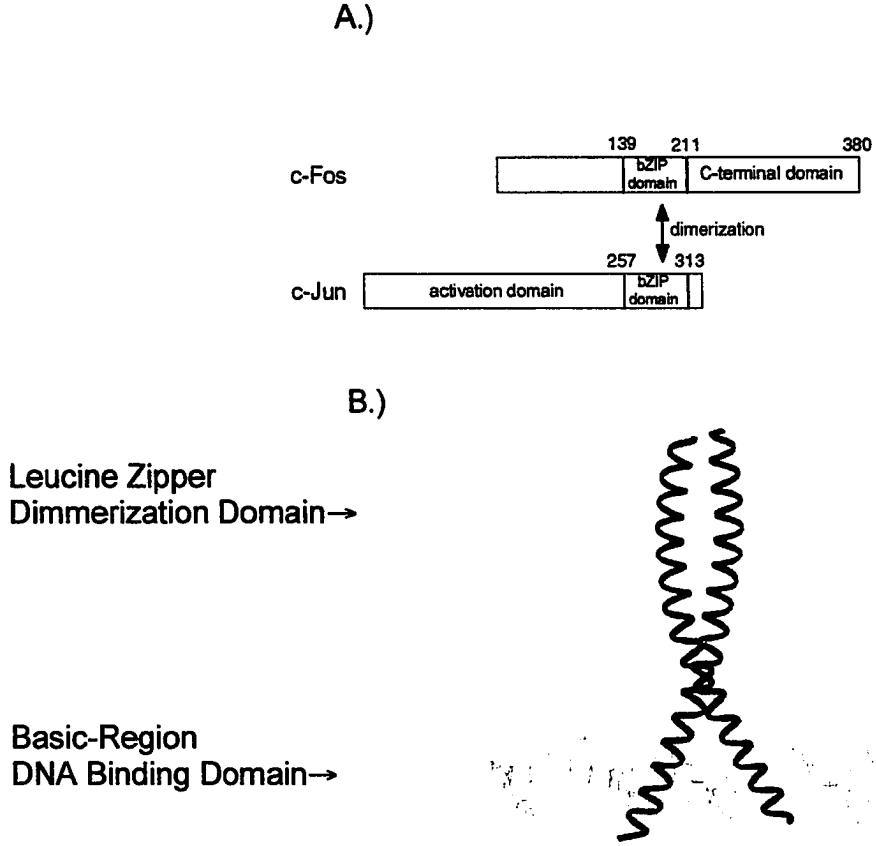

Figure 1.3. (A.) Schematic of human c-Fos and human c-Jun. The leucine zipper of the bZIP domain of c-Fos mediates dimerization with c-Jun (Karin *et al.*, 1997) and the basic region of the bZIP domain binds DNA (Curran & Vogt, 1992). The N- and C-terminal domains of c-Fos (Abate *et al.*, 1991) and the N-terminal of c-Jun (Sutherland *et al.*, 1992) activate transcription. (B) Crystal structure of the bZIP domains of c-Fos and c-Jun bound to DNA (Glover & Harrison, 1995).

c-Jun

c-Jun is required for proper development, since mice lacking c-Jun survive only to embryonic day 12 (Karin *et al.*, 1997; Bohmann, 1999; Jochum *et al.*, 2001). c-Jun regulates the cell cycle by at least one mechanism, which involves repressing p53 expression by binding directly to an AP-1-related element found

in the *p53* promoter (Schreiber *et al.*, 1999). c-Jun also plays a role in differentiation, with *jun* expression in cell culture promoting differentiation of many different cell lineages (Karin *et al.*, 1997; Bohmann, 1999; Jochum *et al.*, 2001). c-Jun activity has been shown to inhibit nerve growth factor withdrawal-induced apoptosis and overexpression of c-Jun has been shown to induce apoptosis (Bohmann, 1999).

c-Jun has phosphorylation sites in the N-terminal domain at Ser 63 and Ser 73, which are phosphorylated by JNK and, in some cell types, by ERK. JNK and ERK are members of the mitogen-activated protein kinase (MAPK) family. JNK is activated in response to stress signals, pathogenic insults and mitogens and ERK is activated by receptor tyrosine kinases and relays proliferation and differentiation signals (Karin *et al.*, 1997; Bohmann, 1999). The role of c-Jun phosphorylation at Ser 63 and Ser 73 is unclear. In fibroblasts, cells have a proliferation defect when the *c-jun* gene is replaced with a gene encoding c-Jun with Ser63Ala and Ser73Ala mutations (Behrens *et al.*, 1999). The phosphorylation sites were, however, found to be unimportant using directed expression of *c-jun* mutants to rescue *c-jun -/-* cells (Wisdom *et al.*, 1999). Phosphorylation has been shown to increase trans-activation (Forrest & Curran, 1992). However, this might be due to reduction in c-Jun ubiquitination and consequent stabilization of c-Jun levels *in vivo* (Musti *et al.*, 1997). The role phosphorylation plays in the interaction between c-Jun and the KIX domain of the CREB-binding protein (CBP) is also unclear. Although formation of the c-Jun-

CBP complex was once thought to be enhanced by phosphorylation (Arias *et al.*, 1994; Karin *et al.*, 1997), other studies suggest that Jun phosphorylation is not a prerequisite for binding CBP (Bannister *et al.*, 1995; Van Orden *et al.*, 1999a).

Human c-Jun has a modular structure consisting of an N-terminal activation domain and a bZIP domain (Fig. 1.A). Prior to starting my thesis research, the structural basis of transcriptional regulation by the N-terminal domain of c-Jun was limited to circular dicroism (CD) studies of a fragment corresponding to residues 61-98 of c-Jun (Matthias *et al.*, 1996). CD indicated that this peptide was essentially unstructured and that phosphorylation of Ser 63 and Ser 73 did not significantly change the secondary structure of the peptide, although, the c-Jun fragments did become more helical at low pH and in the presence of trifluoroethanol.

c-Fos

c-Fos is rapidly induced in response to growth factors (Karin *et al.*, 1997; Bohmann, 1999; Jochum *et al.*, 2001). However, c-Fos appears to be not required for cell proliferation since fibroblasts and embryonic stem cells lacking *c-fos* have no proliferation defect (Karin *et al.*, 1997; Bohmann, 1999). *c-fos* knockout mice also suggest that *c-fos* is not essential for the viability, proliferation and differentiation of most cell types. *c-fos* -/- mice are however, growth-retarded and have deficiencies in bone remodeling and tooth eruption (Karin *et al.*, 1997; Bohmann, 1999). A study using specific antibodies to the Fos

proteins (c-Fos, FosB, Fra-1 and Fra2), showed that although none of these proteins are individually essential for cell proliferation, the neutralization of all four blocked cell proliferation (Piechaczk & Blanchard, 1994). This suggests that the function of c-Fos in knockout mice might be compensated for by other Fos or AP-1 proteins (Karin *et al.*, 1997). c-Fos has been shown to induce apoptosis in many cell lines *in vitro* and *c-fos* is expressed *in vivo* in cells undergoing apoptosis (Jochum *et al.*, 2001). c-Fos also appears to protect cells from apoptosis, since fibroblasts deficient in c-Fos are more likely to undergo UV-induced cell death (Jochum *et al.*, 2001).

Human c-Fos has a modular structure consisting of an N-terminal activation domain, the bZIP domain and a C-terminal domain (Fig. 1A). The C-terminal domain of Fos can act both as a transcriptional activator (Abate *et al.*, 1991) and as a phosphorylation-dependent transcriptional repressor (Wilson & Treisman, 1988; Ofir *et al.*, 1990). Prior to starting my thesis research, the structural basis of transcriptional regulation by the C-terminal domain of c-Fos was essentially limited to deletion studies that identified regions of the primary sequence required for regulation (Abate *et al.*, 1991; Sutherland *et al.*, 1992; Metz *et al.*, 1994; Bannister & Kouzarides, 1995).

1.1.D. The Fos-Jun Leucine Zipper Dimerization Domain

Fos and Jun heterodimerize via the leucine zipper, which is a classic example of a heterodimeric coiled coil [(O'Shea *et al.*, 1989b; Glover & Harrison, 1995);

Figure 1.4]. Coiled coils are widespread oligomerization motifs in naturally occurring proteins, where two or more helices assemble in either a parallel or anti-parallel orientation (Lupas, 1996; Burkhard *et al.*, 2001). The sequences of coiled coils are characterized by a heptad amino-acid repeat denoted **a** to **g** (McLachlan & Stewart, 1975; Stone *et al.*, 1975). Most of the residues at positions **a** and **d** are hydrophobic and constitute the core of the helical, dimer interface, while the residues at positions **e** and **g** are mostly charged (Lupas, 1996; Burkhard *et al.*, 2001). However, the Fos leucine zipper is unusual with charged (Lys) or neutral polar (Thr) at four of the five **a** positions. The crystal structure of the human Fos-Jun leucine zipper shows that the aliphatic regions of the two **a** position Lys sidechains form hydrophobic packing interactions at the heterodimer interface, with the sidechain amino groups positioned to form inter-helical hydrogen bonds with **g'** position glutamine residues of the proceeding heptad of Jun (Glover & Harrison, 1995). Fos does not form a stable homodimer, because of unfavorable interhelical **g'**→**e** electrostatic interactions in the Fos homodimer that are relieved upon heterodimer formation (O'Shea *et al.*, 1992).

A.)

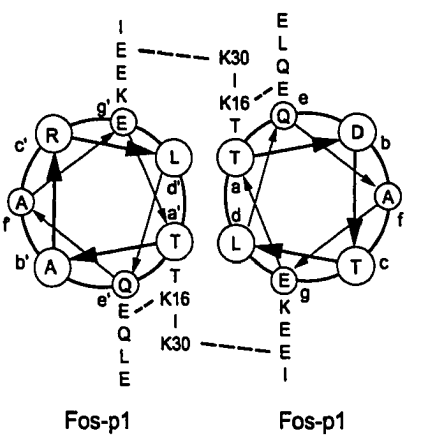

B.) Ac-LTDTLQAETDLEDKKSALQTEIANLLKEKEKLEFILAAY-CONH$_2$

Figure 1.4. (A.) Helical-wheel representation of the heterodimeric c-Fos/c-Fos leucine zipper. (B.) Amino acid sequence for Fos-p1.

1.1.E. The Designed Heterodimeric Coiled Coil ACID-p1/BASE-p1

An example of a designed coiled-coil is ACID-p1/BASE-p1, which was designed based on principals derived from studies of the Fos-Jun and GCN4 leucine zippers [Figure 1.5; (O'Shea *et al.*, 1993)]. The interface between the ACID-p1 and BASE-p1 helices consists of hydrophobic leucine residues, with the exception of Asn 14 at position **a**. ACID-p1 and BASE-p1 are predominantly unfolded in isolation because of destabilizing **g'** to **e** electrostatic interactions in the homodimer (O'Shea *et al.*, 1993). However, ACID-p1 and BASE-p1 associate to form a stable, parallel coiled coil, in which unfavorable electrostatic interations are releaved (O'Shea *et al.*, 1993). ACID-p1/BASE-p1 also has native-like tertiary structure, which is rare for designed proteins (O'Shea *et al.*, 1993; Lumb & Kim, 1995). When Asn 14 is substituted by leucine in both ACID-p1 and BASE-p1 (termed ACID-pLL and BASE-pLL), the peptides form a

heterotetramer instead of a heterodimer (Lumb & Kim, 1995). The tetramer is more stable than ACID-p1/BASE-p1 and the helices do not have a unique orientation and the core is poorly packed. Thus, Asn14 promotes specificity of the heterodimer at the expense of stability (Lumb & Kim, 1995).

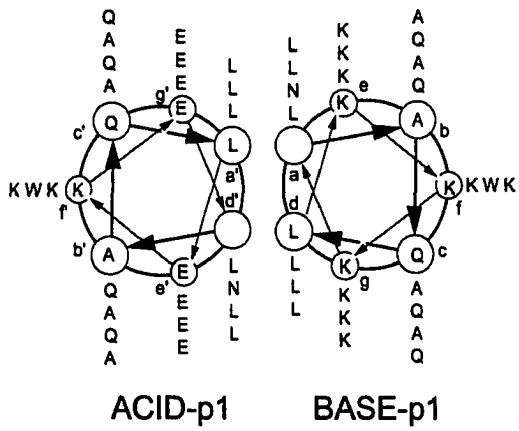

Figure 1.5. Helical-weel representation of the ACID-p1/BASE-p1 heterodimeric leucine zipper (O'Shea *et al.*, 1993b).

1.1.F. Targets of AP-1 during Gene Expression

The TATA-Box Binding Protein (TBP)

TBP has been shown to interact with a number of transcriptional activators, including p53, E1A, VP16, c-Myc, E2F-1, c-Jun and c-Fos (Stringer *et al.*, 1990; Seto *et al.*, 1992; Geisberg *et al.*, 1994; Metz *et al.*, 1994; Emili & Ingles, 1995; Franklin *et al.*, 1995; McEwan *et al.*, 1996; Hermann *et al.*, 2001). Strong evidence exists for activator interactions with TBP *in vivo* (Triezenberg, 1995) and competition for TBP binding exists between the acidic activator VP16 and at least one TAF (*Drosophilia* $TAF_{II}230$) (Nishikawa *et al.*, 1997).

The evidence for a physiologically relevant interaction between the C-terminal domain of c-Fos and cTBP is strong (Metz *et al.*, 1994), *In vitro*, GST-pulldown assays show that GST-c-Fos binds to the conserved C-terminal domain of TBP, but not to the divergent N-terminus, and that GST-c-Fos interacts with TFIID from HeLa nuclear extract. c-Fos was affinity purified with TBP from sf9 cells coinfected with baculoviruses expressing c-Fos and GST-TBP, suggesting a c-Fos-TBP interaction *in vivo*, and this interaction was abolished by deletion mutations that abolish the c-Fos-TBP interaction *in vitro*. In addition, c-Fos and TBP were coimmunoprecipitated from c-Fos-transformed or serum-stimulated NIH 3T3 cells. Finally, the c-Fos mutants that abolish binding to TBP also abolish transcriptional activation *in vivo*. Thus, c-Fos provides one of the best-established examples of a functional *in vivo* interaction between an activator and TBP.

The Human Coactivator and Histone Acetyltransferase CBP

CBP (CREB-Binding Protein) was originally identified as a protein that associates with CREB when Ser 133 of CREB is phosphorylated (Chrivia *et al.*, 1993). Further studies have determined that CBP (and the paralog p300) is a transcriptional co-activator (Orphanides *et al.*, 1996; Ptashne & Gann, 1997; Lemon & Tjian, 2000; Näär *et al.*, 2001). Co-activators differ from activators in that co-activators do not bind DNA directly. Instead co-activators are recruited to the transcription complex by activators. CBP has been shown to interact with many transcriptional activators (Figure 1.6), including c-Jun. CBP also interacts

either directly or indirectly with several general transcription factors, including TFIIB, TFIID, and RNA polymerase II (Goldman *et al.*, 1997; Montminy, 1997; Shikama *et al.*, 1997; Martínez-Balbás *et al.*, 1998; Goodman & Smolik, 2000). CBP also contains nucleosomal histone acetyltransferase activity. Therefore, CBP can stimulate transcription by recruiting the general transcription factors and by remodeling chromatin by acetylation (Goldman *et al.*, 1997; Montminy, 1997; Shikama *et al.*, 1997; Martínez-Balbás *et al.*, 1998; Goodman & Smolik, 2000).

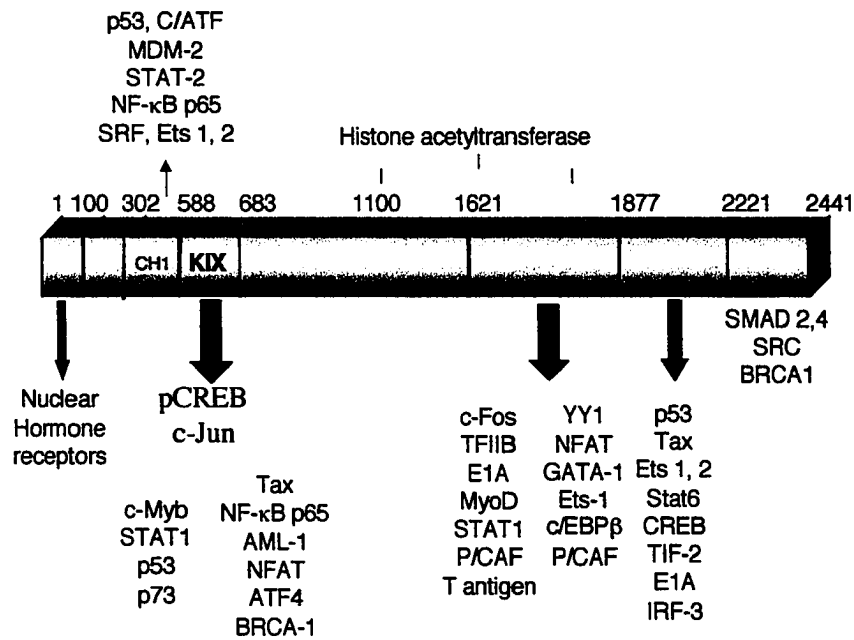

Figure 1.6. Schematic of domain structure of CBP. Transcription factors which have been shown to bind CBP are listed.

CBP has a fundamental role in cell growth and differentiation. Chromosomal translocations in CBP are associated with acute and chronic myeloid leukemia and myeloidoysplastic syndrome (Giles *et al.*, 1998; Goodman & Smolik, 2000).

CBP point mutations, translations, and deletions are linked to Rubinstein-Taybi syndrome (Giles *et al.*, 1998; Goodman & Smolik, 2000).

Analysis of the CBP amino acid sequence reveals several globular domains, with more that half of the sequence corresponding to regions of high predicted flexibility (Wright & Dyson, 1999). The structures of the KIX (residues 586-672), TAZ2(CH3) (residues 1764-1850) and IbiD (residues 2066-2111) domains have been solved and are all involved in protein-protein interactions with transcriptional activators and the general transcription machinery (Radhakrishnan *et al.*, 1999; Guzman *et al.*, 2000; Lin *et al.*, 2001). In addition, there is a HAT (histone acetyl-transferase) domain and a bromodomain, which are associated with chromatin remodeling (Wright & Dyson, 1999).

The N-terminal activation domain of c-Jun binds the KIX domain of CBP (Bannister *et al.*, 1995; Van Orden *et al.*, 1999a), and the interaction between full-length c-Jun and CBP stimulates transcription in vivo (Bannister *et al.*, 1994). Phosphorylated c-Jun binds CBP (Arias *et al.*, 1994) although c-Jun phosphorylation is not required for the formation of the c-Jun-CBP complex (Bannister *et al.*, 1994; Van Orden *et al.*, 1999a).

1.1.G. Gaps to be Filled

Buried polar residues at **a** positions of coiled coils have been shown to dictate coiled-coil oligomerization and helix orientation (O'Shea *et al.*, 1991; Harbury *et*

al., 1993; Junius *et al.*, 1995; Lumb & Kim, 1995; Gonzalez *et al.*, 1996a; Gonzalez *et al.*, 1996b; Zeng *et al.*, 1997; Oakley & Kim, 1998; Suzuki *et al.*, 1999; Wagschal *et al.*, 1999a; Wagschal *et al.*, 1999b; Zhu *et al.*, 2000; Akey *et al.*, 2001). The Fos leucine zipper is unusual with charged (Lys) or neutral polar (Thr) at four of the five **a** positions, which are usually occupied by hydrophobic residues in coiled coils. We saught to determine if these **a**-position Lys residues were responsible for the oligomerization state of Fos by replacing them with the unnatural amino acid norleucine, which corresponds to a deletion of the charged Lys ε–amino group. This work was begun by Aaron Sholders (as an undergraduate summer research student) and I continued this work when he left the laboratory (Chapter 2). The results from this project lead to protein design studies, which furthered our understanding of Lys at **a** postions in coiled-coils (Chapter 3).

When I began my thesis research very little was known about the structural basis of transcriptional activation. Fragments of activation domains of herpes virus VP16, GCN4, human NFκB, human gluticorticoid receptor, yeast heat-shock factor and p53 were shown to be essentially unfolded (Donaldson & Capone, 1992; O'Hare & Williams, 1992; Van Hoy *et al.*, 1992; Schmitz *et al.*, 1994; Chang *et al.*, 1995; Dahlman-Wright *et al.*, 1995; Cho *et al.*, 1996). This suggested that many activation domains lacked structure in isolation. It was unclear whether this was a result of studying peptide fragments, since it was not demonstrated that these peptides maintained their function. These unfolded

domains led to two hypotheses, one suggested that these domains bound non-specifically to their targets (Sigler, 1988), and the second suggested that binding their targets required induced folding of the activation domains (Kim & Frankel, 1991; Tjian & Maniatis, 1994).

We were interested in structurally characterizing a full-length activation domain, which involved determining if it had structure in isolation, showing that it was functional, determining if it bound its target specifically and determining if it adopted secondary structure upon binding its target. We originally decided to characterize the C-terminal domain of c-Fos, because it had not been previously characterized and the Fos-TBP interaction had been well-documented (Metz *et al.*, 1994). We successfully characterized of the C-terminal activation domain of c-Fos and found it to be active for transcription and primarily unstructured (Chapter 4). However, studying the interaction between Fos and TBP proved to be difficult, primarily because the TBP-Fos complex is large and was difficult to study by NMR. This was further complicated by low solubility of TBP and loss of activity with time. We instead decided to characterize a different activator complex.

In the process of studying the TBP-Fos complex, one of the techniques I used was sedimentation equilibrium, which showed that full-length TBP was monomeric at physiological concentrations (Chapter 5). This data was combined with data from Drs. Ryan Ranallo and Laurie Strargell, which also suggested that

TBP was monomeric *in vivo*. Our finding was contrary to the current hypothesis that TBP was dimeric *in vivo* and that dimer dissociation was a rate-limiting step in DNA binding (Coleman *et al.*, 1995; Taggart & Pugh, 1996; Coleman & Pugh, 1997; Jackson-Fisher *et al.*, 1999a and 1999b).

To persue our original goal of characterizing an activator complex, we decided to study the interaction between the activation domain of c-Jun and the KIX domain of the coactivator CBP. This interaction had been confirmed by two independent laboratories (Bannister & Kouzarides, 1995; Van Orden *et al.*, 1999a) and the domains were of reasonable size for NMR studies. Furthermore, Santano Mestas and Dr. Kevin Lumb had determined an expression and purification scheme, which resulted in large amounts of KIX. Although we were unable to determine the solution structure of the c-Jun activation domain and KIX we were able to greatly increase our understanding of this interaction. We determined that c-Jun and CREB recognize the KIX domain by structurally distinct modes (Chapter 6).

Chapter 2

Contribution of Buried Lysine Residues to the Oligomerization Specificity and Stability of the Fos Coiled Coil

This chapter describes work representing a collaboration with Aaron J. Sholders. Aaron J. Sholders synthesized and purified the peptides and did preliminary circular dichroism and sedimentation equilibrium studies. I fully characterized the peptides, using circular dichroism, sedimentation equilibrium and fluorescence. This work is in press at *Biochemistry* (Campbell *et al.*, 2002). Experimental details and results have been expanded beyond that reported in the manuscript.

2.1. ABSTRACT

Coiled coils comprise two or more helices characterized by a heptad repeat of amino acids denoted **a** through **g**. The buried **a** and **d** positions are usually occupied by hydrophobic residues. Fos dimerizes via a coiled coil (leucine zipper) with Jun family members to form the transcription factor AP-1. Fos homodimers are relatively unstable due to unfavorable interhelical electrostatic interactions within the Fos two-stranded coiled coil. The Fos coiled coil contains two polar position-**a** Lys residues (Lys 16 and Lys 30 of Fos-p1, a peptide corresponding to the coiled-coil domain of v-Fos). Lys 16 and 30 of Fos-p1 were replaced individually and together with the unnatural amino acid norleucine (2-aminohexanoic acid), which corresponds to a deletion of the Lys ε-amino group. The midpoint of thermal denaturation (T_m) of Fos-p1 (10 μM) is 30 °C at pH 7. The Lys 16→Nle variant forms predominantly homodimers that are relatively unstable (T_m = 46 °C). The Lys 30→Nle variant forms a stable homotetramer (T_m = 60 °C). The Lys 16/Lys 30→Nle variant forms a very stable homotetramer (T_m = 80 °C). The results show that (i) the effects of buried position-**a** Lys residues on coiled-coil oligomerization are context dependent and (ii) electrostatic destabilization of the Fos homodimer can be mitigated by an oligomerization switch mediated by a single buried Lys residue.

2.2. INTRODUCTION

The coiled coil governs protein-protein interactions in a diverse range of structural and regulatory proteins (Lupas, 1996; Burkhard *et al.*, 2001). The motif is widespread in natural proteins, with over 5% of putative open-reading frames of sequenced genomes predicted to contain coiled coils (Newman *et al.*, 2000). Coiled coils consist of two or more helices that assemble with either a parallel or antiparallel orientation (Lupas, 1996; Burkhard *et al.*, 2001). The hallmark sequence feature of the coiled coil is a heptad repeat of seven amino acids labeled **a** to **g** (McLachlan & Stewart, 1975; Stone *et al.*, 1975). The hydrophobic interface between the helices of a coiled coil comprise residues at positions **a**, **d**, **e** and **g** (O'Shea *et al.*, 1991; Harbury *et al.*, 1993; Harbury *et al.*, 1994). Amino acids at positions **a** and **d** are usually hydrophobic, whereas residues at the **e** and **g** positions are often charged (McLachlan & Stewart, 1975; Stone *et al.*, 1975; Parry, 1982; Conway & Parry, 1990; Lupas *et al.*, 1991; Berger *et al.*, 1995; Woolfson & Alber, 1995; Wolf *et al.*, 1997; Walshaw & Woolfson, 2001). Residues at the **e** and **g** positions may participate in interhelical electrostatic interactions (McLachlan & Stewart, 1975; Stone *et al.*, 1975; Lumb & Kim, 1996).

A classic example of a parallel, coiled-coil heterodimer is the leucine zipper of the Fos-Jun transcription factor (AP-1) (O'Shea *et al.*, 1989b; Glover & Harrison, 1995). AP-1 is implicated in cellular processes such as differentiation, oncogenesis and apoptosis (Karin *et al.*, 1997; Jochum *et al.*, 2001; Shaulian & Karin, 2001). The dimerization specificity of the Fos-Jun heterodimer is

embodied in the leucine-zipper coiled-coil domain (O'Shea *et al.*, 1989b). Jun can form a stable homodimer (Karin *et al.*, 1997). In contrast, the Fos homodimer is destabilized by unfavorable interhelical electrostatic interactions between Glu residues at **e** and **g'** positions in the leucine zipper of the Fos homodimer (Figure 2.1.A) (Nicklin & Casari, 1991; O'Shea *et al.*, 1992; John *et al.*, 1994). These unfavorable interactions are relieved upon heterodimerization with Jun, and so the specificity of Fos-Jun heterodimerization is driven by the instability of the Fos homodimer (O'Shea *et al.*, 1992).

Four of the five **a** positions of the Fos leucine zipper are occupied by either charged (Lys) or neutral polar (Thr) amino acids (Figure 2.1.A). These positions are usually, but not exclusively, occupied by hydrophobic amino acids (McLachlan & Stewart, 1975; Stone *et al.*, 1975; Parry, 1982; Conway & Parry, 1990; Lupas *et al.*, 1991; Berger *et al.*, 1995; Woolfson & Alber, 1995; Wolf *et al.*, 1997; Walshaw & Woolfson, 2001). Buried polar residues at **a** positions of coiled coils can dictate coiled-coil oligomerization and helix orientation (O'Shea *et al.*, 1991; Harbury *et al.*, 1993; Junius *et al.*, 1995; Lumb & Kim, 1995; Gonzalez *et al.*, 1996a; Gonzalez *et al.*, 1996b; Zeng *et al.*, 1997; Oakley & Kim, 1998; Suzuki *et al.*, 1999; Wagschal *et al.*, 1999a; Wagschal *et al.*, 1999b; Zhu *et al.*, 2000; Akey *et al.*, 2001). Position-**a** Lys residues have been observed to impart dimerization specificity (Gonzalez *et al.*, 1996b) and to occur more frequently in two-stranded than in three-stranded coiled coils (Conway & Parry, 1990; Woolfson & Alber, 1995; Walshaw & Woolfson, 2001). Simultaneous

replacement of four or five of the polar position-**a** residues of the Fos leucine zipper with hydrophobic amino acids results in Fos mutants that activate transcription *in vivo*, which was interpreted to result from the formation of stable homodimers by the Fos mutants (Porte *et al.*, 1995).

We show here that the electrostatic mechanism of Fos destabilization can be overcome by an oligomerization switch of the Fos leucine zipper that is mediated by one of the two position-**a** Lys residues of Fos. The effects of the two position-**a** Lys residues on oligomerization are different, and so are depend on context. The results extend our understanding of the basis of Fos-Jun assembly, in that electrostatic destabilization of Fos association relies on dimerization, and illustrate the importance of considering context when using position-**a** Lys residues as a sequence feature for identifying dimeric coiled coils.

2.3. METHODS

2.3.A. Peptide Synthesis

Peptides with acetylated N-termini and amidated C-termini were synthesized by Aaron J. Sholders on MBHA (4-methylbenzhydrylamine hydrochloride salt) resin (100-200 mesh) with manual Boc chemistry (Schnölzer *et al.*, 1992). The following protecting groups were used: Asn(Xan), Asp(Bzl), Gln(Xan), Glu(Bzl), Lys(2-Cl-Z), Ser(Bzl) Thr(Bzl), Tyr(Bzl). Peptides were purified by C_{18} HPLC using linear 0.1%/min water/acetonitrile gradients containing 0.1% (v/v) trifluoroacetic acid. The identity of each peptide was confirmed with electrospray

mass spectrometry, by Don Dick in the Department of Chemistry Central Instrument Facility, with the expected and observed masses agreeing to within 1 Da.

2.3.B. Determination of Protein Concentration

Concentrations of peptide stock solutions were determined by Tyr absorbance in 6 M GuHCl, 10 mM sodium phosphate, and 50 mM NaCl, pH 6.5 using an extinction coefficient at 276 nm of 1450 cm^{-1} M^{-1} (Edelhoch, 1967).

2.3.C. CD Spectroscopy

CD spectroscopy was performed with an Aviv 202 spectrometer. Samples contained 10 μM peptide in 10 mM sodium phosphate and 150 mM NaCl, pH 7.0. Thermal stability was monitored from the change in $[\theta]_{222}$ with temperature. The temperature was increased in steps of 2 °C with an equilibration time of 60 s. The CD signal at 222 nm was averaged over 60 s. The T_m was determined from the maxima of the first derivative of $[\theta]_{222}$ with respect to 1/T (Cantor & Schimmel, 1980).

2.3.D. Sedimentation Equilibrium

Sedimentation equilibrium experiments were performed with a Beckman XL-I analytical ultracentrifuge. Samples were dialyzed for at least 12 hours against the reference buffer (10 mM sodium phosphate, 150 mM NaCl, pH 7.0). Data were collected at 5 °C at 35, 40 and 45 krpm on samples of initial loading

concentrations of 70 and 140 μM using two-sector centerpieces. Peptide concentrations spanned approximately 20 to 700 μM at equilibrium. Sapphire windows were used, which alleviated apparent sticking of the Fos peptides to quartz windows. A directly measured solvent density of 1.008 g ml^{-1} and calculated partial molar volumes of 0.744 ml g^{-1} (Fos-p1), 0.745 ml g^{-1} (single Nle variants) and 0.747 ml g^{-1} (double Nle variant) were used (Laue *et al.*, 1992). Data were fit using ORIGIN (Beckman) to single-species and self-associating models both as individual data sets and as a global fit of all six data sets for each peptide. The validity of different models evaluated by the distribution of residuals and the variance. Results are reported as the mean mass of the individual data sets ± the standard error and as the mass and variance obtained from global fits.

2.3.E. Fluorescence Spectroscopy

ANS binding was monitored at 5 °C with an Aviv ATF105 fluorometer. Emission spectra were collected from 400 to 600 nm using an excitation wavelength of 355 nm. Samples contained 10 μM peptide and 1 μM ANS (Molecular Probes) in 10 mM sodium phosphate 150 mM NaCl, pH 7.0. ANS concentration was determined for a stock solution in methanol by absorbance at 372 nm using an extinction coefficient of 7.8 x 10^3 cm^{-1} M^{-1} (Molecular Probes).

Intrinsic Tyr fluorescence was monitored at 5 °C by exciting at 276 nm and collecting emission scans from 290 to 380 nm. Samples contained 10 μM peptide in 10 mM sodium phosphate, 150 mM NaCl, pH 7.0.

2.4. RESULTS

2.4.A. Biophysical characterization of Fos-P1

Fos-p1 (Figure 2.1) corresponds to the leucine-zipper region of v-Fos (residues 161-200) and is identical to the leucine zipper of human c-Fos with the exception of a single **g**-position amino-acid substitution; Glu 175 of human c-Fos is substituted with Lys in v-Fos (van Straaten *et al.*, 1983). Although Fos-p1 forms a helical dimer at μM concentrations, the dissociation constant for dimerization (approximately 5.6 μM at 25 °C, pH 7) precludes dimerization at nanomolar concentrations (O'Shea *et al.*, 1989b).

A.)

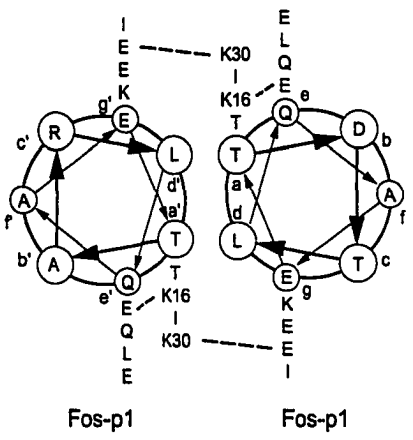

B.) Ac-LTDTLQAETDLEDKKSALQTEIANLLKEKEKLEFILAAY-CONH$_2$

Figure 2.1. (A.) Helical-wheel representation of the Fos-Fos leucine zipper, shown as a parallel, two-stranded coiled coil (O'Shea *et al.*, 1989b). A view down the helix from the amino terminus is shown. The **d**-position residues are all Leu, and are omitted after the first heptad for clarity, as are the **b**, **c** and **f**-position residues. Putative intra- and interhelical polar interactions involving Lys 16 and Lys 30 (shown in bold) are indicated with dashed lines. (B.) Amino-acid sequence of Fos-p1 (O'Shea *et al.*, 1989b). The N-terminus is acetylated and the C-terminus is amidated.

To evaluate the contribution of position-**a** polar Lys residues to the formation of the Fos leucine zipper, Lys 16 and Lys 30 were substituted separately and together with the unnatural amino-acid norleucine (Nle; 2-aminohexanoic acid). This substitution corresponds to a deletion of the side chain ε-amino moiety of Lys while leaving the remainder of the hydrophobic side chain intact. Lys 16 and Lys 30 of Fos-p1 correspond to Lys 176 and Lys 190, respectively, of full-length human c-Fos and v-Fos (van Straaten *et al.*, 1983).

In accord with previously published results (O'Shea *et al.*, 1989b), CD indicates that Fos-p1 is helical (Figure 2.2) and is relatively unstable (Figures 2.3 and 2.4), with a T_m of 30 °C at a total peptide concentration of 10 μM. The molecular mass determined by sedimentation equilibrium indicates that Fos-p1 is dimeric at micromolar concentrations and 5 °C (expected mass for the dimer of 9218 Da; observed 9100 ± 500 Da; Figure 2.5).

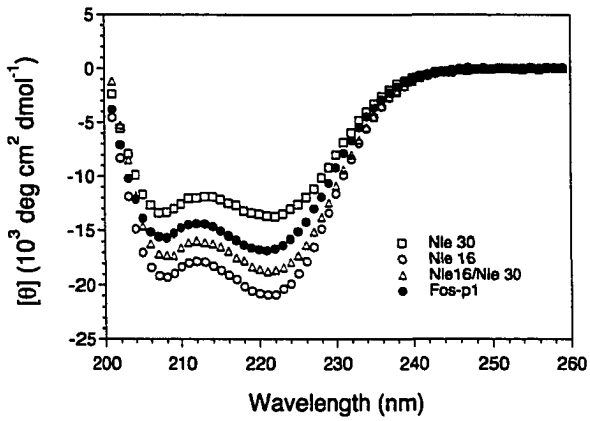

Figure 2.2. CD spectra of Fos-p1 and the Lys→16Nle, Lys 30→Nle, and Lys 16/Lys30→Nle variants. The minima at 208 and 222 nm indicate that the peptides form helical structures. The origin of the different magnitudes of the CD spectra is unclear (see section 2.4.E.), but do not simply reflect changes in the fraction of globally unfolded peptide.

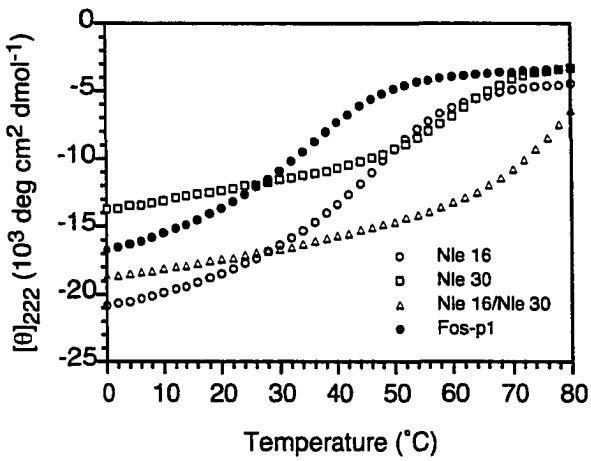

Figure 2.3. Temperature dependence of $[\theta]_{222}$ for Fos-p1 (T_m = 30°C), Lys 16→Nle (T_m = 46°C), Lys 30→Nle (T_m = 60°C) and Lys 16/Lys30→Nle (T_m = 80°C) variants.

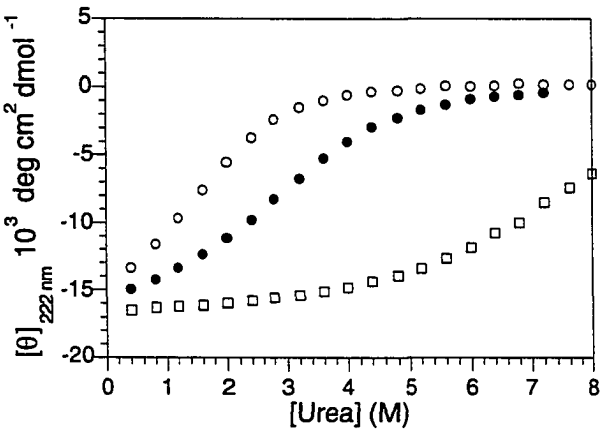

Figure 2.4. Urea melts for Fos-p1(O), Lys 16→Nle (●) and Lys 16/Lys30 →Nle (□) variants. The lack of folded baselines for Fos-p1 and Lys 16→Nle and lack of unfolded baseline for Lys 16/Lys30 →Nle, precluded determination of ΔG.

The thermal and urea unfolding curves of Fos-p1 are sigmoidal (Figure 2.3 and Figure 2.4) and Fos-p1 does not bind ANS (Figure 2.6). These results suggest that the Fos-p1 dimer adopts a well-packed structure typical of native proteins. In contrast, molten globules and many designed proteins that lack structural uniqueness exhibit linear unfolding transitions and bind ANS (Kuwajima, 1989; Betz *et al.*, 1993; Lumb & Kim, 1995).

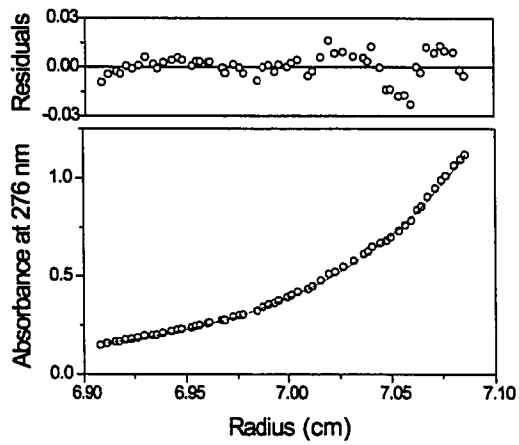

Figure 2.5. Sedimentation equilibrium data for Fos-p1. Data fit to a single species model gave the mass expected for a dimer.

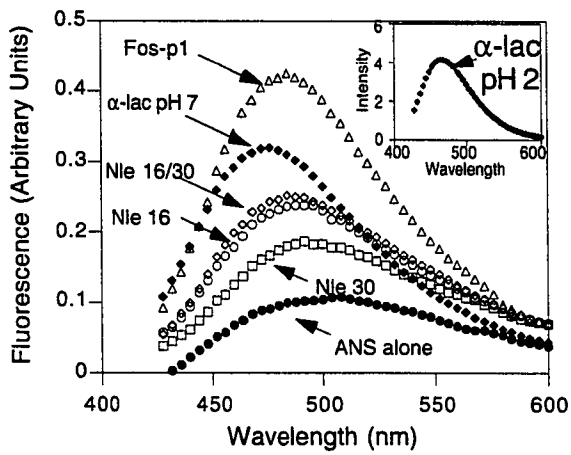

Figure 2.6. ANS binding by Fos-p1 and the Fos leucine zipper variants. ANS binding to proteins is accompanied by a significant increase in ANS emission intensity and a decrease in emission wavelength from 500 nm to approximately 470 nm (Stryer, 1965; Goto & Fink, 1989; Semisotnov *et al.*, 1991). Such large changes in ANS fluorescence are induced by the pH 2 molten-globule form of α-lactalbumin, in accord with previous results (Semisotnov *et al.*, 1991). In contrast, such large changes in ANS fluorescence are not induced by the Fos leucine-zipper peptides.

2.4.B. Biophysical Characterization of the Lys 16→Nle Variant

The Lys 16→Nle variant is helical (Figure 2.2) with a higher thermal stability than Fos-p1; the T_m at 10 μM peptide concentration is 46 °C (Figure 2.3). The sigmoidal thermal and urea unfolding curves (Figures 2.3 and 2.4) and lack of ANS binding (Figure 2.6) suggest that the Lys 16→Nle variant adopts a well-packed structure typical of native proteins.

The apparent molecular mass of the Lys 16→Nle variant determined from individual fits of the six sedimentation equilibrium data sets is 10.9 ± 0.4 kDa, which is 19% higher than expected for a dimer (9188 Da) and 21% lower than expected for a trimer (13782 Da). The apparent mass obtained from a global fit to a single-species model is 11.1 kDa (variance = 1.4). Of various models, the sedimentation equilibrium data is best accounted for by a dimer-tetramer equilibrium as judged by the distribution of the residuals for fits to individual data sets (Figure 2.7). In addition, the variance, which approaches 1 as the fit improves, of a global fit of the six data sets is lowest for the dimer-tetramer model at 1.06. Significant deviations of residuals are observed for fits to models other than dimer-tetramer, and higher variances are seen for global fits to other possible models such as single-species trimer (variance = 13.0) and monomer-tetramer (variance = 2.76). The distribution of the residuals (Figure 2.7) and the variance of the global fit at 1.11 for the monomer-trimer model is only slightly less favorable than for the dimer-tetramer model (variance = 1.06). However, the thermal denaturation behavior of the Lys 16→Nle variant is inconsistent with the

presence of unfolded monomers (see Figure 2.3. legend), and therefore inconsistent with equilibria involving monomeric peptides that are likely to be largely unfolded. The Lys 16→Nle variant therefore exists in a mixture of oligomerization states and is predominantly dimeric (>80%, assuming that the apparent mass reflects the weight-average distribution of the dimer and tetramer).

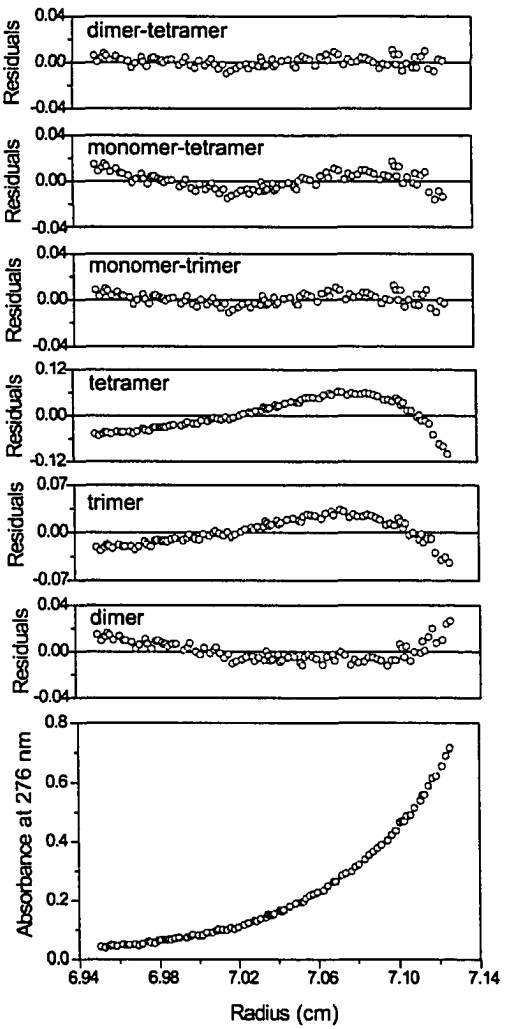

Figure 2.7. Sedimentation equilibrium data for the Lys 16→Nle. Of various models, the distribution of residuals to individual fits and variances of the global fits (see text) indicate that the data are best accounted for by a dimer-tetramer equilibrium. The apparent dissociation constant for the dimer-tetramer equilibrium is 1.0 ± 0.2 mM, and so the Lys 16→Nle variant is predominantly dimeric at low micromolar concentrations.

2.4.C. Biophysical Characterization of the Lys 30→Nle Variant

Replacement of Lys 30 with Nle results in a helical structure (Figure 2.2) of significantly higher thermal stability; the T_m is increased to 60 °C (Figure 2.3). The sigmoidal thermal and urea unfolding curves (Figure 2.3 and 2.4) and lack of ANS binding (Figure 2.6) suggest that the Lys 30→Nle variant adopts a well-packed structure typical of native proteins.

The apparent molecular mass of the Lys 30→Nle variant determined from a single-species fit of sedimentation equilibrium data is 17.6 ± 0.4 kDa (Figure 2.8). The mass obtained from a global fit of the six data sets is also 17.6 kDa, and the variance of the global fit is 1.4. These apparent masses are significantly higher than expected for a trimer (13782 Da) and approximately 4% lower than expected for a tetramer (18376 Da). The single-species tetramer (variance = 1.47), monomer-tetramer (variance = 1.52) and dimer-tetramer (variance = 1.47) models provide essentially equivalent descriptions of the data, and a systematic change in apparent mass with loading concentration is not observed. The sedimentation equilibrium data therefore indicate that the Lys 30→Nle variant is essentially tetrameric.

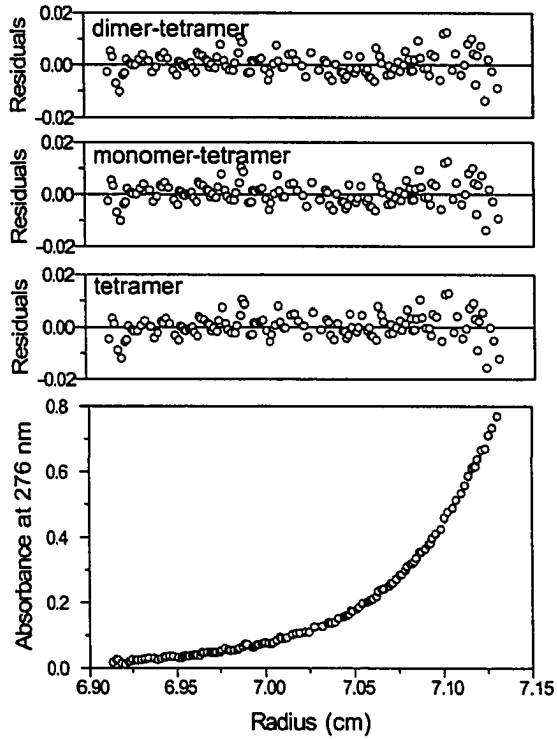

Figure 2.8. Sedimentation equilibrium data for the Lys 30→Nle variant. The quality of fits to various models involving the tetramer indicate that the Lys 30→Nle variant is essentially tetrameric.

2.4.D. Biophysical Characerization of Lys 16/Lys 30→Nle.

Simultaneous substitution of Lys 16 and Lys 30 with Nle results in a helical structure (Figure 2.2) with increased thermal stability relative to the Lys 30→Nle variant (T_m = 80 °C; Figure 2.3). The molecular mass determined by sedimentation equilibrium indicates that the double variant is tetrameric (Figure 2.9). The average molecular mass obtained from individual fits of the six data sets is 18.5 ± 0.7 kDa, and the mass obtained from a global fit of all six data sets is 18.7 kDa (variance = 1.7). The expected mass for the tetramer is 18316 Da.

The Lys 16/Lys 30→Nle variant exhibits the native-like properties of a sigmoidal unfolding curve (Figures 2.3 and 2.4) and lack of ANS binding (Figure 2.6).

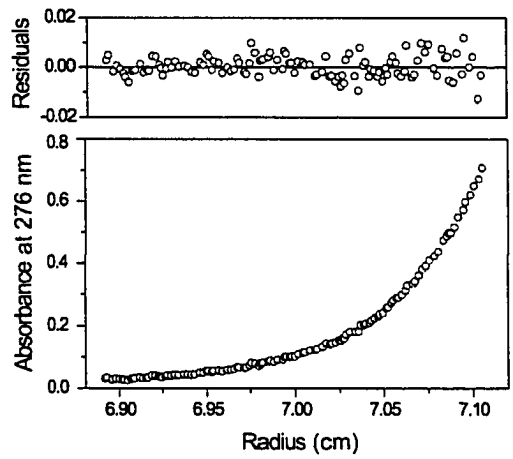

Figure 2.9. Sedimentation equilibrium indicates that the Lys 16/Lys30→Nle variant is tetrameric. The random distribution of residuals and the molecular weight within error of the tetramer, indicates that a single-species tetramer accounts for the data.

2.4.E. Differences in $[\theta]_{222}$ for Fos-p1 Variants

The variant Fos peptides exhibit differences in $[\theta]_{222}$ at low temperatures that are unrelated to T_m. If $[\theta]_{222}$ reflects helix content only, then the Lys 30→Nle variant is apparently less helical than Fos-p1 at low temperatures but has a higher T_m than Fos-p1, and the Lys 16/Lys 30→Nle variant is slightly less helical than the Lys 16→Nle variant at low temperatures, but has a higher T_m than Lys 16→Nle (Figure 2.3). The reason for this behavior is unclear, and is seen with peptides that have been once and twice purified by C_{18} HPLC with shallow (0.1%/min)

gradients, making the presence of impurities unlikely. The values of $[\theta]_{222}$ may reflect an aromatic contribution from Tyr 40 to the CD spectra (Woody & Dunker, 1996). Tyr 40 is at the C-terminal **a** position in each of the Fos peptides and may be sensitive to conformational changes or oligomerization switches due to the Nle substitutions. Tyr 40 of each peptide is, however, largely solvent exposed since the fluorescence emission maximum of each peptide and of the free amino-acid L-Tyr is 303 nm (Figure 2.10), as expected for a solvent-exposed Tyr (Creighton, 1993). The differences in $[\theta]_{222}$ at low temperature may also reflect local unfolding of the Fos variant coiled coils, as seen for a variant GCN4 coiled coil (Lumb *et al.*, 1994). The presence of folded baselines for the three variant peptides suggests the absence of an equilibrium between globally unfolded and folded peptides (Lumb *et al.*, 1994).

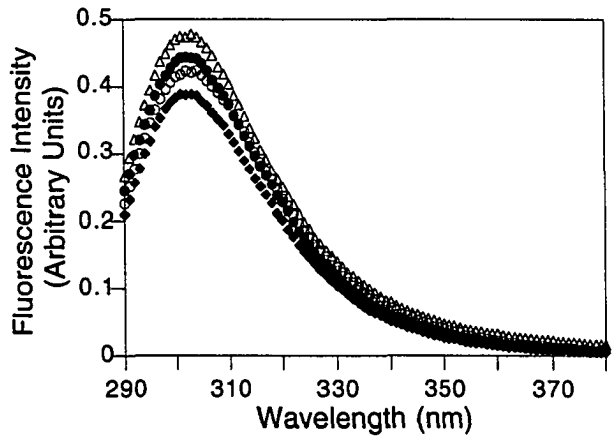

Figure 2.10. Tyrosine fluorescence for Fos-p1(O), Lys 16→Nle (Δ), Lys 30→Nle (♦) and Lys 16/Lys30 →Nle (●) variants. The similarity of fluorescence maxima for each variant suggests that Tyr 40 of each peptide is largely solvent exposed.

2.5. DISCUSSION

Coiled coils form a widespread protein oligomerization motif (Lupas, 1996; Burkhard *et al.*, 2001), with over 5% of all putative open reading frames predicted to contain coiled-coil domains (Newman *et al.*, 2000). The hallmark sequence feature of the motif, the **3,4** hydrophobic repeat at positions **a** and **d** (McLachlan & Stewart, 1975; Stone *et al.*, 1975), is a useful predictor of putative coiled coils (McLachlan & Stewart, 1975; Stone *et al.*, 1975; Conway & Parry, 1990; Lupas *et al.*, 1991; Berger *et al.*, 1995; Woolfson & Alber, 1995; Wolf *et al.*, 1997; Walshaw & Woolfson, 2001). Since the helices of coiled coils can adopt multiple oligomerization states in homo- and heteromeric complexes (Lupas, 1996; Burkhard *et al.*, 2001), it is desirable to identify sequence features that identify oligmerization orders and partners of coiled-coil assemblies.

Buried polar residues can dictate the specificity of coiled-coil oligomerization and association (O'Shea *et al.*, 1991; Harbury *et al.*, 1993; Junius *et al.*, 1995; Lumb & Kim, 1995; Gonzalez *et al.*, 1996a; Gonzalez *et al.*, 1996b; Zeng *et al.*, 1997; Oakley & Kim, 1998; Suzuki *et al.*, 1999; Wagschal *et al.*, 1999a; Wagschal *et al.*, 1999b; Zhu *et al.*, 2000; Akey *et al.*, 2001). For example, Asn residues at position **a** are a common feature of two-stranded coiled coils (Conway & Parry, 1990; Lupas *et al.*, 1991; Berger *et al.*, 1995; Woolfson & Alber, 1995; Walshaw & Woolfson, 2001), including the c-Jun homodimer (Junius *et al.*, 1995). In several natural and designed coiled coils, Asn at position **a** imparts specificity for dimerization (Harbury *et al.*, 1993; Betz *et al.*, 1995; Junius *et al.*, 1995; Lumb &

Kim, 1995; Gonzalez *et al.*, 1996b; Zeng *et al.*, 1997; Wagschal *et al.*, 1999b) and helix orientation (Lumb & Kim, 1995; Oakley & Kim, 1998), presumably by destabilizing alternative conformations in which the hydrogen-bonding potential of the Asn side chain is unsatisfied (O'Shea *et al.*, 1991; Betz *et al.*, 1995; Lumb & Kim, 1995).

Lys is a relatively common buried polar residue in coiled coils. Position-**a** Lys residues are significantly more common in dimeric than trimeric coiled coils (Conway & Parry, 1990; Woolfson & Alber, 1995; Walshaw & Woolfson, 2001). A position-**a** Lys directs formation of dimers in the context of the GCN4 coiled coil, and analysis of GCN4 coiled-coil structures suggests that the oligomerization preference may be due to preferential solvation of the Lys ε-amino group in the dimer relative to the trimer (Gonzalez *et al.*, 1996b). Indirect evidence for a contribution of position-**a** Lys to oligomerization specificity comes from studies of a designed coiled coil in which two peptides are crosslinked with a disulfide bond (Wagschal *et al.*, 1999b). In this context, Lys at position **a** decreases the stability of the dimer without resulting in an oligomerization switch (Wagschal *et al.*, 1999b). Taken together, these findings suggest that position-**a** Lys residues promote dimer formation.

Fos forms a homodimer at micromolar concentrations, but does not have a position-**a** Asn. There are, however, two position-**a** Lys residues. Our results indicate that dimerization of the Fos leucine zipper is mediated by Lys 30, since

replacement of Lys 30 with Nle results in tetramer formation. Lys 16, in contrast, does not impart dimerization specificity to the same extent, since the Lys 16→Nle variant is predominantly dimeric at micromolar concentrations. Simultaneous replacement of Lys 16 and Lys 30 with Nle results in a very stable homotetramer. Thus, Lys 30 plays a central role in imparting dimerization specificity to Fos at the expense of stability.

The different effects of Lys 16 and Lys 30 on oligomerization specificity indicate that the effects of position-**a** Lys residues on coiled-coil assembly are context dependent. The influence of context may reflect different ionic interactions of the ε-amino groups of the two Lys residues. In the parallel Fos homodimer, Lys 30 has the potential to form an interhelical **g'**→**a** polar interaction with a **g'**-position Glu of the preceding heptad of the opposing helix (Figure 1A). Such interactions are seen in the crystal structure of the parallel Fos-Jun coiled-coil heterodimer (Glover & Harrison, 1995) and may contribute to dimerization specificity. In contrast, Lys 16 in an analogous **g'**→**a** interaction would be paired with a **g'**-position Lys of the opposing helix (Figure 1A), which is expected to be destabilizing (O'Shea *et al.*, 1993; Vinson *et al.*, 1993). Instead, Lys 16 could form an intrahelical electrostatic interaction with an **e**-position Glu of the preceding heptad (Figure 1A), as seen in the crystal structure of a GCN4 variant with a Lys at position **a** (Gonzalez *et al.*, 1996b). Such intrahelical interactions may not discriminate between alternative quaternary assemblies such as dimers,

trimers and tetramers, which have different interhelical packing arrangements (Harbury *et al.*, 1993; Harbury *et al.*, 1994).

Interhelical electrostatic interactions provide a mechanism to impart homo- and heteroassociation specificity (O'Shea *et al.*, 1992; O'Shea *et al.*, 1993; Lumb & Kim, 1996). Fos homodimers are destabilized by the juxtaposition of Glu residues that form unfavorable interhelical **g'→e** electrostatic interactions in the homodimer (Nicklin & Casari, 1991; O'Shea *et al.*, 1992; John *et al.*, 1994). We find that the destabilization of the Fos homodimer by unfavorable electrostatic interhelical **g'→e** interactions can be alleviated, however, by an oligomerization switch to the homotetramer. The results reveal an additional facet to the mechanism of Fos destabilization, which is the role of dimerization specificity, mediated by the position-**a** Lys residues, in placing like-charged residues in the correct context to disfavor self-association by Fos. Since Fos-Jun dimerization is driven by the instability of the Fos homodimer (O'Shea *et al.*, 1992), imparting specificity for dimerization is a key element of the molecular basis of the specificity of the Fos-Jun protein-protein interaction.

Chapter 3

Complementation of Buried Lysine and Surface Polar Residues in a Designed Heterodimeric Coiled Coil

This chapter describes work accepted for publication by *Biochemistry* (Campbell & Lumb, 2002a). Experimental details and results have been expanded beyond those reported in the manuscript.

3.1. ABSTRACT

The coiled coil is an attractive target for protein design. The helices of coiled coils are characterized by a heptad repeat of residues denoted **a** to **g**. Residues at positions **a** and **d** form the interhelical interface and are usually hydrophobic. An established strategy to confer structural uniqueness to two-stranded coiled coils is placing paired buried polar Asn residues at position **a**, which imparts specificity at the expense of stability. The results show that polar interactions involving buried position-**a** Lys residues that can interact favorably only with surface **e'** or **g'** Glu residues also impart structural uniqueness to a designed heterodimeric coiled coil with the native-like properties of sigmoidal unfolding transitions, slow hydrogen exchange and lack of ANS binding. The position-**a** Lys residues do not, however, confer a single preference for helix orientation, likely reflecting the ability of Lys at position **a** to form favorable interactions with **g'** or **e'** Glu residues in the parallel and antiparallel orientations, respectively. The Lys-Glu polar interaction is less destabilizing than the Asn-Asn **a**→**a'** interaction, presumably reflecting a higher desolvation penalty associated with the completely buried polar position-**a** groups. Our results extend the range of approaches for two-stranded coiled-coil design and illustrate the role of complementing polar groups associated with buried and surface positions of proteins in protein folding and design.

3.2. INTRODUCTION

Protein design provides a critical test of ideas regarding protein folding and stability, and holds promise for the rational creation of proteins with new properties. A popular target for protein design is the α-helical coiled coil (Kohn & Hodges, 1998; Schneider *et al.*, 1998; Micklatcher & Chmielewski, 1999; Oakley & Hollenneck, 2001). Naturally occurring coiled coils govern protein-protein interactions in a wide variety of biological processes (Lupas, 1996; Burkhard *et al.*, 2001) and over 5% of putative open reading frames in sequenced genomes are predicted to contain coiled-coil domains (Newman *et al.*, 2000). Rules derived from coiled-coil design, therefore, have implications for predicting and understanding the properties of natural coiled coils as well as extending the repertoire of approaches to designing new sequences that fold and assemble in a predetermined manner.

The helices of the coiled coil are characterized by a heptad repeat of seven amino acids labeled **a** to **g** (McLachlan & Stewart, 1975; Stone *et al.*, 1975). Residues at positions **a** and **d** are usually hydrophobic, whereas residues at **e** and **g** positions are often charged (McLachlan & Stewart, 1975; Stone *et al.*, 1975). The hydrophobic interface between the helices of a coiled coil comprise the side chains of residues at positions **a** and **d**, and the methylene groups of the **e** and **g** residues (Cusack *et al.*, 1990; O'Shea *et al.*, 1991; Harbury *et al.*, 1993). Polar side chains at positions **e** and **g** can also participate in intra- and

interhelical electrostatic interactions (Cusack *et al.*, 1990; O'Shea *et al.*, 1991; Harbury *et al.*, 1993; Harbury *et al.*, 1994).

Coiled-coil designs have utilized a variety of structural features such as hydrophobic packing at the **a-d** interface, interhelical **a**→**a'** buried polar interactions, and interhelical **g'**→**e** electrostatic interactions (Kohn & Hodges, 1998; Schneider *et al.*, 1998; Micklatcher & Chmielewski, 1999; Oakley & Hollenneck, 2001). The potential of exploiting interhelical interactions between normally buried position-**a** residues of one helix and normally solvent-exposed **e'** and **g'** side chain groups of the opposing helix has yet to be explored.

ACID-p1/BASE-p1 is a designed parallel coiled-coil heterodimer. ACID-p1 and BASE-p1 heterodimerize with high specificity, but the individual peptides do not form stable homodimers at neutral pH (O'Shea *et al.*, 1993). The ACID-p1/BASE-p1 heterodimer exhibits sigmoidal thermal- and urea-induced unfolding transitions, slow hydrogen exchange, and a lack of ANS binding (O'Shea *et al.*, 1993; Lumb & Kim, 1995). These native-like properties suggest the presence of conformational specificity or structural uniqueness, i.e., a well-defined, single fold (or family of very closely related folds) with a well-packed hydrophobic interior (O'Shea *et al.*, 1993; Lumb & Kim, 1995).

An explicit design feature of ACID-p1/BASE-p1 is a buried polar interaction between two position-**a** Asn residues (O'Shea *et al.*, 1993). Substitution of the

position-**a** Asn with Leu to form the peptides ACID-pLL and BASE-pLL results in the formation of a very stable heterotetramer. The ACID-pLL/BASE-pLL heterotetramer does not fold in a unique conformation, since the helices lack a single orientation and the heterotetramer exhibits the molten-globule properties of low protection from hydrogen exchange and ANS binding (Lumb & Kim, 1995). The Asn residues presumably impart structural uniqueness by destabilizing conformations that do not satisfy the hydrogen-bonding potential of the Asn side chains (Lumb & Kim, 1995). The conformationally plastic peptides ACID-pLL and BASE-pLL provide a platform to test the ability of different interactions to confer structural uniqueness to protein structure.

In a parallel two-stranded coiled coil, Lys at position **a** can form polar interactions with position-**g'** residues of the preceding heptad of the opposing helix (Glover & Harrison, 1995). In an antiparallel coiled coil, polar residues at position **a** can form polar interactions with position-**e'** residues of the opposing helix (Cusack *et al.*, 1990). Two position-**a** Lys residues were placed into the context of BASE-pLL to make BASE-pK (Figure 3.1), with the expectation that interhelical polar interactions between the position-**a** Lys residues of BASE-pK and **e'** or **g'** Glu residues of ACID-pLL could impart structural uniqueness and dimerization specificity. In a dimeric assembly, the only residues able to make a favorable polar interaction with the position-**a** Lys ε-amino groups of BASE-pK are the **e'** or **g'** Glu residues of ACID-pLL in the antiparallel or parallel orientations, respectively (Figure 3.1).

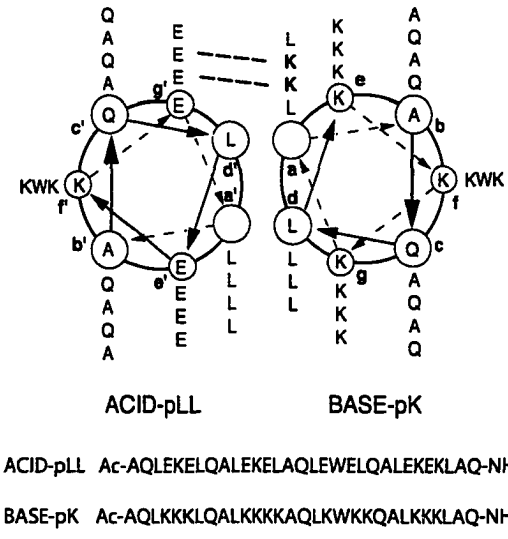

Figure 3.1. Helical-wheel representation of the ACID-pLL/BASE-pK heterodimer. In the parallel ACID-pLL/BASE-pK heterodimer, the α-amino group of the position-**a** Lys can only form favorable polar interactions with position-**g'** Glu residues of ACID-pLL, shown using dashed lines. In the antiparallel orientation, the α-amino group of the position-**a** Lys can only form favorable polar interactions with position-**e'** Glu residues of ACID-pLL The position-**d** Leu residues of ACID-pLL are omitted for clarity.

We find that the position-**a** Lys residues do indeed impart a significant level of structural uniqueness: ACID-pLL and BASE-pK associate to form a heterodimer with the properties expected of a native globular protein. There is not, however, a significant preference in helical orientation (parallel or antiparallel) in the ACID-pLL/BASE-pK heterodimer. Our results enlarge the range of combinatorial interactions that can be utilized in coiled-coil prediction, design and assembly.

3.3. METHODS

3.3.A. Peptide Purification

The peptides ACID-p1, BASE-p1, ACID-pLL (corresponding to ACID-p1 with Asn 14 substituted for Leu: Figure 3.1), ACID-pLL^N (corresponding to ACID-pLL with an N-terminal Ac-Cys-Gly-Gly), and ACID-pLL^C (corresponding to ACID-pLL with a C-terminal Gly-Gly-Cys-NH_2) were kind gifts of Peter S. Kim (O'Shea *et al.*, 1993; Lumb & Kim, 1995). BASE-pK (Figure 3.1) was synthesized with Fmoc chemistry by the Macromolecular Resources Facility at Colorado State University. Peptides were purified by reversed phase C_{18} HPLC using linear water/acetonitrile gradients containing 0.1% (v/v) trifluoroacetic acid. The identity of each peptide was confirmed with electrospray mass spectrometry by Don Dick in the Department of Chemistry Central Intrument Facility, and in all cases the expected and observed masses agreed to within 1 Da.

3.3.B. Peptide Synthesis of BASE-pK^N

BASE-pK^N, corresponding to BASE-pK with an N-terminal Ac-Cys-Gly-Gly and amidated C-terminus was prepared with manual Boc chemistry at the 0.25 mmol scale, using MBHA resin (0.373 g) (Schnolzer et al., 1992). The following protecting groups were used: Gln(Xan), Lys(ClZ), Cys(MeBzl) andTrp(CHO) (Nova Biochem).

1 mmol of the first (C-terminal) Boc-amino acid was mixed with 0.359 g HBTU, 2.5 ml DMF and 0.3 ml DIEA in a test tube. The mixture was sonicated until

clear. After waiting two minutes, the amino acid was added to the resin and the solution was mixed with shaking for 40 minutes (12 minutes for subsequent amino acids). The resin was rinsed with DMF. Coupling was confirmed by the Kaiser ninhydrin test (Kaiser *et al.*, 1970). A negative Kaiser test indicates that coupling is complete, whereas a positive Kaiser test results in a blue product and indicates the presence of a free amine. If the test was positive, coupling of the same amino acid was repeated. If the test was negative then the Boc group was removed with TFA (2 rounds of 3 ml TFA for 1 minute), the resin was rinsed with DMF and the next amino acid was coupled. After the coupling of the final amino acid, the N-terminal was acetylated by adding 3 ml acetic anhydride, 2 ml DMF and 2 ml DIEA and shaking for 12 minutes.

When synthesis was complete, the resin was rinsed with DMF, CH_2Cl_2 and diethyl ether and desiccated under vacuum overnight to remove residual solvents. The peptide was cleaved from the resin and the remaining protecting groups were removed by HF cleavage, for two hours, in an HF reaction apparatus (Stewart & Young, 1984) using 10 ml HF per g of dried resin and 1 ml anisole per g of dried resin. After the HF evaporated, the resin was resuspended with diethyl ether, rinsed with ether and the peptide was eluted from the resin with water. BASE-pK^N was treated with 100 mM DTT at pH 8 and then purified by reverse-phase C_{18} HPLC using a linear 0.1% per minute acetonitrile/water gradient containing 0.1% TFA. The identity of the peptide was confirmed with electrospray mass spectrometry by Don Dick in the Department of Chemistry

Central Instrument Facility. The expected and observed mass agreed to within 1 Da.

3.3.C. Determination of Peptide Concentration

Concentrations of peptide stock solutions were determined by Trp absorbance in 6 M GuHCl, 10 mM sodium phosphate, and 50 mM NaCl, pH 6.5 using an extinction coefficient at 280 nm of 11380 M^{-1} cm^{-1} and 5690 M^{-1} cm^{-1} for disulfide bonded and non-disulfide bonded peptides, respectively (Edelhoch, 1967).

3.3.D. CD Spectroscopy

CD spectra were acquired with Aviv 202 or Jasco J720 CD spectrometers. Samples contained 10 μM peptide in 10 mM sodium phosphate and 150 mM NaCl, pH 7.0.

Thermal stability was monitored from the change in the CD signal at 222 nm with temperature with an Aviv 202 CD spectrometer. Samples contained 10 μM peptide in 10 mM $NaPO_3$, 150 mM NaCl, pH 7.0. The temperature was increased in steps of 2 °C with an equilibration time of 60 s. The CD signal at 222 nm was averaged over 60 s. The T_m was determined from the maxima of the first derivative of $[\theta]_{222}$ with respect to 1/T (Cantor & Schimmel, 1980).

The free energy of unfolding at 25 °C was determined from the change in the CD signal at 222 nm, with urea concentration, with an Aviv 202 CD spectrometer.

Samples contained 10 μM ACID-pLL/BASE-pK in 10 mM $NaPO_3$, 150 mM NaCl, pH 7.0 (PBS buffer). Urea concentration was increased in steps of 0.4 M with a 600 s equilibration time and the CD signal at 222 nm averaged over 60 s. Data were fit to an unfolded monomer-folded dimer equilibrium to obtain the equilibrium constant for unfolding at each urea concentration, K_u, given by $(2 \cdot c \cdot f_u^2)/(1-f_u)$, where c is the total peptide concentration and f_u is the fraction unfolded. The change in $\Delta G_u°$, given by $-RTlnK_u$, with urea concentration ([urea]) in the transition region was fit to $\Delta G_u°(urea) = \Delta G_u°(PBS) + m[urea]$ to obtain $\Delta G_u°(PBS)$ and m (Pace, 1986). Urea concentration was determined with refractometry (Nozaki, 1972).

3.3.E. Sedimentation Equilibrium

Sedimentation equilibrium experiments were performed with a Beckman XL-I analytical ultracentrifuge. Samples were dialyzed for at least 12 hours against the reference buffer (10 mM $NaPO_3$, 150 mM NaCl, pH 7.0). Data were collected at 25 °C at rotor speeds of 40 and 48 krpm using two-sector and six-sector centerpieces. For BASE-pK, eight data sets were collected at 280 nm with loading concentrations ranging from 20 to 80 μM. For ACID-pLL/BASE-pK, six and fourteen data sets were collected at 230 and 280 nm, respectively, with loading concentrations ranging from 10 to 100 μM. A solvent density of 1.004 g ml^{-1} and calculated partial specific volumes of 0.783 ml g^{-1} (BASE-pK) and 0.762 ml g^{-1} (ACID-pLL/BASE-pK) were used (Laue *et al.*, 1992). Data in the approximate concentration range 6 to 90 μM were fit using ORIGIN (Beckman

Instruments) to an ideal, single-species model, with the validity of the model evaluated by the distribution of residuals. Masses are reported as the mean mass of the individual fits ± the standard error.

3.3.F. Helix Orientation

Helix orientation was determined from the concentration dependence of stability of disulfide-bonded peptides (O'Shea *et al.*, 1989a and 1989b). The helices of ACID-pLL and BASE-pK were constrained to be parallel by forming the disulfide between ACID-pLL^N and BASE-pK^N, and were constrained to be antiparallel by forming the disulfide between ACID-pLL^C and BASE-pK^N. The disulfide-bonded peptides were prepared by incubating the HPLC-purified reduced peptides in 6 M GuHCl, pH 8 at room temperature overnight. The desired disulfide-bonded heterodimer (i.e., ACID-pLL^N/BASE-pK^N or ACID-pLL^C/BASE-pK^N) was separated from the reduced peptides or the unwanted disulfide-bonded homodimers by C_{18} HPLC. The identities of the disulfide-bonded products were confirmed with MALDI mass spectrometry, and the expected and observed masses agreed to within 1 Da. The T_m values of the disulfide-bonded peptides were determined with CD spectroscopy as described above except samples were prepared in 10 mM sodium phosphate, 150 mM NaCl, and 3 M GuHCl, pH 7.0 containing peptide at total concentrations of 5, 10, 20 and 30 μM. The GuHCl concentration was determined with refractometry.

3.3.G. Hydrogen Exchange

Hydrogen exchange experiments were performed with Varian Unity Inova NMR spectrometer operating at 500.13 MHz for ^1H. Samples contained 0.5 mM ACID-pLL/BASE-pK in 10 mM $NaPO_3$, 150 mM NaCl, pH 7.0, and were internally referenced to DSS at zero ppm (Wishart *et al.*, 1995). One-dimensional ^1H spectra were acquired at 25 °C with a spectral width of 6000.1 Hz. Data sets consisted of 2048 transients defined by 8192 complex points. Data were resolution enhanced with a shifted Gaussian function and zero filled once prior to Fourier transformation, and the baseline was corrected using VNMR 6.1b software (Varian). Hydrogen exchange studies were initiated by dissolving lyophilized samples in D_2O. The pH of the solution was checked after the experiment and found to be 7.01, uncorrected for the isotope effect. The observed hydrogen exchange rate (k_{ex}) was obtained from fitting the change in amide resonance intensity (I) with time (t) to $I = I_0 \exp(-k_{ex}t) + I_\infty$. The intrinsic exchange rate (k_{int}) was taken to be 31 s^{-1} (Lumb & Kim, 1995), corresponding to three times the rate of amide exchange for poly-DL-alanine at pH 7.0 and 25 °C (Englander *et al.*, 1972). The observed protection factor was calculated as k_{ex}/k_{int}. The expected protection factor was calculated from $1/f_u$, which assumes a global unfolding mechanism of hydrogen exchange for a stable protein ($f_u << 1$) (Bai *et al.*, 1994). F_u was calculated from $K_u = (2 \cdot c \cdot f_u^2)/(1-f_u)$ where K_u is the equilibrium constant for unfolding determined by urea denaturation as described above and c is the total peptide concentration.

3.3.H. ANS Binding

Fluorescence studies of ANS binding were performed at 25 °C with an Aviv ATF105 fluorometer. Emission spectra were collected using an excitation wavelength of 355 nm and an emission wavelength of 400-600 nm. Samples contained 5 μM ANS (Molecular Probes) and 0 to 100 μM bovine α-lactalbumin in 10 mM $NaPO_3$, 150 mM NaCl, pH 2 or 0 to100 μM ACID-pLL/BASE-pK in 10 mM $NaPO_3$, 150 mM NaCl, pH 7.0. ANS concentration was determined for a stock solution in methanol by absorbance at 372 nm using an extinction coefficient of 7.8×10^3 cm^{-1} M^{-1} (Molecular Probes).

3.4. RESULTS

3.4.A. Properties of the Isolated ACID-pLL and BASE-pK Peptides

The CD spectrum of ACID-pLL indicates that the peptide forms a partially helical structure (Figure 3.2), in accord with previous results (Lumb & Kim, 1995). The temperature dependence of $[\theta]_{222}$ indicates that the helical structure is marginally stable, in accord with previous results (Lumb & Kim, 1995), with an apparent T_m of approximately 0 °C (Figure 3.3). CD indicates that BASE-pK also forms a marginally stable helix with an apparent T_m of approximately 0 °C (Figures 3.2). Since BASE-pLL forms a stable, helical homodimer at neutral pH (Lumb & Kim, 1995), the substitution of Leu with Lys at position **a** of BASE-pK is destabilizing.

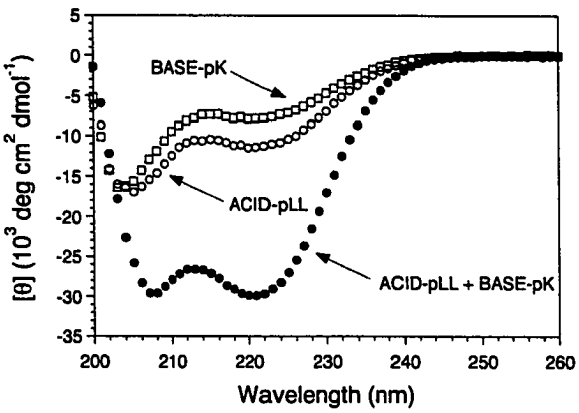

Figure 3.2. CD spectra of ACID-pLL, BASE-pK, and ACID-pLL/BASE-pK. The minima at 208 and 222 nm indicate that the peptides form helical structures. The CD spectrum of an equimolar mixture of ACID-pLL and BASE-pK is not the average of the spectra of the isolated ACID-pLL and BASE-pK peptides, indicating that the peptides associate to form a heterospecies.

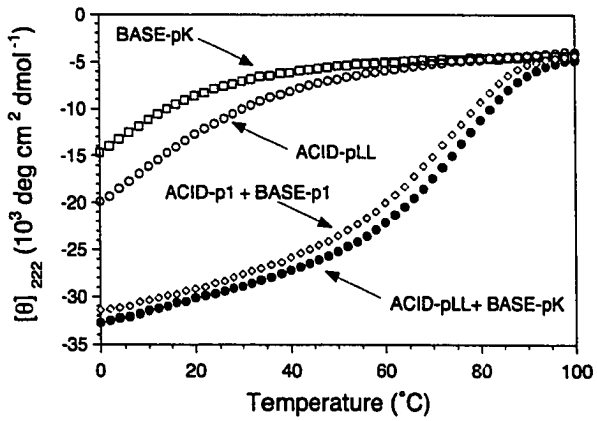

Figure 3.3. Thermal stability of ACID-pLL, BASE-pK, and ACID-pLL/BASE-pK monitored by the temperature dependence of $[\theta]_{222}$. Thermal melts were reversible (the forward and reverse melts were superimposable, with over 98% of the starting signal regained on cooling).

Sedimentation equilibrium indicates that BASE-pK is predominantly monomeric. The expected mass for the monomer is 3,585 Da and the apparent mass obtained from a single-species fit is 4.70 kDa ± 0.4 kDa (Figure 3.4). Previous studies show that ACID-pLL exists in a monomer-dimer-tetramer equilibrium that favors the monomer at low micromolar concentrations (Lumb & Kim, 1995).

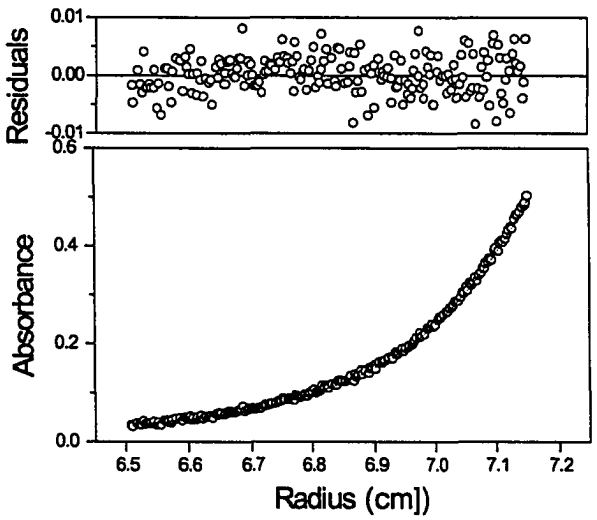

Figure 3.4. Sedimentation equilibrium indicates that BASE-pK is a monomer. The observed molecular mass is 4.70 ± 0.4 kDa (expected for monomer: 3,585 Da).

3.4.B. Heterodimerization of ACID-pLL and BASE-pK

On mixing, changes in the CD spectrum show that ACID-pLL and BASE-pK associate to form a new helical species with a helix content significantly greater than the isolated peptides (Figure 3.2). Sedimentation equilibrium indicates that the ACID-pLL and BASE-pK peptides form a dimer (Figure 3.5). The observed molecular mass is 7.60 ± 0.4 kDa (expected for the heterodimer: 7.148 kDa). The random distribution of residuals indicates that a single-species model

accounts for data. Systematic changes in apparent molecular mass with total peptide concentration or rotor speed are not observed.

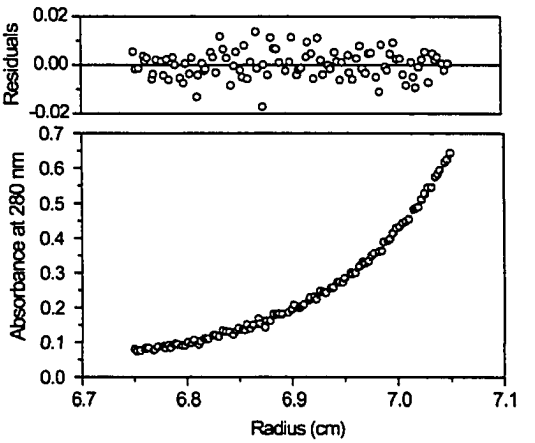

Figure 3.5. Sedimentation equilibrium indicates that ACID-pLL/BASE-pK is dimeric. The observed molecular mass is 7.60 ± 0.4 kDa (expected for the heterodimer: 7.148 kDa).

The helical content of the heterodimer is maximal when ACID-pLL and BASE-pK are mixed in equimolar amounts, indicating that the ACID-pLL and BASE-pK peptides associate with a 1:1 stoichiometry (Figure 3.6). The ACID-pLL/BASE-pK heterodimer is dramatically more stable than either of the two isolated peptides, with a T_m of 74 °C (Figure 3.3) and a free energy of unfolding (ΔG_u^o) measured by urea denaturation of 11.7 + 0.2 kcal mol^{-1} (Figure 3.7). The ACID-pLL/BASE-pK heterodimer is more stable than the ACID-p1/BASE-p1 heterodimer, for which the T_m is 72 °C (Figure 3.3) and $\Delta G_u°$ is 10.1 kcal mol^{-1} (O'Shea *et al.*, 1993). ACID-pLL and BASE-pK therefore assemble to form a stable, helical heterodimer.

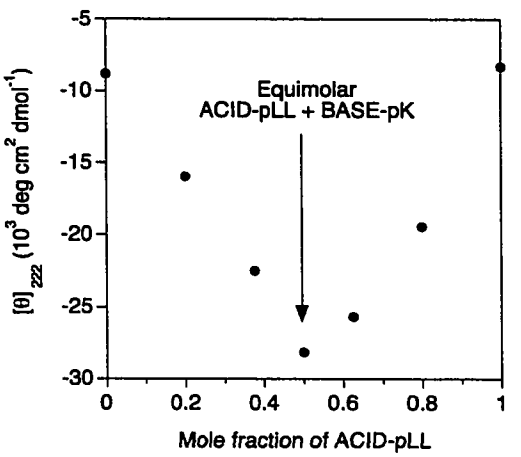

Figure 3.6. ACID-pLL/BASE-pK associate with a 1:1 stoichiometry. The helix content of the ACID-pLL + BASE-pK solution is maximal when the peptides are mixed in equimolar amounts.

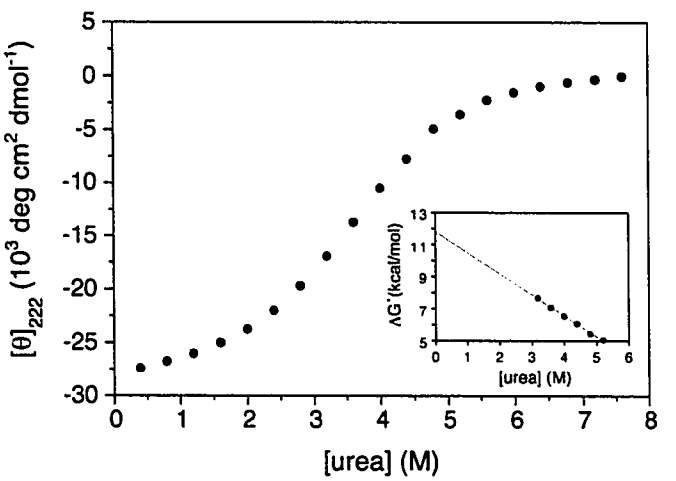

Figure 3.7. Stability of the ACID-pLL/BASE-pK heterodimer. The change in $[\theta]_{222}$ with urea concentration fit a monomer-dimer equilibrium (insert) to yield an apparent ΔG_u° of 11.7 ± 0.2 kcal mol^{-1} (m = 1.3 kcal mol^{-1}).

3.4.C. Helix Orientation of the ACID-pLL/BASE-pK Heterodimer

Helix orientation in coiled coils can be determined from the concentration dependence of stability of disulfide-bonded peptides (O'Shea *et al.*, 1989a and 1989b). The stability of a disulfide-bonded dimer is independent of concentration when the helices are joined in the preferred orientation. Conversely, stability is dependent on concentration when helices are covalently crosslinked in the unfavorable orientation, arising from the intermolecular association of higher-order assemblies with the helices in the preferred orientation (O'Shea *et al.*, 1989a and 1989b). ACID-pLL and BASE-pK crosslinked in both the parallel orientation and antiparallel orientations have T_m values that are independent of concentration. The T_m values of the parallel disulfide-bonded ACID-pLL^N/BASE-pK^N and antiparallel disulfide-bonded ACID-pLL^C/BASE-pK^N exceed 100 °C in 10 mM $NaPO_3$, 150 mM NaCl, pH 7. In 10 mM $NaPO_3$, 150 mM NaCl, 3 M GuHCl, pH 7.0, the T_m values of both disulfide-boded peptides is 58 ± 2 °C at total peptide concentrations of 5, 10, 20 and 30 mM (Figure 3.8), suggesting that both helix orientations are equally stable at the T_m. However, at low temperature there is a concentration dependence of $[\theta]_{222}$ for the antiparallel disulfide bonded ACID-pLL^C/BASE-pK^N. The helices of the ACID-pLL/BASE-pK heterodimer, therefore, do not exhibit a strong preference for a unique orientation, but the antiparallel orientation is prefered at low temperatures.

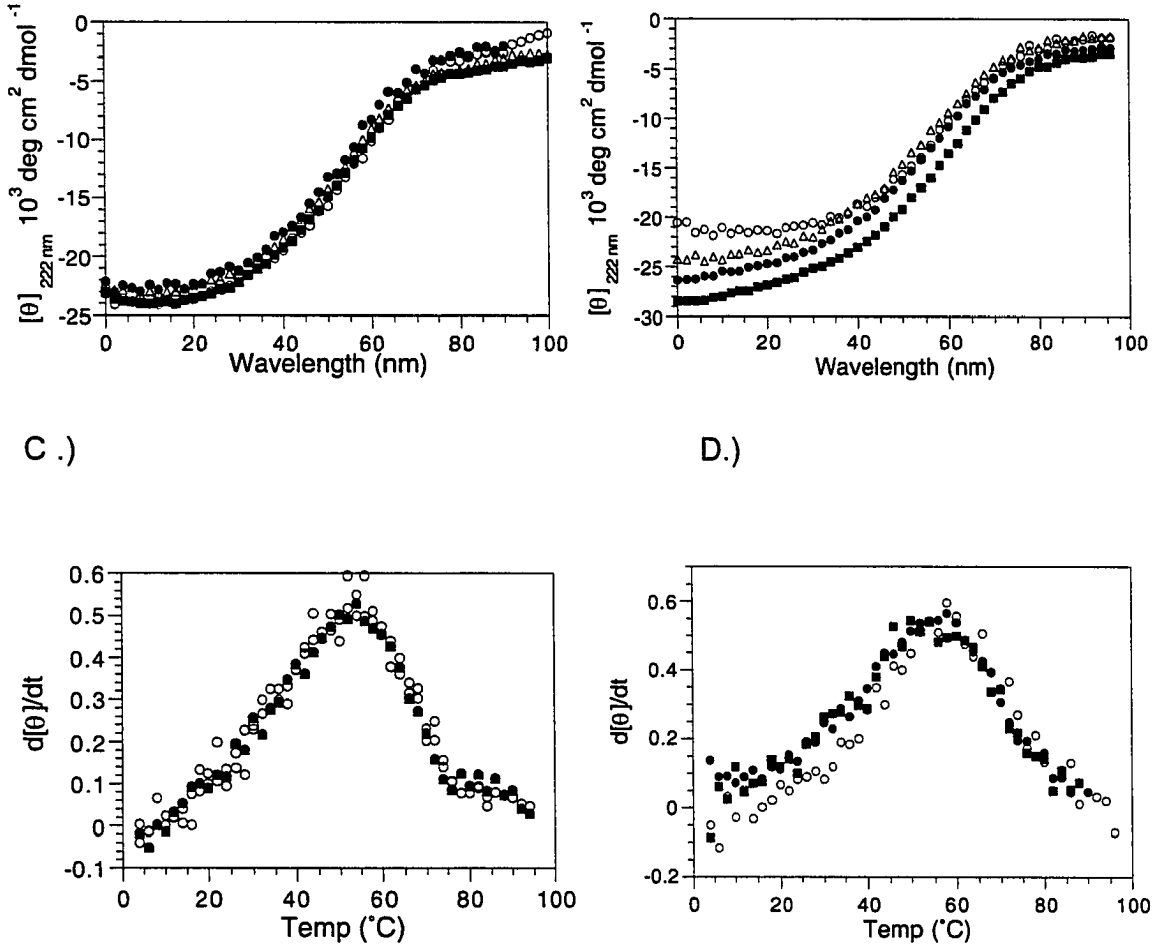

Figure 3.8. ACID-pLL/BASE-pK helix orientation. ACID-pLL/BASE-pK do not have a strong preference for helical orientation as shown by monitoring $[\theta]_{222}$ of (A.) parallel ACID-pLL^N/BASEpK^N and (B.) antiparallel ACID-pLL^C-BASEpK^N with increasing temperature. The T_m of the disulfide-bonded peptides does not change with increasing peptide concentration (O) 5 μM, (●) 10 μM, (Δ) 20 μM, and (■) 30 μM. The T_m was calculated by the derivative of $[\theta]_{222}$ vs. temperature (°C) for (C.) parallel ACID-pLL^N/BASEpK^N and (D.) anti-parallel ACID-pLL^C-BASEpK^N.

3.4.D. Native-like Properties of the ACID-pLL/BASE-pK Heterodimer

Native, globular proteins have sigmoidal unfolding transitions, do not bind ANS, and have a subset of amide protons with hydrogen exchange protection factors comparable to those expected if exchange occurred only from the globally unfolded state. In contrast, molten globules and designed proteins with ill-defined or loosely packed structures exhibit linear thermal unfolding transitions, ANS binding, and low hydrogen exchange protection factors (Kuwajima, 1989; Richardson *et al.*, 1992; Betz *et al.*, 1993).

The predicted protection factor (k_{int}/k_{ex}) when hydrogen exchange occurs only from a globally unfolded protein is $1/f_u$ (Bai *et al.*, 1994). The slowest-exchanging amide protons of native globular proteins often have protection factors comparable to or greater than those expected if exchange occurred from the globally unfolded state (Bai *et al.*, 1994; Lumb & Kim, 1995). This empirical observation forms the basis for using hydrogen exchange as a probe of native-like, globular structure.

The slowest-exchanging amide protons of ACID-pLL/BASE-pK have protection factors of 10^6 (Figure 3.9 and 3.10), which is comparable to the protection factors observed in well-packed proteins and higher than the predicted value of 10^3 if exchange occurred from the globally unfolded state. A higher than predicted protection factor is seen for natural proteins (Bai *et al.*, 1994; Lumb & Kim, 1995) and for other coiled coils based on the ACID/BASE parent sequence with native-

like properties (O'Shea *et al.*, 1993; Lumb & Kim, 1995; Oakley & Kim, 1998; Sia & Kim, 2001). For the ACID/BASE family of peptides with slowly exchanging protons, the higher than predicted protection factor may reflect residual structure in the unfolded state, differences in stability in D_2O and H_2O, or deviations from a strict two-state unfolding mechanism (Bai *et al.*, 1994; Sia & Kim, 2001). The presence of slowly exchanging amide protons in the ACID-pLL/BASE-pK heterodimer suggests the presence of a well-packed hydrophobic core typical of natural, globular proteins.

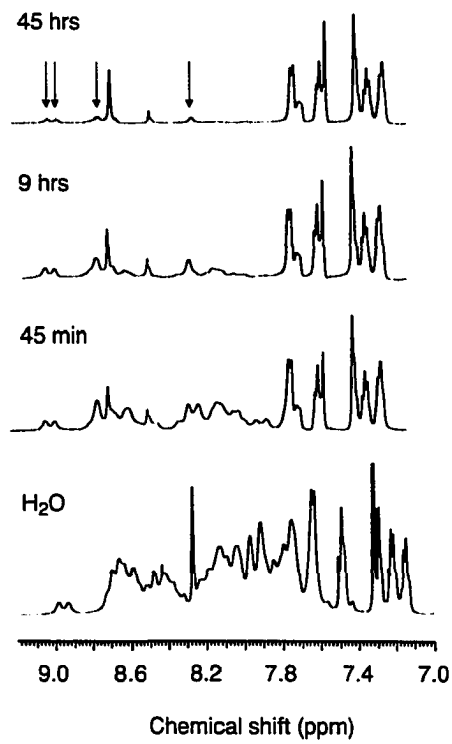

Figure 3.9. ^1H amide hydrogen exchange studies of the ACID-pLL/BASE-pK. One-dimensional spectra are shown of ACID-pLL/BASE-pK in 90% H_2O/10% D_2O and at various time points after dissolution in D_2O. The four most slowly exchanging amide resonances were used to calculate the protection factor and are indicated here with arrows.

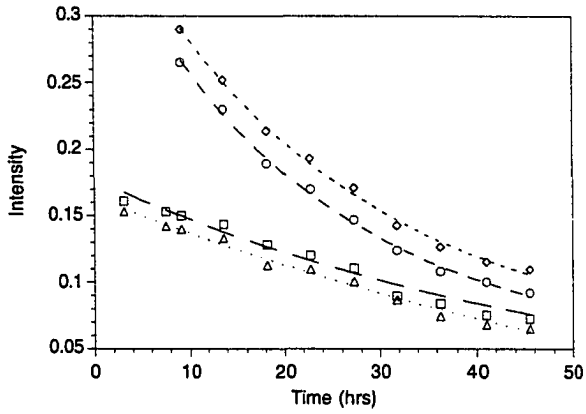

Figure 3.10. ^{1}H amide exchange suggests that ACID-pLL/BASE-pK has a well-packed interior. Fits of the change in amide intensity with time of the four most slowly exchanging amide resonances (indicated with arrows in Figure 3.7) yield protection factors of 10^6, which exceeds the predicted protection factor ($1/f_u$) of 10^3, suggesting the presence of a well-packed interior.

ANS binding to proteins is accompanied by a significant increase in ANS emission intensity and a decrease in emission wavelength from 500 nm to approximately 470 nm (Stryer, 1965). Molten globules and designed proteins that lack structural uniqueness bind ANS, presumably because these proteins are loosely packed (Goto & Fink, 1989; Semisotnov *et al.*, 1991; Handel *et al.*, 1993). Such large changes in ANS fluorescence are induced by the pH 2 molten-globule form of α-lactalbumin, in accord with previous results (Semisotnov *et al.*, 1991). In contrast, minimal changes in ANS fluorescence are induced by the ACID-pLL/BASE-pK heterodimer, indicating that ANS does not bind the heterodimer to an appreciable extent (Figure 3.11).

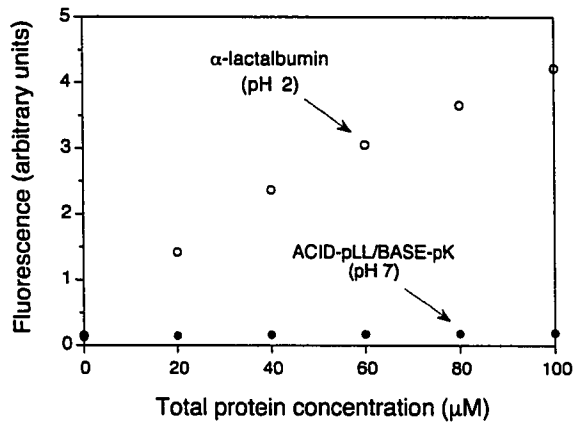

Figure 3.11. Fluorescence studies of ANS binding. The pH 2 α-lactalbumin molten globule induces a significant increase in ANS fluorescence intensity and a shift in the ANS emission maximum form 484 to 470 nm, indicating that the α-lactalbumin molten globule binds ANS in accord with previous results (Semisotnov *et al.*, 1991). In contrast, the ACID-pLL/BASE-pLL heterodimer at pH 7.0 does not induce significant changes in ANS fluorescence, indicating that the heterodimer does not bind to ANS.

The heterodimer lacks structural uniqueness in the sense that there is not a single, preferred orientation of helices. However, the sigmodal thermal and urea unfolding transitions (Figures 3.2 and 3.7), slow hydrogen exchange (Figure 3.9 and 3.10), and lack of ANS binding (Figure 3.11) of the ACID-pLL/BASE-pK heterodimer are consistent with the properties expected of a native protein with a well-defined fold, as opposed to a fluctuating or poorly packed structure reminiscent of the molten globule.

3.5. DISCUSSION

Successful protein design requires a balance of hydrophobic interactions for stability and directional interactions to confer structural uniqueness. Approaches

to imparting structural uniqueness include considerations of core packing and binary patterns of hydrophobic and polar residues (Hill *et al.*, 2000; Moffet & Hecht, 2001). Another approach is the use of buried polar interactions, with the intent of destabilizing conformations that do not satisfy the hydrogen-bonding or salt-bridging potential of polar groups (O'Shea *et al.*, 1993; Betz *et al.*, 1995; Lumb & Kim, 1995; Raleigh *et al.*, 1995; Schneider *et al.*, 1997; Oakley & Kim, 1998).

Asn and Lys at position **a** are the most common buried polar residues in two-stranded natural coiled coils (Berger *et al.*, 1995; Woolfson & Alber, 1995; Walshaw & Woolfson, 2001). The role of position-**a** Asn residues has often been studied. Asn at position **a** strongly promotes dimer formation in both natural and designed coiled coils (O'Shea *et al.*, 1991; Harbury *et al.*, 1993; Potekhin *et al.*, 1994; Betz *et al.*, 1995; Junius *et al.*, 1995; Lumb & Kim, 1995; Wendt *et al.*, 1995; Gonzalez *et al.*, 1996b; Zeng *et al.*, 1997; Wagschal *et al.*, 1999b; Zhu *et al.*, 2000) and imparts structural uniqueness in the designed heterodimeric coiled coil ACID-p1/BASE-p1 (Lumb & Kim, 1995).

Position-**a** Lys residues have received less attention (Gonzalez *et al.*, 1996b; Wagschal *et al.*, 1999b). Lys at position **a** can form an *intra*helical electrostatic interaction with an **e**-position residue of the preceding heptad, as seen in the crystal structure of a parallel GCN4 variant dimer with an **a**-position Lys (Gonzalez *et al.*, 1996b). In this case, the hydrophobic side chain of Lys forms

part of the hydrophobic interface of the coiled coil and the polar ε-amino group forms a polar interaction with the **e**-position polar group. In the context of ACID-pLL/BASE-pK, juxtaposition of the position **a** and **e** Lys residues of BASE-pK is expected to be destabilizing and unfavorable for coiled-coil formation.

Lys at position **a** can form an *inter*helical **g'**→**a** polar interaction with a **g'**-position polar residue of the preceding heptad of the opposing helix in a parallel dimer, as seen in the crystal structures of the Fos-Jun parallel coiled coil (Glover & Harrison, 1995). In an antiparallel dimer, a polar residue such as Lys at position **a** can form an *inter*helical **e'**→**a** polar interaction with a **e'**-position polar residue of the preceding heptad of the opposing helix, as seen in crystal structures of the antiparallel coiled coils of seryl-tRNA synthetase and GreA (Cusack *et al.*, 1990; Stebbins *et al.*, 1995). Interhelical interactions involving Lys at position **a** paired with an appropriate partner at position **e'** or **g'** may therefore offer an alternative route to position-**a** Asn residues for imparting fold specificity in designed coiled coils. Polar **g'-a** interactions involve partially buried position-**a** Lys residues and solvent-accessible **e'** or **g'** side chains on the surface of the coiled-coil interface, and so differ from **a-a'** interactions that are completely buried.

In the context of the ACID/BASE system, Lys at position **a** of BASE-pK has the potential to form an interhelical polar interaction with a position-**g'** Glu of the preceding heptad of the opposing helix of ACID-pLL in the parallel heterodimer (Figure 3.1), and with an **e'**-position Glu in the antiparallel heterodimer. These

are the only stabilizing interactions available to the position-**a** Lys residues of BASE-pK, since formation of intrahelical electrostatic interactions between Lys residues at positions **a** and **e** is expected to be destabilizing. Incorporation of the position-**a** Lys residues in BASE-pK confers both dimerization specificity and a native level of core packing but no preferred orientation of helices to the ACID-pLL/BASE-pK heterodimer.

Various approaches have been used to confer specificity for the antiparallel and parallel orientations of helices, including pairing of position-**a** Asn residues and complementary **g'-e** electrostatic interactions (Oakley & Hollenneck, 2001). The position-**a** Lys residues of BASE-pK can conceivably form both interhelical **g'→a** and **e'→a** interactions in the parallel and antiparallel orientations, respectively (see above), and so it is perhaps not surprising that there is not a strong preference for a single helix orientation under all conditions. Imparting specificity for a single orientation might be attained by placing residues at **e'** or **g'** that form unfavorable interactions with the position-**a** Lys in the unwanted, but not in the desired, orientation.

Buried polar residues typically destabilize coiled coils relative to substitution with hydrophobic residues (Harbury *et al.*, 1993; Potekhin *et al.*, 1994; Betz *et al.*, 1995; Junius *et al.*, 1995; Lumb & Kim, 1995; Wendt *et al.*, 1995; Gonzalez *et al.*, 1996b; Eckert *et al.*, 1998; Suzuki *et al.*, 1999; Wagschal *et al.*, 1999b; Tripet *et al.*, 2000; Zhu *et al.*, 2000; Akey *et al.*, 2001), which reflects the energetic cost of

desolvating a buried polar group (Hendsch & Tidor, 1994). This is seen here also; the ACID-pLL/BASE-pK heterodimer (for which $\Delta G_u° = 11.7 \pm 0.2$ kcal mol^{-1}) is less stable than the ACID-pLL/BASE-pLL heterotetramer [for which $\Delta G_u° =$ 33.3 kcal mol^{-1} (Lumb & Kim, 1995)], and BASE-pK is destabilized relative to BASE-pLL. The ACID-pLL/BASE-pK heterodimer, however, is 1.6 kcal mol^{-1} more stable than the ACID-p1/BASE-p1 heterodimer [for which $\Delta G_u° = 10.1$ kcal mol^{-1} (O'Shea *et al.*, 1993)]. The position-**a** Lys residues therefore impart dimerization specificity and native-like levels of structural uniqueness at the expense of stability, compared to substitution with the hydrophobic residue Leu, but with a lower energetic penalty than incurred with two buried position-**a** Asn residues. This likely reflects a smaller desolvation penalty for the surface-exposed Lys and Glu side chains than for the completely buried Asn side chains.

Buried polar interactions occur frequently in natural proteins and are expected to destabilize conformations in which the buried polar groups are not involved in hydrogen bonds or salt brides (Barlow & Thornton, 1983; Rashin & Honig, 1984). Buried polar groups apparently do not contribute to structural uniqueness in an SH2 domain and Arc repressor (Waldburger *et al.*, 1995; Maxwell & Davidson, 1998). Buried polar interactions do, however, impart conformational specificity in natural and designed coiled coils (Harbury *et al.*, 1993; Lumb & Kim, 1995; Gonzalez *et al.*, 1996b; Oakley & Kim, 1998), designed helical bundles (Hill *et al.*, 2000) and the globular protein thioredoxin (Bolon & Mayo, 2001). These results, together with the findings reported here, support the notion that directional polar

interactions can contribute in a defining way to protein folding and structural uniqueness.

In conclusion, complementary interactions between buried polar groups, which lack a buried polar interaction partner, and surface polar groups can impart native levels of structural uniqueness to protein folding and design with a smaller energetic penalty than incurred through the use of a completely buried polar interaction. The application of buried-surface electrostatic interactions provides an alternative route to the established role of buried polar interactions for introducing organization and specificity to protein design.

Chapter 4

Intrinsic Structural Disorder of the C-Terminal Domain from the bZIP Transcription Factor Fos

This chapter describes work published in *Biochemistry* (Campbell *et al.*, 2000a) and represents a collaboration with Drs. Paul Laybourn and Andrea Terrell, who performed the transcription assays (Figure 4.2). Experimental detail and analysis have been expanded beyond that reported in the paper.

4.1. ABSTRACT

The bZIP proto-oncoprotein c-Fos activates transcription of a wide variety of genes involved in cell growth. The C-terminal activation domain of c-Fos is functionally independent of the remainder of the protein. Fos-AD corresponds to the C-terminal activation domain of human c-Fos (residues 216-380). Fos-AD suppresses (squelches) transcription *in vitro*, as expected for a functional activation domain lacking a DNA-binding domain. Fos-AD is unstructured and highly mobile, as demonstrated by CD spectra indicative of unfolded proteins, a lack of ^{1}H chemical-shift dispersion, and negative ^{1}H-^{15}N heteronuclear NOE intensities. The hydrodynamic properties of Fos-AD are also consistent with an extended structure. We conclude that the C-terminal domain of human c-Fos is biologically active yet intrinsically disordered. Our results suggest that conformational disorder is an integral aspect of the diverse contributions to transcriptional regulation by c-Fos.

4.2. INTRODUCTION

The enzymatic synthesis of protein-coding RNA is performed in eukaryotes by a large protein complex called RNA polymerase II (Orphanides *et al.*, 1996; Lemon & Tjian, 2000). Although assembly of RNA polymerase II and the general transcription factors at the promoter is sufficient for transcription at basal levels *in vitro*, transcription at elevated levels requires DNA-binding transcriptional activator proteins. Activators may enhance various steps in transcription, such as assembly of the polymerase II preinitiation complex at the promoter, clearance, and elongation (Orphanides *et al.*, 1996). Moreover, activators may be generally required *in vivo* to overcome the repressive effects of chromatin and suppresser proteins and for competitive recruitment of general transcription factors (Orphanides *et al.*, 1996; Lemon & Tjian, 2000).

Members of the Fos family of mitogen-inducible transcriptional activators dimerize with the Jun or ATF/CREB activators to form the transcriptional regulator AP-1 (Curran & Morgan, 1995; Karin *et al.*, 1997). AP-1 activates transcription of genes involved in a diverse range of biological processes, including cell proliferation, differentiation, neuronal development, and apoptosis (Curran & Morgan, 1995; Karin *et al.*, 1997). The Fos proteins have a strong oncogenic potential, especially when transduced by retroviruses (Ransone & Verma, 1990; Curran & Vogt, 1992), and provide a model system to understand the mechanism of transcriptional activation using molecular biology and genetic approaches (Lech *et al.*, 1988; Wilson & Treisman, 1988; Ofir *et al.*, 1990; Abate

et al., 1991; Sutherland *et al.*, 1992; Wisdom & Verma, 1993; Metz *et al.*, 1994; Bannister & Kouzarides, 1995; Chen *et al.*, 1996; Funk *et al.*, 1997; McBride & Nemer, 1998; Zhang *et al.*, 1998).

Human c-Fos has a modular structure consisting of an N-terminal activation domain, a bZIP dimerization/DNA-binding domain, and a C-terminal domain (Figure 4.1). The C-terminal domain of c-Fos contains both acidic and proline-rich activation domains (Abate *et al.*, 1991) and is functionally independent of the rest of the molecule. For example, the C-terminal domain activates transcription when the bZIP domain is replaced with the LexA DNA-binding domain (Funk *et al.*, 1997) and when the N-terminal domain is deleted (Abate *et al.*, 1991).

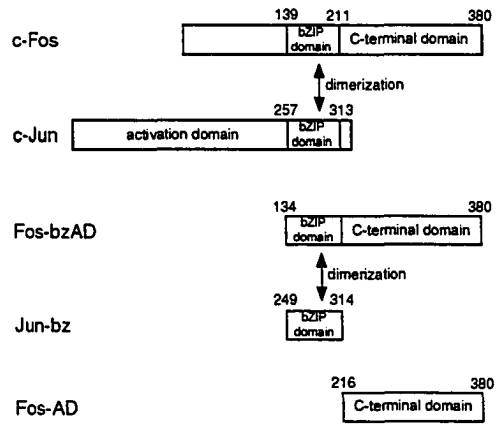

Figure 4.1. Schematic of human c-Fos and human c-Jun. The leucine zipper of the bZIP domain of c-Fos moderates dimerization with c-Jun (Siegel & Monty, 1966) and the basic region of the bZIP domain binds DNA (Curran & Vogt, 1992). The N- and C- terminal domains of c-Fos activate transcription (Abate *et al.*, 1991).

Several transcriptionally important protein-protein interactions involving c-Fos are mediated by the C-terminal domain. In particular, the C-terminal domain

interacts with TBP, a central component of the general transcription factor TFIID, the acetyltransferase and coactivator CBP, and the regulatory transcription factor Smad3 (Metz *et al.*, 1994; Bannister & Kouzarides, 1995; Zhang *et al.*, 1998). In addition, regions of the C-terminal domain that participate in activation have been mapped in several deletion and mutagenesis studies and regulatory effects of phosphorylation of the C-terminal domain have been described (Lech *et al.*, 1988; Wilson & Treisman, 1988; Ofir *et al.*, 1990; Abate *et al.*, 1991; Sutherland *et al.*, 1992; Wisdom & Verma, 1993; Metz *et al.*, 1994; Bannister & Kouzarides, 1995; Chen *et al.*, 1996; Funk *et al.*, 1997; McBride & Nemer, 1998; Zhang *et al.*, 1998).

While the C-terminal domain of Fos has been extensively characterized using molecular biology techniques, the domain has yet to be defined in structural terms. We show here that the C-terminal activation domain of human c-Fos (residues 216-380; Figure 4.1), although functionally active, is essentially devoid of the stable helical or β-sheet structure typical of globular proteins. We conclude that c-Fos contains an intrinsically disordered yet biologically active activation domain.

4.3. METHODS

4.3.A. Expression and Purification of Fos-bzAD

Fos-bzAD corresponds to residues 134-380 of human c-Fos *i.e.*, the bZIP dimerization and DNA-binding domain and the C-terminal activation domain

(Figure 4.1). A pET-11a vector, encoding residues 134-380 of the natural human c-Fos gene sequence, did not express in *Escherichia coli* strain BL21(DE3) or BL21 (DE3) pLysS. The problem was overcome by constructing a plasmid (pFos 134-380) with optimized codon usage in the bZIP domain [cf. the approach of Abate *et al.* (1991) for expressing rat c-Fos]. Two PCR products encoding residues 134-205 of human c-Fos, amplified from a plasmid encoding the bZIP domain of human c-Fos with codon usage optimized for *Escherichia coli* (pFF70, gift of P.S. Kim), and residues 206-380 of human c-Fos, amplified from pGEX2TKN-hcfos (gift of J. A. Goodrich) were ligated between the *Nde* I and *Bam* HI sites of pET-15b. DNA sequences were confirmed with dRhodamine sequencing (Colorado State University Molecular Resources Facility).

Fos-bzAD was expressed using the T7 system (Studier *et al.*, 1990) as an N-terminal His-tag fusion protein and purified with Ni-affinity chromatography (Novagen) and HPLC. Fos-bzAD were expressed in *Escherichia coli* strain BL21 (DE3) grown in LB at 37 °C to an optical density of 0.6 and induced with 0.5 mM IPTG at 37 °C for 3 hours. The cells were harvested by centrifugation, resuspended in 50 ml His-Bind buffer (5 mM imidazole, 500 mM NaCl, 1 mM PMSF, 20 mM Tris-HCl, pH 7.9) and lysed by sonication. The cell lysate was centrifuged. The soluble fraction was filtered (0.45 μM filter) and loaded onto a 10 ml His-bind column (Novagen 70666) charged with 50 mM $NiSO_4$ and equilibrated in His-bind buffer (5 mM imidazole, 500 mM NaCl, 20 mM Tris-HCl, pH 7.9). The column was washed with 100 ml His-bind buffer and 50 ml His-

wash buffer (60 mM imidazole, 500 mM NaCl, 20 mM Tris-HCl, pH 7.9). Fos-bzAD was eluted from the column with 1 M imidazole, 500 mM NaCl, 20 mM Tris-HCl, pH 7.9. The eluted fraction was dialysed for 4 hours against 4 L of thrombin cleavage buffer (150 mM NaCl, 2.5 mM $CaCl_2$, 20 mM Tris-HCl, pH 8.4). The His-tag sequence was cleaved with 15 units of thrombin (Novagen 69671) for 16 hours at 25 °C. The proteolyzed product was passed over a 10 ml His-bind column to remove uncleaved fusion protein and the His-tag. 1 mM EDTA and 10 mM DTT were added and final purification of Fos-bzAD was by reverse-phase C_4 HPLC using 0.1%/min linear acetonitrile/water gradients containing 1% v/v trifluoroacetic acid. Fos-bzAD has three additional N-terminal amino acids (Gly-Ser-His) derived from the His-tag sequence. The identity of Fos-bzAD was confirmed with MALDI mass spectrometry (Colorado State University Macromolecular Resources Facility), with the expected and observed masses agreeing to within 1 Da. The final protein yield of Fosbz-AD was approximately 0.5 mg/ L of LB culture.

4.3.B. Expression and Purification of Fos-AD

Fos-AD corresponds to residues 216-380 of human c-Fos, *i.e.*, the C-terminal activation domain (Figure 4.1). The plasmid for Fos-AD was constructed by ligating a PCR product encoding residues 216-380 of human c-Fos amplified from pGEX2TKN-hcfos (gift of J.A. Goodrich) between the *Nde* I and *Bam* HI sites of pET-15b. DNA sequences were confirmed with dRhodamine sequencing (Colorado State University Molecular Resources Facility). Fos-AD was

expressed and purified in the same way as Fos-bzAD. Fos-AD has three additional N-terminal amino acids (Gly-Ser-His) derived from the His-tag sequence. The identity of Fos-AD was confirmed with N-terminal sequencing and MALDI mass spectrometry (Colorado State Macromolecular Resources Facility), with the expected and observed masses agreeing to within 1 Da. Final Fos-AD protein yield was approximately 1 mg/ L of LB culture.

Uniformly ^{15}N labeled Fos-AD was expressed in M9 minimal medium supplemented with thiamine (McIntosh and Dalhquist, 1990), containing 1g/L $^{15}NH_4(SO_4)_2$ as the sole nitrogen source. ^{15}N-labeled Fos-AD was purified using the same protocol as above and gave comparable yields.

4.3.C. Expression and Purification of Jun-bz

Jun-bz corresponds to residues 249-314 of human c-Jun with an additional N-terminal Met and C-terminal Tyr-Gly-Gly-Cys (Figure 4.1). Jun-bz was expressed using the T7 expression plasmid pJJ70 (gift of P. S. Kim). *Escherichia coli* strain BL21 (DE3) pLysS transformed with pJJ70 was incubated at 37 °C until the optical density reached 0.6 at 600 nm. The cells were then induced with 1 mM IPTG at 37 °C for three hours. The cells were resuspended in 1 mM EDTA, 1 mM DTT, 20 mM Tris-HCl, pH 8, lysed by sonication and centrifuged. The soluble fraction was filtered (0.45 μM) and loaded on a Q Sepharose column (Pharmacia 17-1153-05) equilibrated in 1 mM EDTA, 1 mM DTT, 20 mM TRIS-HCl, pH 8. Jun-bz flowed through this column and was

loaded on a SP Sepharose column (Pharmacia 17-0406-05). Jun-bz also flowed through this column. Final purification was by reverse phase C_{18} HPLC, using linear 0.1%/minute acetonitrile/water gradients, containing 1% v/v trifluroaceticacid. Jun-bz is easily oxidized and must be kept in ≥ 1 mM fresh-DTT.

4.3.D. Transcription Assays

Transcription assays were performed by Drs. Andrea R. Terrell and Paul J. Laybourn in *Saccharomyces cerevisiae* whole-cell extract from strain BJ926 with a template [pS(GCN4)2CG$^-$] containing a G-less transcript under control of two AP-1 (Gcn4p) sites (gift of R. D. Kornberg), as described in Campbell *et al.* (2000a). Reactions were performed three times with reproducible results.

4.3.E. CD Spectroscopy

CD spectroscopy was performed with a Jasco J720 spectrometer. Samples were prepared in 10 mM sodium phosphate, 0-1 M NaCl, 1 mM DTT, pH 7.0, and contained 10 μM protein. Protein concentrations for FosA-D, Fos-bzAD, and Jun-bz were determined by absorbance in 6 M GuHCl, 10 mM sodium phosphate, pH 6.5 at 25 °C using extinction coefficients at 280 nm of 9530 M^{-1} cm^{-1}, 9530 M^{-1} cm^{-1}, and 1280 M^{-1} cm^{-1} respectively (Edelhoch, 1967). Helix content was estimated from $f_H = -([\theta]_{222}/30{,}300 + 2340/30{,}300)$ where f_H is fraction of helix (Chen *et al.*, 1972).

4.3.F. NMR Spectroscopy

NMR spectroscopy was performed with a Varian Unity Inova spectrometer operating at 500.1 MHz for ^{1}H. Samples were prepared in 10 mM sodium phosphate, 150 mM NaCl, 1 mM d_{10}-DTT, and 10% (v/v) D_2O, pH 6.5. Homonuclear ^{1}H experiments were performed on 0.35 mM Fos-AD. Heteronuclear ^{1}H-^{15}N experiments were performed on 90 μM or 0.93 mM ^{15}N-labeled Fos-AD. Data were collected at 25 °C using States phase-TTPI discrimination in the indirectly detected dimension. The water resonance was suppressed using gradient techniques rather than solvent presaturation to minimize cross saturation of the amide N^{H} protons. ^{1}H chemical shifts were referenced with internal DSS at zero ppm (Wishart *et al.*, 1995). Magic-angle-gradient DQF-COSY spectra (van Zijl *et al.*, 1995) consisted of 256 complex increments defined by 16 transients. Sensitivity-enhanced gradient HSQC spectra (Kay *et al.*, 1992) consisted of 256 complex increments defined by 24 (0.93 mM Fos-AD) or 96 (90 μM Fos-AD) transients. Steady-state ^{1}H-^{15}N NOE values were measured at 25 °C from 2D ^{1}H-^{15}N NOE correlation spectra (Farrow *et al.*, 1994). Spectra were recorded with and without a 3 s ^{1}H saturation period using relaxation delays of 5 s and 8 s, respectively, and consisted of 128 complex increments defined by 24 transients.

4.3.G. Sedimentation Equilibrium

Sedimentation equilibrium was performed at 25 °C with a Beckman XL-A analytical ultracentrifuge at the University of Colorado Health Sciences Center.

Samples were dialyzed against the reference buffer (10 mM sodium phosphate, 150 mM NaCl, 1 mM DTT, pH 7.0) for at least 12 hours. Initial loading concentrations of 26, 52 and 87 μM were used. Data were collected at 30 and 40 krpm using 12 mm pathlength six-sector centerpieces and an An-60Ti rotor. Data were analyzed with ORIGIN (Beckman Instruments). Discrimination between different models (*i.e.*, ideal versus nonideal single species) was based on the distribution of residuals. The solvent density of 1.0 was measured directly and the partial specific volume of 0.724 cm^3/g was calculated as described elsewhere (Laue *et al.*, 1992).

4.3.H. Determination of the Stokes Radius of Fos-AD

The Stokes' radius of Fos-AD was determined with gel filtration (Siegel & Monty, 1966). A Sephacryl S-100 column equilibrated in 10 mM sodium phosphate, 150 mM NaCl, 1 mM DTT, pH 7 was used at a flow rate of 0.2 ml/min. The column was calibrated with 0.5 mg bovine ribonuclease A, bovine chymotrypsinogen A, hen ovalbumin and bovine serum albumin, which have Stokes' radii of 16.4 Å, 20.9 Å, 30.5 Å, 35.5 Å, respectively, and with Blue Dextran 2000 to determine the void volume. Protein elution was monitored by UV at 230 nm. The elution volume of the standards (in ml) was used to plot $[-\log(K_{AV})]^{1/2}$ vs. Stokes' radius, with $K_{AV}= (v_e - v_o)/ (v_t - v_o)$, where v_e is the elution volume, v_o is the void volume of the column, and v_t is the total column volume. This plot resulted in a straight line, which could be fit to the equation y = 0.022728(x) + 0.25059. The Stokes'

radius of Fos-AD (0.3 mg) was estimated using this equation where x is the Stokes' radius and $y = [-\log(K_{AV})]^{1/2}$.

4.4. RESULTS AND DISCUSION

4.4.A. Transcriptional Activity of Fos-AD

Since transcriptional activators must bind to regulatory DNA elements to function efficiently (Ptashne, 1988) it is generally not possible to assay directly transcriptional activation by an activation domain lacking a DNA-binding domain. However, a functional activation domain lacking a DNA-binding domain would be expected to suppress (squelch) transcription by sequestering target transcription factors, making them unavailable to participate in transcription (Ptashne, 1988).

A yeast-based transcription assay for c-Fos activity at an AP-1 promoter was used, since human c-Fos activates transcription in yeast (Lech *et al.*, 1988). To show that the yeast extract was responsive to transcriptional activation by the human c-Fos C-terminal domain, we used an N-terminal deletion mutant of human c-Fos corresponding to the bZIP DNA-binding domain and C-terminal activation domain (called Fos-bzAD; Figure 4.1). Fos-bzAD activates transcription from an AP-1 regulated promoter when paired with Jun-bz (a peptide corresponding to the human c-Jun bZIP domain; Figure 4.1), in accord with previous studies (Abate *et al.*, 1991). Jun-bz lacks an activation domain, and actually suppresses transcription in the absence of Fos-bzAD (Figure 4.2). Suppression by Jun-bz presumably occurs because the c-Jun bZIP domain can

form a stable homodimer (O'Shea *et al.*, 1989b) that competes with endogenous AP-1 activity for DNA-binding sites. The suppression by Jun-bz indicates that transcriptional activation by Fos-bzAD/Jun-bz is not due to Jun-bz alone. Thus, the c-Fos C-terminal domain can activate transcription in the assay when bound to DNA.

In contrast to Fos-bzAD/Jun-bz, Fos-AD suppresses transcription of an AP-1-regulated gene (Figure 4.2), as expected for a functional activation domain lacking a DNA-binding domain (Ptashne, 1988). We conclude that Fos-AD is functional for interactions with the target transcription factors of c-Fos in a biological context.

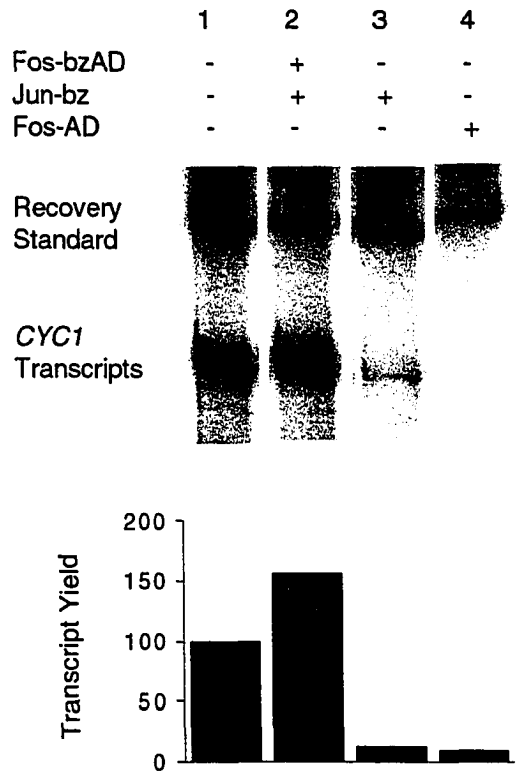

FIGURE 4.2. Transcriptional activity at an AP-1 promoter in yeast whole-cell extract. The extract contains endogenous AP-1 activity (*i.e.*, Gcn4p) responsible for the intrinsic transcription of a 350-nucleotide gene product under control of the AP-1 site (lane 1). The presence of several bands indicates multiple start sites. Fos-bzAD paired with Jun-bz activates transcription (lane 2). Jun-bz alone suppresses transcription (lane 3). Fos-AD suppresses (squelches) transcription (lane 4). Results are shown for 40 nM Jun-bz/Fos-bzAD (lane 2), 50 nM Jun-bz (lane 3) or 50 nM Fos-AD (lane 4). The bar chart illustrates the average of three independent experiments.

4.4.B. Structural and Dynamic Properties of Fos-AD

CD provides information on protein secondary structure. The CD spectrum of Fos-bzAD at neutral pH exhibits a strong negative band at 202 nm (Fig. 4.3), indicative of a disordered conformation (Woody, 1992). The shoulder centered at 220 nm likely reflects both the disordered conformation indicated by the negative

band at 202 nm and formation of the helical c-Fos leucine zipper, since the CD studies are performed at a protein concentration (10μM) above the c-Fos leucine-zipper dissociation constant. The value of $[\theta]_{222}$ observed for Fos-bzAD corresponds to an estimated helix content of 8%, which is comparable to the expected helix content of 10% due to folding of the c-Fos leucine zipper, since 78 residues of the leucine zipper domain of a total of 246 residues of Fos-bzAD would adopt a helical structure. Thus the CD spectrum of Fos-bzAD is consistent with helix formation by the c-Fos leucine zipper, with the remainder of Fos-bzAD being largely disordered.

Since DNA binding by c-Fos requires dimerization with the bZIP domain of Jun, CD spectra of the Fos-bzAD-Junbz complex were collected, to rule out the possibility of a large conformational change in Fos-bzAD upon Jun-bz binding. The CD spectrum of the Fos-bzAD-Jun-bZIP complex contains a strong negative band at 205 nm (Figure 4.3), indicative of a disordered conformation (Woody, 1992). The negative contribution at 222 nm reflects formation of the c-Fos/c-Jun leucine zipper (O'Shea *et al.*, 1989b). The value of $[\theta]_{222}$ observed for Fos-bzAD/Jun-bZIP corresponds to an estimated helix content of 24%, which compares with the expected value of 25% for complete formation of the 78-residue c-Fos/c-Jun leucine zipper (Glover & Harrison, 1995). Thus, the CD spectrum of the Fos-bzAD-Jun-bZIP complex is consistent with helix formation by the c-Fos/c-Jun leucine zipper, with the remainder of Fos-bzAD being largely disordered. In addition, the CD spectrum of the Fos-bzAD/Jun-bZIP complex

rules out the possibility of a large-scale conformational change induced in the c-Fos C-terminal domain on formation of the complex.

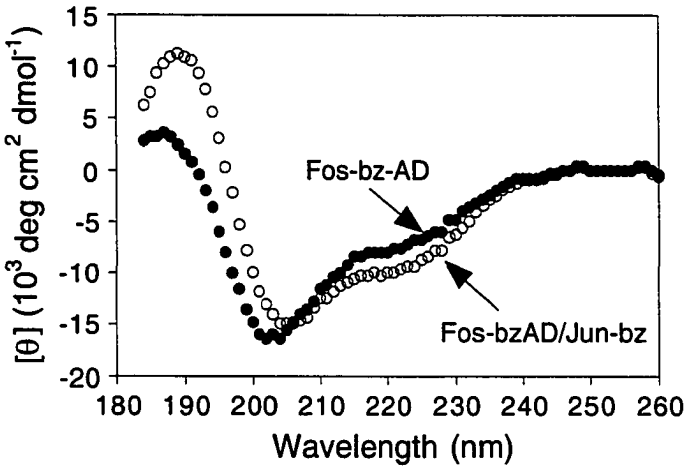

Figure 4.3. CD spectrum of Fos-bzAD and the Fos-bzAD/Jun-bZIP complex.

The CD spectrum of Fos-AD at neutral pH lacks the spectral features in the far-UV region that are characteristic of significant helical or β-sheet secondary structure (Figure 4.4). Instead, the spectrum contains a negative band at 198 nm and a shoulder centered at 220 nm (above 5 °C), which are indicative of a disordered conformation (Woody, 1992). Changes with temperature in the CD spectrum of Fos-AD are linear up to at least 80 °C (Figure 4.4), which is also characteristic of an unfolded protein. In addition, the increase in negative ellipticity at 222 nm with temperature is often observed in peptides with extended or disordered conformations (Woody, 1992).

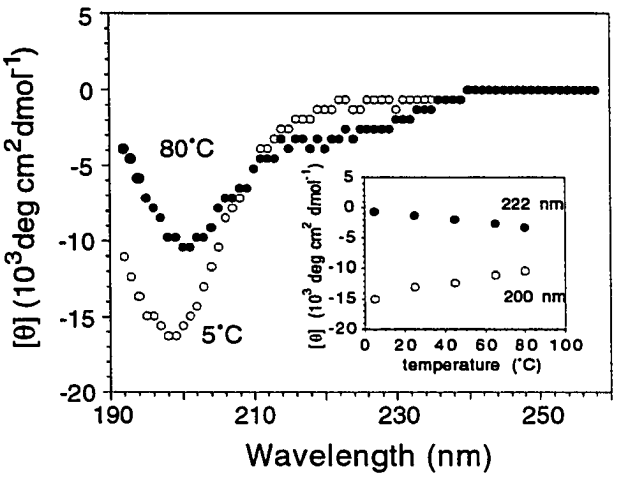

FIGURE 4.4. CD spectra of Fos-AD. The CD spectra at 5 °C and 80 °C are characteristic of an unfolded protein. Changes in the CD spectrum with temperature are linear (insert), indicating that any structure formation is not cooperative.

The CD spectrum of Fos-AD is independent of pH in the range 2 to 8 (Figure 4.5; except at pH 4, where Fos-AD is insoluble). Helical or β-sheet structure is not induced in Fos-AD by changes in pH, in contrast to the behavior of some peptide fragments of activation domains (Van Hoy *et al.*, 1993). Thus, the CD data indicate a lack of stable, cooperatively folded helical or β-sheet structure in Fos-AD.

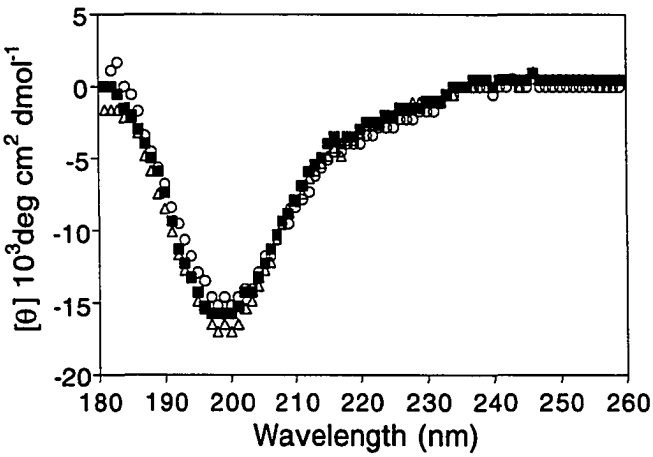

Figure 4.5. CD spectra of Fos-AD is independent of pH. Spectra are similar at pH 2 (O), pH6 (Δ) and pH 8 (■).

The ^{1}H chemical-shift provides information on secondary and tertiary structure formation in proteins (Wishart & Sykes, 1994). ^{1}H chemical shifts of Fos-AD were obtained from DQF-COSY and ^{1}H-^{15}N HSQC spectra. The H^{N} chemical shifts fall between 7.6 and 8.5 ppm and the H^{α} chemical shifts fall between 3.8 and 4.7 ppm in DQF COSY spectra (Figure 4.6). The ^{1}H chemical shifts of Fos-AD are within the chemical shift ranges expected for unfolded proteins (Wishart & Sykes, 1994). The chemical shift analysis is limited by ^{1}H chemical-shift degeneracy and cannot rule out formation of marginally stable secondary structure that exists in fast exchange on the chemical-shift timescale with a random-coil conformation. Nonetheless, the chemical-shift data suggest strongly that Fos-AD lacks stable secondary and tertiary structure typical of globular proteins.

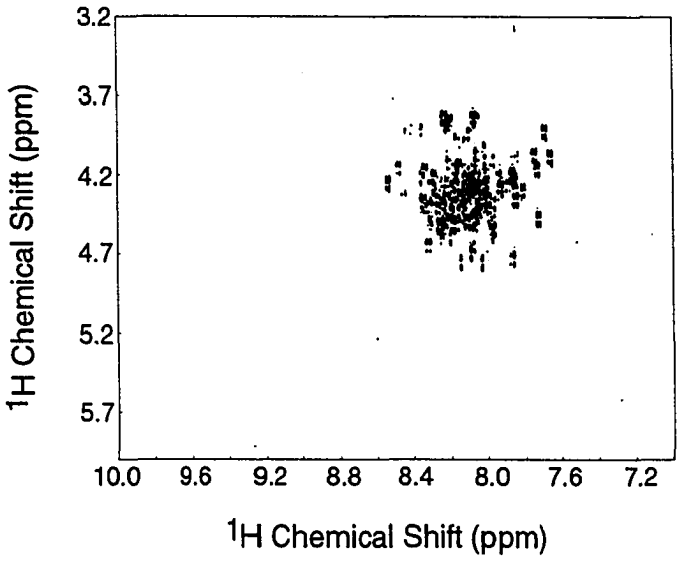

Figure 4.6. DQF COSY spectrum of Fos-AD lacks chemical shift dispersion. The H^{α} chemical shifts fall between 3.8 and 4.7 ppm and the H^{N} chemical shifts fall between 7.6 and 8.5 ppm.

The heteronuclear ^{1}H-^{15}N NOE provides information on mainchain flexibility. In particular, ^{1}H-^{15}N NOEs are positive in folded, globular proteins and reduced or negative in unfolded and disordered proteins (Cho *et al.*, 1996; Donne *et al.*, 1997; Farrow *et al.*, 1997; Sem *et al.*, 1997; Penkett *et al.*, 1998). The ^{1}H-^{15}N HSQC spectrum of Fos-AD is expected to contain 147 amide ^{1}H-^{15}N correlations (168 residues minus Gly 1 and 20 prolines). The HSQC spectrum of Fos-AD at pH 6.5 contains 95 completely resolved crosspeaks and numerous partially resolved or overlapped resonances (Figure 4.7). The ^{1}H-^{15}N NOE was measured for each completely resolved crosspeak. In all cases, the ^{1}H-^{15}N NOE was negative (Figure 4.8), ranging from -0.86 to -3.4. In addition, the bulk NOE of the partially resolved or degenerate crosspeaks was negative in all cases,

ranging from -1.3 to - 2.1 (Figure 4.8). This result indicates that the Fos-AD mainchain is flexible, with motion on a timescale characteristic of unfolded proteins.

^{1}H-^{15}N HSQC spectra of Fos-AD were essentially identical at concentrations of 0.93 mM (where the ^{1}H-^{15}N NOE measurements were performed) and at 90 μM ruling out concentration-dependent effects on the NMR spectra of Fos-AD.

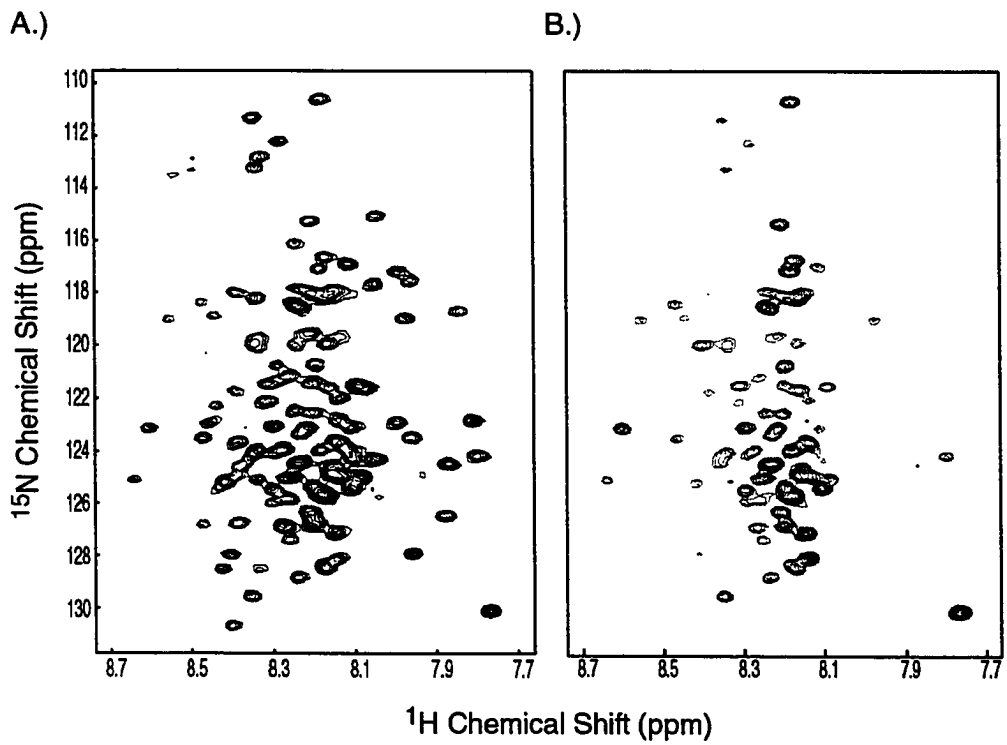

Figure 4.7. HSQC spectra for ^{15}N Fos-AD. Spectra shown are both without (A.) and with (B.) a 3 s proton saturation.

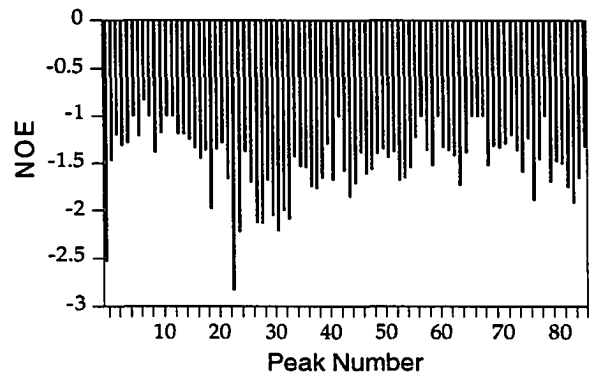

Figure 4.8. ^{1}H-^{15}N NOE intensities of Fos-AD. ^{1}H-^{15}N NOE intensities were calculated for the well-resolved crosspeaks with $NOE=I-I_o/I_o$, where I is the crosspeak intensity with ^{1}H saturation and I_o is the intensity without ^{1}H saturation. Peaks are numbered in order of increasing chemical shift.

A global property of Fos-AD is the Stokes' radius, which reflects compactness. An apparent Stokes' radius of 35 Å for Fos-AD was obtained with gel filtration (Figure 4.9). Given that Fos-AD has a dynamic structure, as indicated by the ^{1}H-^{15}N NOE measurements, the observed Stokes' radius of Fos-AD should be considered an average value of the ensemble of the structures accessible to Fos-AD. Sedimentation equilibrium indicates that Fos-AD is monomeric (Figure 4.10), and the expected Stokes' radius for a globular protein with this molecular weight is 17 Å (Siegel & Monty, 1966). Fos-AD therefore has a Stokes' radius that is twice the size expected for a compact globular fold, consistent with the properties expected of an unfolded protein.

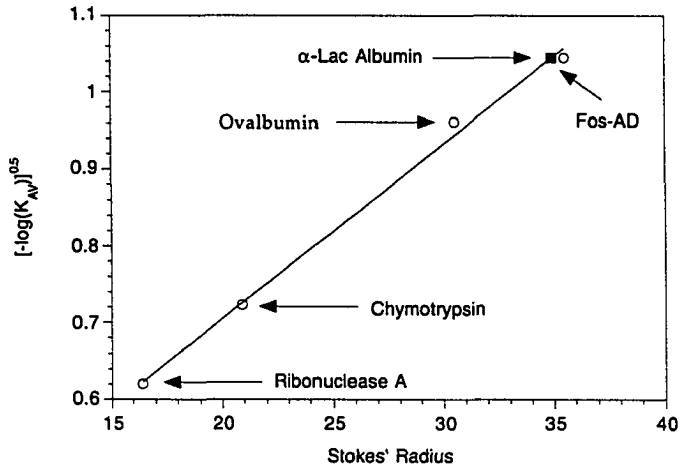

Figure 4.9. Stokes' radius of Fos-AD was determined by gel-filtration. The column was equilibrated with ribonuclease A, bovine chymotrypsinogen A, hen ovalbumin and bovine serium albumin.

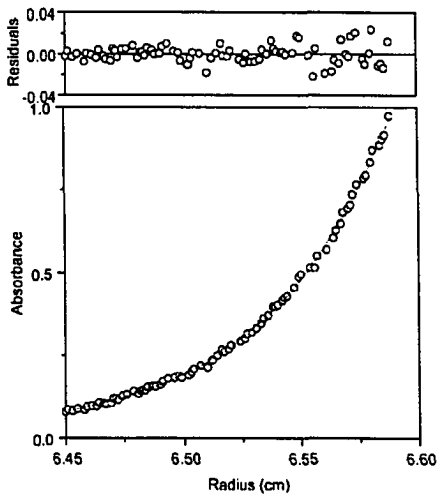

Figure 4.10. Sedimentation equilibrium data for Fos-AD. The data fit to single-species, non-ideal model, as indicated by the random distribution of residuals, with a mass expected of a monomer (expected 17.61 kDa; observed 17.59 ± 0.23 kDa). The data shown span a concentration range of approximately 9 to 90 μM.

The spectroscopic and hydrodynamic data collectively indicate that Fos-AD lacks stable helical and β-sheet structure, has an extended conformation and is monomeric. The data cannot rule out the formation of β-turn structure (Dyson & Wright, 1996) or hydrophobic clusters (Neri *et al.*, 1992; Lumb & Kim, 1994). However, the negative amide ^{1}H-^{15}N NOEs indicate that the mainchain of Fos-AD is highly flexible and exists in a motional regime expected of an unfolded protein. We conclude that human c-Fos contains a biologically active yet intrinsically disordered domain.

4.4.C. Implications for Fos function

Biological activity and molecular recognition often result from well-defined structures that place functional groups in key positions to interact with and discriminate between other molecules. Globular proteins, for example, typically lose biological activity when unfolded. However, a combination of biophysical probes collectively indicate that the biologically active acidic and proline-rich C-terminal activation domain of human c-Fos is structurally disordered, with properties reminiscent of an unfolded protein. The entire activation domain was used, and so the disorder is not due to deletion of sequence required for structure. Structural disorder has also been observed for the full-length acidic activation domains from VP16, NF-κB, and p53 (O'Hare & Williams, 1992; Schmitz *et al.*, 1994; Chang *et al.*, 1995) as well as peptide fragments of other acidic activation domains at neutral pH (Van Hoy *et al.*, 1993; Dahlman-Wright *et al.*, 1995). Our findings, along with results for the p53 proline-rich activation

domain (Chang *et al.*, 1995), also indicate that proline-rich activation domains can exhibit structural disorder.

Several mechanistic advantages to using disordered protein domains have been proposed, including increased binding specificity at the expense of thermodynamic stability, regulation by proteolysis, and the ability to recognize a range of different proteins (Frankel & Kim, 1991; Kriwacki *et al.*, 1996; Penkett *et al.*, 1997). The C-terminal activation domain of c-Fos interacts directly with the transcription factors TBP, CBP and Smad3 (Metz *et al.*, 1994; Bannister & Kouzarides, 1995; Zhang *et al.*, 1998), and activates transcription in a diverse range of cellular processes (Curran & Morgan, 1995; Karin *et al.*, 1997). In addition, the c-Fos C-terminal domain contains a number of phosphorylation sites that moderate Fos activity (Wilson & Treisman, 1988; Ofir *et al.*, 1990; Chen *et al.*, 1996). The structural requirements for Fos phosphorylation and for interactions of Fos with other transcription factors may well be different, as proposed for the intrinsically disordered KID activation domain of CREB (Radhakrishnan *et al.*, 1997; Hua *et al.*, 1998). Our results raise the intriguing possibility that the conformational freedom of the structurally disordered C-terminal activation domain contributes to the functional diversity of c-Fos by permitting formation of a greater variety of protein complexes, both with other transcription factors and with regulatory kinases, than could be achieved with a single, pre-defined structure.

Chapter 5

Reevaluation of Transcriptional Regulation by TATA-Binding Protein Oligomerization: Predominance of Monomers

This chapter describes work published in *Biochemistry* (Campbell *et al.*, 2000b). This work represents a collaboration with Drs. Ryan Ranallo and Laurie Stargell, who performed the DNA-binding assays and the immunoprecipitations (Figures 5.4 and 5.8). Experimental detail and analysis have been expanded beyond that reported in the paper.

5.1. ABSTRACT

The TATA-binding protein (TBP) plays an important role in transcriptional initiation by all three nuclear RNA polymerases. TBP contains a conserved C-terminal domain (cTBP) that binds DNA. Crystal structures of cTBP from various species and molecular biology studies of cTBP and mixed cTBP/TBP species have led to the view that DNA binding by TBP is regulated by TBP dimerization. Sedimentation equilibrium indicates that yeast cTBP forms dimers with a dissociation constant of 7±1 μM. In contrast, the physiologically relevant full-length yeast TBP forms dimers with a dissociation constant is 51±5 μM. This dissociation constant precludes formation of stable dimers at physiological concentrations. Moreover, no evidence for TBP oligomerization in the context of TFIID was found using immunoprecipitation techniques from yeast whole-cell extract. We conclude that yeast TBP is predominantly monomeric under physiological conditions, thus precluding a role for TBP dimerization in the regulation of TBP and transcriptional initiation.

5.2. INTRODUCTION

Initiation of gene transcription on a TATA-containing RNA polymerase II promoter is a complex process, involving a large number of interactions between multiple transcription factors (Orphanides *et al.*, 1996; Lemon & Tjian, 2000). The RNA polymerase II general transcription factor TFIID consists of both TBP and TAFs. An initial regulatory step in transcription initiation by polymerase II is the binding of the TBP to DNA, which serves to nucleate pre-initiation complex assembly (Burley & Roeder, 1996; Orphanides *et al.*, 1996), and is proposed to be a major rate-limiting step in RNA polymerase II transcription initiation (Colgan & Manley, 1992; Kuras & Struhl, 1999; Li *et al.*, 1999). In addition, TBP is a central component in transcription by RNA polymerases I and III (Burley & Roeder, 1996; Orphanides *et al.*, 1996). Accurate prediction of transcription patterns and an understanding of the mechanism of transcription initiation will require a description of the factors that regulate TBP.

The DNA-binding region of TBP is located in the conserved 180-residue C-terminal domain (Burley & Roeder, 1996). The crystal structures of yeast, human and plant TBP C-terminal domains have been solved (Chasman *et al.*, 1993; Kim *et al.*, 1993; Burley & Roeder, 1996). In all cases, the TBP C-terminal domain crystallizes as a dimer (Figure 5.1.A.). However, crystal structures of the TBP C-terminal domain bound to DNA show that the C-terminal domain binds DNA as a monomer (Figure 5.1.B) (Chasman *et al.*, 1993; Kim *et al.*, 1993; Burley & Roeder, 1996). The dimerization interface of the C-terminal domain occludes the

DNA-binding site, and so dimerization and DNA-binding by the C-terminal domain are mutually exclusive on structural grounds (Figure 5.1). Taken together with cross-linking and pull-down assays of solutions containing the TBP C-terminal domain and full-length TBP (Coleman *et al.*, 1995; Taggart & Pugh, 1996; Coleman & Pugh, 1997; Jackson-Fisher *et al.*, 1999a; Jackson-Fisher *et al.*, 1999b), these results have led to the view that DNA binding by TBP is regulated by dimerization, and that TBP dissociation is a key rate limiting step in transcriptional initiation (Coleman *et al.*, 1995; Taggart & Pugh, 1996; Coleman & Pugh, 1997; Jackson-Fisher *et al.*, 1999a; Jackson-Fisher *et al.*, 1999b).

A.) B.)

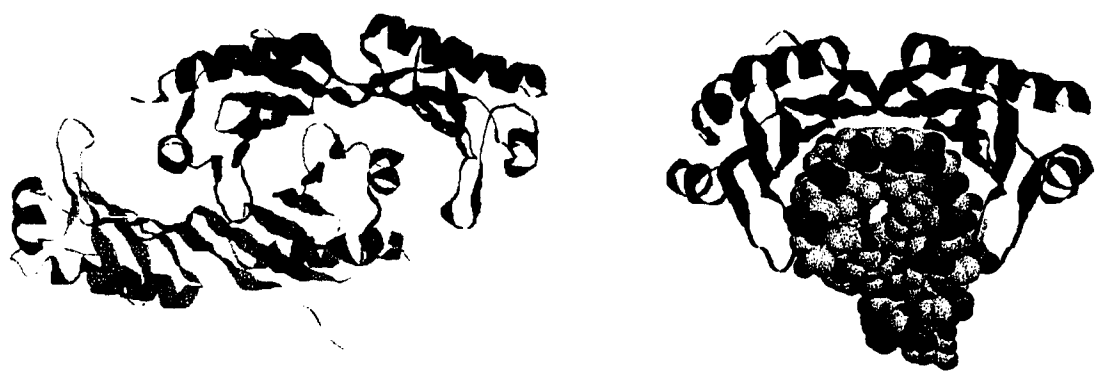

Figure 5.1. The dimerization interface of the C-terminal domain of yeast TBP occludes the DNA-binding surface. (A) Crystal structure of yeast cTBP (Chasman *et al.*, 1993). (B) Crystal structure of human c-TBP bound to DNA (Kim *et al.*, 1993). This figure was produced by Dr. Ryan Ranallo using RASMOL.

We report here the oligomerization properties of the C-terminal domain of yeast TBP (cTBP) and full-length yeast TBP using sedimentation equilibrium and immunological methods. Sedimentation equilibrium is a thermodynamically rigorous method to characterize protein self-association in solution (Hensley, 1996). The technique is sensitive to small amounts of incompetent monomer that are unable to oligomerize, which is detected by a systematic increase in K_d with increasing protein concentration (Yphantis *et al.*, 1978). In contrast to chemical crosslinking, sedimentation equilibrium will not generate artificially high levels of an oligomer due to a reactive crosslinking reagent. In addition, problems due to selectivity in pulldown assays and anomalous mobility during gel filtration are avoided. Using sedimentation equilibrium we find that, while cTBP forms dimers, dimerization of full-length TBP is thermodynamically unfavorable at physiological concentrations. In addition, immunological methods provide no evidence for dimerization of TBP in the context of TFIID. Our results challenge the notion that TBP dimerization plays an important role in regulating transcription initiation.

5.3. METHODS

5.3.A. Expression and Purification of Full-Length Yeast TBP

A T7 expression vector for full-length, yeast TBP was prepared by ligating the *Nde*1/*Bam*H1 fragment from a pET-15b vector encoding His-tagged TBP (gift of Dr. Laurie Stargel; Stargell & Struhl, 1996) into the *Nde*1/*Bam*H1 site of a pET-11a vector. The resulting pET-11a expression vector (called pYTBP) encodes

full-length TBP without the His-tag, and solved the solubility problems encountered while cleaving the His-tag. TBP was grown at 37 °C in *Escherichia coli* strain BL21 (DE3) to an optical density of 1.0 and induced with 1 mM IPTG and shaken for approximately 16 hours at 25 °C. Cells were harvested by centrifugation and resuspended in buffer A (50 mM Tris-HCl, 100 mM KCl, 1 mM EDTA, 10% (v/v) glycerol, 1 mM DTT, pH adjusted to 7.5) containing 1 mM PMSF. Cells were lysed by freezing in liquid nitrogen, thawing and sonicating. The cell lysate was centrifuged and the soluble fraction dialyzed for 4 hrs at 4 °C in buffer A containing 1 mM PMSF. After dialysis, the soluble fraction was centrifuged to remove particulate (since TBP normally sticks to filters) and loaded on a 5 ml HiTrap Q column (Pharmacia) equilibrated in buffer A. TBP flowed through the Q column and was loaded on a 5 ml HiTrap SP column (Pharmacia) equilibrated with buffer A. TBP eluted at about 300 mM KCl from the SP column with a linear KCl gradient in buffer A. The fraction containing TBP was loaded on a HiTrap Heparin (Pharmacia) column equilibrated in buffer A. TBP was eluted at about 500 mM KCl from the Heparin column using a linear KCl gradient in buffer A. TBP was concentrated using a centricon-10 (amicon) at 4°C until the total volume was about 1 ml. The TBP was centrifuged and loaded onto a gel filtration column (Sephacryl S-100) equilibrated in 10 mM sodium phosphate, 250 mM Na_2SO_4, 5 mM $MgCl_2$, 1 mM DTT, 10% (v/v) glycerol, pH adjusted to 7.5. The flow rate was 0.2 ml min^{-1} and the TBP eluted at about 80 ml. Purity of the protein was assessed by SDS-PAGE gel electrophoresis, with TBP as the only observable band.

Purified TBP was frozen as aliquots in liquid nitrogen and stored at -70 °C and was not freeze-thawed more than once, since it has been reported that repeated freeze-thaw cycles significantly affect the oligomerization state of yeast TBP (Perez-Howard *et al.*, 1995). N-terminal sequencing, by E. Towers in the CSU Macromolecular Research Facility, indicated that the N-terminal Met of TBP was processed, as observed for authentic TBP from yeast (Schmidt *et al.*, 1989). The identitiy of TBP was confirmed with electrospray mass spectrometry by Don Dick in the Department of Chemistry Central Instrument Facility, with the expected and observed mass agreeing to within 2 Da.

5.3.B. Expression and Purification of the C-terminal Domain of TBP

cTBP, corresponding to residues 49-240 of yeast TBP, was prepared from purified full-length TBP by trypsin (Sigma T-1426) cleavage of the N-terminal domain (Lieberman *et al.*, 1991) using 35 µg trypsin and stirring 2 hours at 4 °C to cut approximately 5 milligrams of TBP. The reaction product was immediately loaded onto a SP HiTrap column (Pharmacia) equilibrated in buffer A and eluted using a linear NaCl gradient in buffer A.

Purified cTBP was frozen as aliquots in liquid nitrogen and stored at -70 °C and was not freeze-thawed more than once. The identitiy of cTBP was confirmed with electrospray mass spectrometry, with the expected and observed mass agreeing to within 2 Da.

5.3.C. Sedimentation Equilibrium

Sedimentation equilibrium experiments were performed with a Beckman XL-I and An60-Ti rotor. Data were collected using 1.2 cm pathlength six-sector centerpieces at wavelengths of 276 and 280 nm for cTBP and TBP, respectively. Equilibrium was judged to be reached when scans collected three hours apart were indistinguishable, and was generally attained within 12 hours. Solvent densities of 1.060 g ml^{-1} at 5 °C and 1.056 g ml^{-1} at 30 °C and partial molar volumes of 0.754 ml g^{-1} for cTBP and 0.746 ml g^{-1} for TBP were calculated as described elsewhere (Laue *et al.*, 1992).

Data were analyzed with Origin (Beckman) and fit to ideal single species, monomer-dimer, monomer-trimer, monomer-tetramer and monomer-octamer models. The equation used was

$$c_r = c_{m,r_0}\exp[M(r^2-r_0^2)(1-\rho v)\omega^2/2RT] + (c_{m,r_0})nK_{a,abs}\exp[nM(r^2-r_0^2)(1-\rho v)\omega^2/2RT] + E$$

where c_r is the concentration at radius r, r_0 is the radius of the first data point, c_{m,r_0} is the monomer concentration in absorbance units at r_0, M is the molecular mass of the monomer, n is the oligomerization order of the associated species, ρ is the solvent density, ω is the rotor speed, R is the gas constant, T is the

temperature, $K_{a,abs}$ is the association constant in absorbance units, E is the baseline offset (McRorie & Voelker, 1993).

The association constant in terms of concentration, K_a, for a monomer-dimer equilibrium is given by

$K_a = K_{a,abs}\, \varepsilon l/2$

where ε is the extinction coefficient, and l is the pathlength (McRorie & Voelker, 1993).

Discrimination between the different models was based on the distribution of residuals and the variance, which approaches 1 as the fit improves (Beckman Technical Bulletin LXL/A-TB-009C). Parameters that were allowed to vary during fits to the ideal single-species model were molecular mass and baseline offset, unless stated otherwise. Parameters that were allowed to vary during fits to the self-associating models were the log of the dissociation constant and the baseline offset, with the molecular mass held constant at the known monomeric value (21279.0 Da for cTBP and 26871.7 Da for TBP). In all fits the second virial coefficient was held constant at zero (and therefore not included in the equation) and terms for oligomers not considered in the fit were made insignificant by constraining the association constant to10^{-20} (McRorie & Voelker, 1993).

Samples were dialyzed at 4 °C against the reference buffer (10 mM sodium phosphate, 250 mM Na_2SO_4, 5 mM $MgCl_2$, 1 mM DTT, 10% (v/v) glycerol, pH

adjusted to 7.5, unless stated otherwise) for at least 12 hours. For cTBP, data were collected at 5 °C using multiple cTBP loading concentrations spanning 6 to 60 μM and rotor speeds of 20, 30 and 40 krpm and cTBP from three independent preparations (Table 5.1). For TBP, data sets were collected at 5 and 30 °C using multiple cTBP loading concentrations spanning 6 to 60 μM and rotor speeds of 30, 35 and 40 krpm and TBP from four independent preparations (Table 5.2 and 5.3).

Reported errors in K_d values were derived from the standard deviation of the mean K_d value obtained from the fits and the error in the extinction coefficient. Extinction coefficients for cTBP and TBP were experimentally determined in 10 mM sodium phosphate, 250 mM Na_2SO_4, 5 mM $MgCl_2$, 1 mM DTT, 10% (v/v) glycerol, pH adjusted to 7.5 from a linear fit of the change in absorbance with protein concentration to the Beer-Lambert equation. Measurements were made three times to obtain extinction coefficients for cTBP at 276 nm of 10474 ± 3% M^{-1} cm^{-1} and for TBP at 280 nm of 13058 ± 3% M^{-1} cm^{-1}. Concentrations of the stock solutions were determined by absorbance in 6 M GuHCl, 10 mM sodium phosphate, pH adjusted to 6.5 using extinction coefficients for cTBP at 276 nm of 8700 M^{-1} cm^{-1} and for TBP at 280 nm of 13370 M^{-1} cm^{-1} (Edelhoch, 1967).

5.3.D. DNA-Binding Assays

Electrophoretic mobility-shift assays were performed by Dr. Ryan Ranallo, using a ^{32}P-labeled 45-basepair fragment containing the adenovirus early 1B TATA box as described in Campbell *et al.* (2000b).

5.3.E. Analytical Gel Filtration

Apparent molecular masses were determined at room temperature (approximately 20 °C) by gel filtration with a TosoHaas G2000SW$_{XL}$ column equilibrated in 10 mM sodium phosphate, 250 mM Na_2SO_4, 5 mM $MgCl_2$, 1 mM DTT, 10% (v/v) glycerol, pH adjusted to 7.5. A flow rate of 0.5 ml min^{-1} was used. The column was calibrated with lysozyme, chymotrypsinogen A, ovalbumin, albumin and blue dextran, which have molecular weights of 14.3, 25.0, 43.0, 67.0 kDa respectively. The elution volume of the standards (in ml) were used to plot K_{AV} vs. log molecular weight, with $K_{AV} = (v_e - v_o)/ (v_t - v_o)$; where v_e is the elution volume, v_o is the void volume of the column, and v_t is the total column volume. This plot resulted in a straight line, which was fit to obtain the equation $y = -0.76409x + 3.8499$. This equation was used to calculate the apparent molecular mass of TBP from the elution volume of 0.05 mg of TBP.

5.3.F. Immunoprecipitations

Immunoprecipitations were performed by Dr. Ryan T. Ranallo as described in Ranallo *et al.* (1999) and Campbell *et al.* (2000b).

5.4. RESULTS

5.4.A. Sedimentation Equilibrium

Sedimentation equilibrium data sets for cTBP were collected at 5 °C using cTBP from three independent preparations. Twenty-five data sets were fit individually to an ideal, single-species model in which the molecular mass was allowed to vary (Table 5.1). In each case, the apparent molecular mass was higher than expected for a monomer but less than expected for a dimer, indicative of a self-associating species (McRorie & Voelker, 1993). Therefore each data set was fit with the molecular mass held constant at the known monomeric value to single species, monomer-dimer, monomer-trimer, monomer-tetramer and monomer-octamer models. In every case the data were fit best by a monomer-dimer model, as indicated by the random distribution of residuals and variances closest to one (Figure 5.2). Equivalent results were obtained for cTBP that was either never frozen or freeze-thawed once.

The mean K_d value for the cTBP monomer-dimer equilibrium obtained from fits of the single data sets is 7 ± 1 μM. Global fits of data collected for each of the three cTBP preparations yielded a mean K_d of 7.9 ± 1 μM. The value of the monomer-dimer K_d for cTBP did not vary systematically in the 25 independent data sets collected over a 10-fold range of total cTBP concentration and at multiple rotor speeds, indicating that cTBP was essentially fully active for dimerization (Yphantis *et al.*, 1978). These results indicate that cTBP in solution exists in a

monomer-dimer equilibrium at 5 °C at low micromolar concentrations, in accord with the dimeric state of cTBP observed in the crystal structure (Figure 5.1).

Table 5.1. Sedimentation equilibrium data for cTBP at 5 °C. K_d values did not increase systematically with increasing loading concentration, indicating that essentially all of the protein was functional for binding.

Prep. #	Initial loading Conc. (μM)	Rotor speed (rpm)					
		20000		30000		40000	
		K_d (μM)	ΔG kcal/mol	K_d (μM)	ΔG kcal/mol	K_d (μM)	ΔG kcal/mol
1	55	1.8	7.3	2.5	7.1	1.4	7.4
	20	10.1	6.4			7.2	6.5
	10			3.2	7.0		
2	15	1.7	7.3	22.9	5.9	7.4	6.5
	10	4.3	6.8	11.3	6.3	17.7	6.5
	7			3.3	7.0	10.9	6.3
3	85					7.2	6.5
	55					8.7	6.4
	30						
4	50					1.3	7.5
	35	2.7	7.1			11.1	6.3
	20					12.4	6.2
5	60			10.3	6.3	6.9	6.6
	40			8.2	6.5	7.4	6.5
	20					4.6	6.8

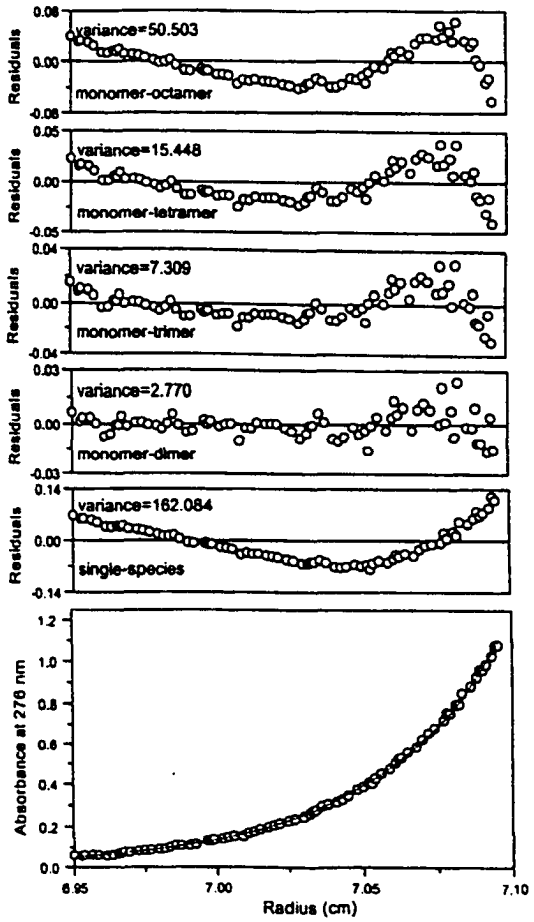

Figure 5.2. Sedimentation equilibrium data for cTBP. The residuals are random for the monomer-dimer fit and the variance is closest to 1 for this model, suggesting that cTBP exists in a monomer-dimer equilibrium at 5 °C.

In contrast to the behavior observed for cTBP, sedimentation equilibrium measurements indicate that full-length yeast TBP is monomeric at 5 °C. TBP from four independent preparations was used and sixteen data sets were fit to an ideal single species model in which the molecular mass was allowed to vary (Table 5.2). In each case, the residuals were random (Figure 5.3), indicating that TBP behaves as a single ideal species at 5 °C. The average molecular mass of

TBP from 16 independent measurements is 27.52 ± 0.79 kDa, which is within experimental error of the expected monomer mass (26.87 kDa). The apparent molecular mass of TBP did not increase systematically with total TBP concentration in the range 6-60 μM, indicating that TBP does not oligomerize significantly at 5 °C (Laue, 1995). Thus, at 5 °C, TBP does not form dimers or higher-order oligomers at micromolar concentrations.

Table 5.2. Sedimentation equilibrium data for TBP at 5°C.

Prep. #	Initial loading conc. (μM)	Rotor speed (rpm)			
		30000		40000	
		MW	% error	MW	% error
10 mM sodium phosphate, 250 mM Na_2SO_4, 5 mM $MgCl_2$, 1 mM DTT, 10% (v/v) glycerol, pH 7.5					
1	38	26,419	1.7	27,187	1.2
	30	25,759	4.1	28,826	7.2
	15	23,637	-12.0		
2	45	30,994	15.3	26,789	-0.3
	30	33,363	24.2	27,093	0.8
	15			28,547	6.2
3	60	29,506	9.8	26,197	-2.5
	40	27,408	2.0	24,162	-10.1
	20	28,418	5.8	25,975	-3.3
20 mM HEPES, 120 mM KCl, 1 mM DTT, 1 mM EDTA, 10% (v/v) glycerol, pH 7.5					
4	60			28,345	5.5
	40			27,775	3.4
	20			28,222	5.0

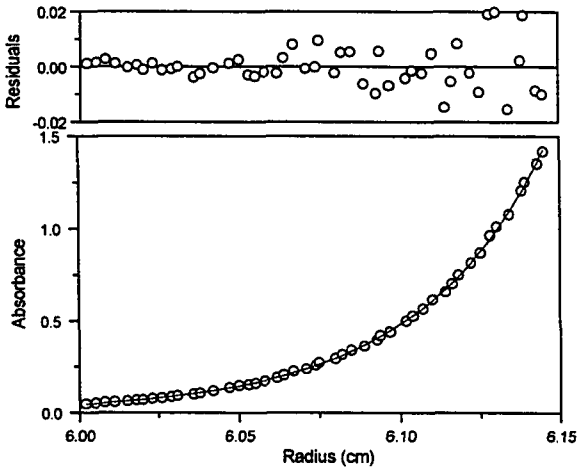

Figure 5.3. Sedimentation equilibrium indicates that TBP is monomeric at 5 °C. The data fit a single-species model, as indicated by random distribution of residuals and a molecular mass expected for a monomer.

Sedimentation equilibrium studies of full-length TBP from four independent preparations were also performed at 30 °C (a standard yeast culturing temperature). Twenty-one data sets were first fit individually to an ideal single-species model in which the molecular mass was allowed to vary (Table 5.3). In each case, the apparent molecular mass was higher than expected for a monomer but less than expected for a dimer, indicative of a self-associating species (McRorie & Voelker, 1993). The data were therefore fit to ideal single species, monomer-dimer, monomer-trimer, monomer-tetramer and monomer-octamer models in which the molecular mass was held constant at the known value for TBP.

Seventeen data sets exhibited a concentration change of >0.2 absorbance units across the cell, which is necessary for a reliable discrimination between different

models (Laue, 1995). All of these data sets were accounted for best by a monomer-dimer model, as indicated by a random distribution of residuals and variances closest to one (Figure 5.4). The four data sets collected at the lowest total concentration (6-15 μM) spanned only a limited concentration range across the cell (approximately 0.1 absorbance units) and exhibited limited curvature. These data sets could also be accounted for by a monomer-dimer model. Equivalent results were obtained for TBP that was either never frozen or freeze-thawed once.

The mean of the monomer-dimer K_d determinations from individual fits for TBP at 30 °C is 51 ± 16 μM. The K_d did not vary systematically over a 10-fold range of total TBP concentration and at multiple rotor speeds (Figure 5.5), indicating that the TBP was essentially fully active for dimerization (Yphantis *et al.*, 1978). Global fits of data collected for each of the four TBP preparations yielded a mean K_d of 63 ± 16 μM.

Table 5.3. Sedimentation equilibrium data for TBP at 30 °C. K_d values did not increase systematically with increasing loading concentration, indicating that essentially all of the protein was functional for binding.

Prep. #	Initial loading conc. (μM)	Rotor speed (rpm)					
		30000		35000		40000	
		K_d (μM)	ΔG kcal/mol	K_d (μM)	ΔG kcal/mol	K_d (μM)	ΔG kcal/mol
10 mM sodium phosphate, 250 mM Na_2SO_4, 5 mM $MgCl_2$, 1 mM DTT, 10% (v/v) glycerol, pH 7.5							
1	45	30.3	6.3			75.3	5.7
	30	30.3	6.3			60.1	5.9
	15	42.9	6.1			24.4	6.4
2	60					67.5	5.8
	40					122.8	5.4
	20					58.5	5.9
3	30	35.5	6.2	25.0	6.4		
	20	58.0	5.9	47.7	6.0		
	10	58.0	5.9	27.6	6.3		
4	30	38.2	6.1	53.2	5.9		
	20	63.5	5.8	42.6	6.1		
	6	61.4	5.8	47.3	6.0		
10 mM sodium phosphate, 150 mM Na_2SO_4, 5 mM $MgCl_2$, 1 mM DTT, 10% (v/v) glycerol, pH 7.5							
5	30	25.0	6.4	42.5	6.1		
	20	39.9	6.1	36.8	6.1		
	8	19.4	6.5	25.2	6.4		
20 mM HEPES, 120 mM KCl, 1 mM DTT, 1 mM EDTA, 10% (v/v) glycerol, pH 7.5							
6	60			23.2	6.4		
	35			47.3	6.0		
	18			79.8	5.7		

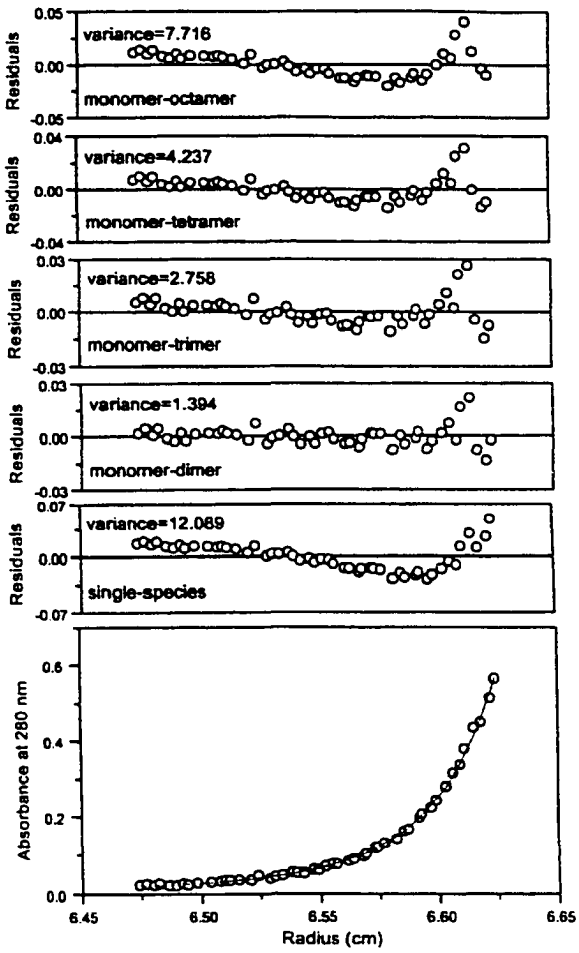

Figure 5.4. Sedimentation equilibrium data of TBP at 30 °C indicates that TBP is in a monomer-dimer equilibrium at 30 °C. The residuals are random for the monomer-dimer model fit and the variances are closest to one for this model.

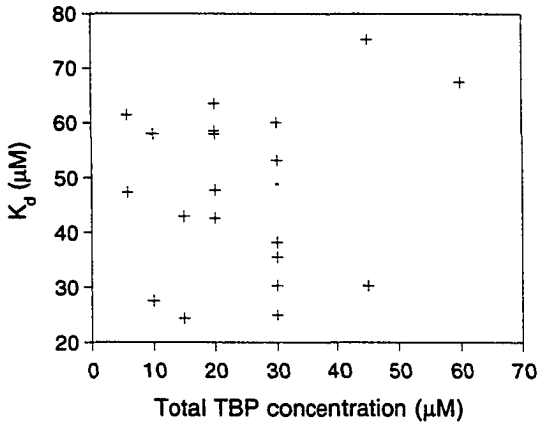

Figure 5.5. The K_d for the TBP monomer-dimer equilibrium obtained from the single-channel fits does not vary systematically with total TBP concentration.

A preponderance of TBP monomers was also observed under conditions of different ionic strength (20 mM HEPES, 120 mM KCl, 1 mM DTT, 1 mM EDTA, 10% glycerol, pH adjusted to 7.5 and 10 mM sodium phosphate, 150 mM Na_2SO_4, 5 mM $MgCl_2$, 1 mM DTT, 10% glycerol, pH adjusted to 7.5).

A previous sedimentation equilibrium study reported that yeast TBP forms tetramers and octamers (Daugherty *et al.*, 1999). The study was performed at total TBP concentrations of 9 and 15 μM and at two rotor speeds (16 and 24 krpm) (Daugherty *et al.*, 1999). The final pH of the buffer used in the study (Daugherty *et al.*, 1999) was not reported, and so we repeated the experiments using the same buffer components (20 mM HEPES, 120 mM KCl, 1 mM DTT, 1 mM EDTA) with the pH adjusted to 7.5. The TBP aggregated visibly in this buffer in two independent attempts. The experiments were not pursued further, since

others have reported that TBP is rapidly inactivated in the buffer where tetramers and octamers were observed (Jackson-Fisher *et al.*, 1999b), and the physiological relevance of residual, soluble TBP under aggregating conditions is questionable. Inclusion of 10% glycerol in the buffer alleviated the aggregation and gave results that fit a monomer-dimer equilibrium, as described above.

5.4.B. DNA-Binding Assays

The functional activity of TBP was not altered during sedimentation equilibrium, since the TBP was equally active for binding the early 1B TATA element before and after sedimentation equilibrium at 30°C (Figure 5.6).

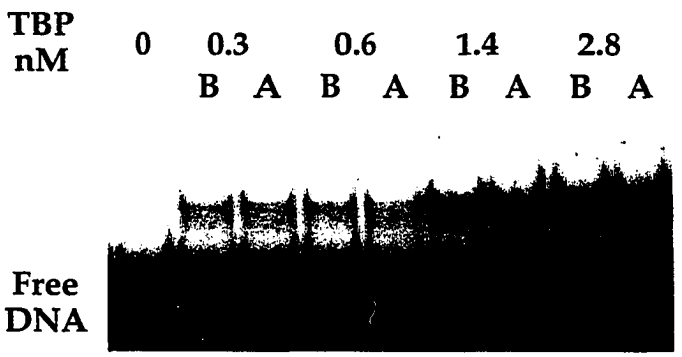

Figure 5.6. TBP exhibited no detectable difference in DNA binding before (B) or after (A) ultracentrifugation at 30°C. TBP (60 pM-22 nM) and ^{32}-P-labeled DNA (5.4 nM) were incubated at 25 °C for 30 minutes. The intensities of the TBP-DNA bands at a particular TBP concentration are the same to within 3%. Experiment performed by Dr. Ryan T. Ranallo.

5.4.C. Analytical Gel Filtration

The apparent molecular mass of TBP was also estimated with gel filtration. A single peak was observed, with an apparent molecular mass of 31.6 kDa (Figure

5.7). This mass is within 18% of the known monomeric mass of TBP. The gel filtration results are consistent with the conclusions from the sedimentation equilibrium analysis that TBP is predominantly monomeric at micromolar concentrations.

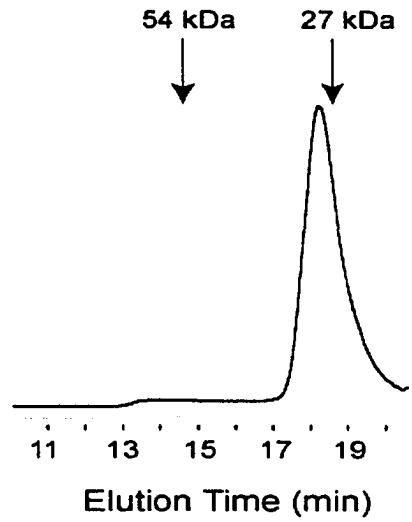

Figure 5.7. TBP elutes during gel filtration as a single peak with an apparent molecular mass of 31.6 kDa. Expected elution times for monomeric and dimeric TBP are indicated.

5.4.D. Immunoprecipitations

TBP is associated *in vivo* with TAFs to form the general transcription factor TFIID (Burley & Roeder, 1996). To test whether the presence of TAFs could favor TBP dimerization, Drs. Laurie Stargell and Ryan Ranallo used immunological methods to evaluate if TBP dimerizes in the context of TFIID. Since TBP monomers and oligomers cannot be distinguished by immunoprecipitation or immunodetection, TBP was tagged with a myc epitope (mycTBP) to allow isolation and detection of putative mycTBP/TBP heterodimers.

TBP and mycTBP were coexpressed in yeast and the presence of mycTBP/TBP heterodimers was probed by immunoprecipitation of mycTBP followed by immunoblotting with anti-TBP antibodies. If TBP dimerizes in the context of TFIID, then immunoprecipitation of mycTBP should result in coimmunoprecipitation of TBP. We found that TBP was not present in the mycTBP immunoprecipitations, indicating that TBP does not oligomerize with mycTBP (Figure 5.8). Dilution experiments of the extract containing TBP and mycTBP indicate that 2% dimer formation could have been detected (data not shown). Moreover, TFIID formation is not disrupted by immunopreciptation or the myc-tag, since TAF130 and TAF61 are present in the immunoprecipitate (Figure 5.8). Furthermore, the myc-tag does not interfere with TBP functions since yeast strains in which TBP or mycTBP were the sole source of TBP were identical for growth at 30 and 37 °C, on alternative carbon sources (raffinose and galactose), in high levels of copper (500 μM) and on aminotriazole (15 mM). Thus, TBP does not self-associate in the context of TFIID.

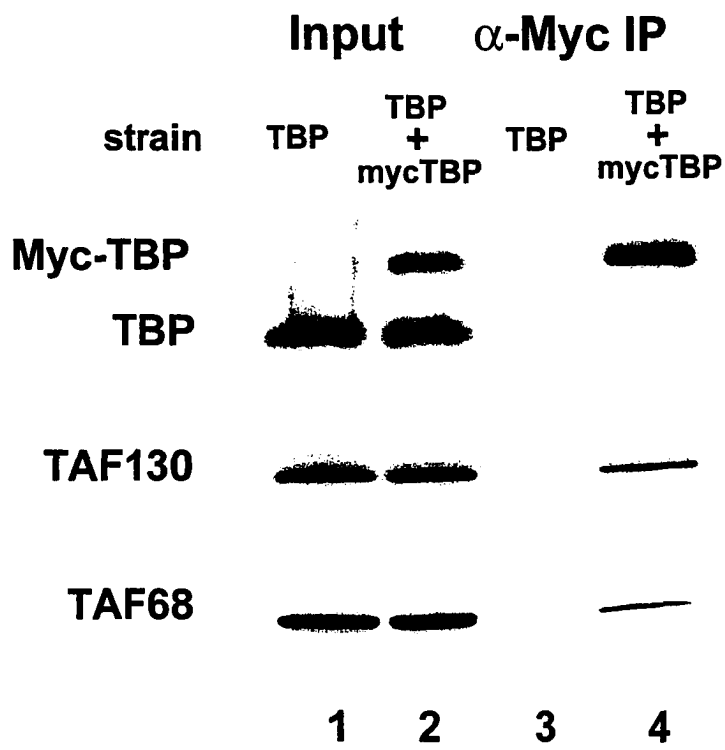

Figure 5.8. Immunoprecipitation assays indicate that TBP is not dimeric in yeast. Whole-cell extracts were prepared from two different strains; one that expresses only TBP (labeled TBP; lanes 1 and 3) and one that expresses both TBP and mycTBP (labeled TBP+mycTBP; lanes 2 and 4). The extract starting material is indicated (labeled Input; lanes 1 and 2). Extracts were immunoprecipitated using myc antibodies (denoted α-Myc IP, lanes 3 and 4), and probed with polyclonal antibodies specific to TBP, TAF68 or TAF130. As expected, immunoprecipitation with anti-myc antibodies of extracts derived from the strain expressing only TBP did not result in isolation of TBP or TFIID (lane 3). Immunoprecipitation of extracts derived from strains coexpressing TBP and mycTBP resulted in isolation of only mycTBP and TAFs and not TBP (lane 4). Experiment performed by RyanT.Ranallo.

5.5. DISCUSSION

The C-terminal domains of TBP from several species, including yeast, are dimeric in crystal structures (Chasman *et al.*, 1993; Burley & Roeder, 1996). Comparison of the free and DNA-bound yeast cTBP crystal structures show that

the TBP dimerization interface occludes the DNA-binding surface (Figure 5.1). This structural feature raises the possibility that TBP is regulated by dimerization, and that slow dissociation of dimers provides a regulatory step in DNA binding by TBP and transcription initiation. Indeed, several experimental studies have been interpreted on the basis that TBP is regulated by dimerization (Coleman *et al.*, 1995; Taggart & Pugh, 1996; Coleman & Pugh, 1997; Jackson-Fisher *et al.*, 1999a and 1999b).

In accord with the dimeric state of yeast cTBP observed in the crystal structure (Chasman *et al.*, 1993), we find that, in solution, cTBP forms dimers at 5 °C with a K_d of 7 ± 1 μM. Since the completion of this study (Campbell *et al.*, 2000b), others have reported a K_d for dimerization for cTBP of 2.8-4.5 μM, in agreement with our results (Liu & Schepartz, 2001). In marked contrast to the dimerization properties of cTBP at 5 °C, the physiologically relevant, full-length TBP is monomeric at micromolar concentrations. Even at 30 °C, TBP dimerization is thermodynamically unfavorable at physiological concentrations. Since the mean K_d for TBP dimerization is 51 μM at 30 °C, and the nuclear concentration is estimated to be 1-6 μM (Kato *et al.*, 1994; Taggart & Pugh, 1996), TBP will be predominantly monomeric at physiological concentrations (Figure 5.9). Moreover, TBP dimers were not observed in immunoprecipitates in the context of TFIID, suggesting that the TAFs or other proteins present *in vivo* do not promote TBP or TFIID oligomerization.

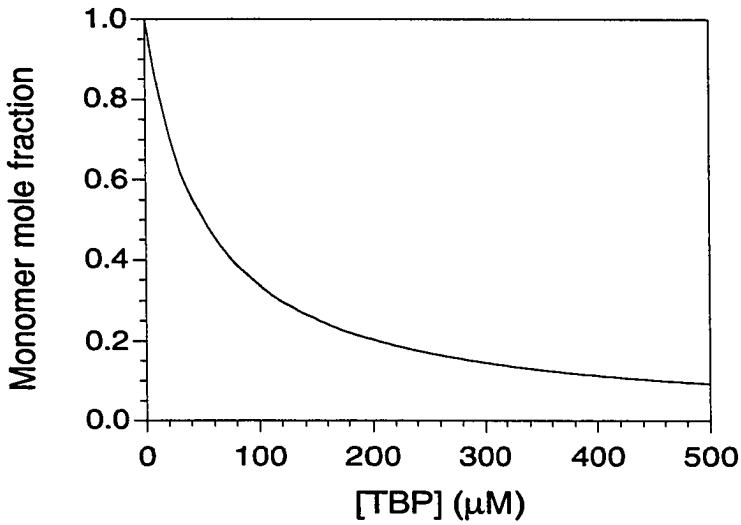

Figure 5.9. The change in mole fraction of monomeric TBP with total TBP concentration. The percentage of dimeric TBP will depend on the total TBP concentration. Since the K_d for dimerization is 51 μM at 30 °C, and the nuclear concentration is estimated to be 1-6 μM (Taggart & Pugh, 1996), TBP will be monomeric at physiological concentrations.

Our results challenge the model for a regulatory role for TBP dimerization in transcription initiation. Our results also demonstrate that TBP dimerization is unfavored by the presence of the N-terminal domain. Since the dimerization interface of cTBP coincides with the DNA-binding surface (Figure 5.1), and the N-terminal domain interferes with TBP dimerization, it is possible that the N-terminal domain occludes the dimerization interface of TBP in solution. Indeed, removal of the N-terminal domain of yeast TBP results in faster binding to DNA and a more stable TBP-DNA complex (Lieberman *et al.*, 1991; Lee *et al.*, 1992). It is an intriguing possibility that any TBP mutation or transcription factor capable of disrupting the interaction between the N- and C-terminal domains will result in potentially elevated levels of transcription.

Chapter 6

Structurally Distinct Modes of Jun and CREB Recognition of the KIX Domain of CBP

This chapter describes work submitted to *Proceedings of the National Academy of Sciences* (Campbell & Lumb 2002b). Experimental detail, results and analysis have been expanded beyond those reported in the paper.

6.1. ABSTRACT

Gene expression is coordinated in part by interactions between transcriptional activators and other transcription factors such as coactivators. The KIX domain of the coactivator and histone acetyltransferase CBP binds numerous mammalian and viral transcriptional activators such as CREB, c-Jun, c-Myb, p53, papillomavirus E2 and HTLV-1 Tax. Formation of the CREB-CBP complex involves the induced folding of the KID region of CREB upon binding a hydrophobic groove on the KIX domain of CBP. Circular dichroism indicates that the activation domain of c-Jun is essentially unfolded and the domain of c-Jun necessary for binding KIX is localized in residues 47-89. In contrast to the mode of binding exhibited by CREB, NMR spectroscopy indicates that the c-Jun activation domain binds to a distinctly different surface of KIX than used by CREB. Moreover, NMR spectroscopy shows that the activation domains of c-Jun and CREB can simultaneously bind the KIX domain of CBP. Literature results suggest that c-Myb, p53, and Tax also utilize the c-Jun-binding site of KIX. The results illustrate a new mode of binding and combinatorial recruitment via the KIX domain of CBP by multiple transcriptional activators.

6.2. INTRODUCTION

The expression of protein-coding genes involves the assembly of a large number of proteins such as RNA polymerase II, general transcription factors, activators, coactivators and architectural proteins (Orphanides *et al.*, 1996; Ptashne & Gann, 1997; Lemon & Tjian, 2000; Näär *et al.*, 2001). Specificity for a given gene is directed in large part by transcriptional activators that bind regulatory DNA sequences (Ptashne & Gann, 1997). Activators contain a functionally independent DNA-binding domain and one or more activation domains that bind and localize other components of the transcription machine to the target gene (Ptashne & Gann, 1997). Coactivators are important binding partners for activation domains, and contribute to transcription by acting as bridging molecules or enzymes that introduce regulatory modifications such as histone acetylation (Orphanides *et al.*, 1996; Ptashne & Gann, 1997; Lemon & Tjian, 2000; Näär *et al.*, 2001).

The coactivator CREB-Binding Protein (CBP) is a large (265 kDa) multi-domain protein containing a histone acetyltransferase domain and several protein-interacting domains that bind RNA polymerase II, the general transcription factors TFIIB and TFIID and a legion of mammalian and viral transcriptional activators (Goodman & Smolik, 2000). One region of CBP that mediates CBP interactions with activators is the autonomously folded, helical KIX domain (Parker *et al.*, 1996; Radhakrishnan *et al.*, 1997). KIX binds inducibly to the KID region of CREB (CRE-Response Element Binding protein) in response to cAMP-

dependent phosphorylation of CREB at Ser 133 (Chrivia *et al.*, 1993; Kwok *et al.*, 1994; Parker *et al.*, 1996). KIX also binds constitutively to a range of activators such as BRCA1, c-Jun, c-Myb, p53, and SREBP, and to viral activators such as papillomavirus E2 and HTLV-1 Tax (Bannister & Kouzarides, 1995; Dai *et al.*, 1996; Janknecht & Nordheim, 1996; Oelgeschlager *et al.*, 1996; Oliner *et al.*, 1996; Van Orden *et al.*, 1999a; Van Orden *et al.*, 1999b; Lee *et al.*, 2000; Pao *et al.*, 2000). The wide range of activator complexes involving CBP mirrors the diverse roles for CBP in processes such as cell growth, transformation and development (Goodman & Smolik, 2000).

Of the numerous protein-protein complexes involving KIX, the interaction between CBP and the KID region of CREB is the best understood in molecular terms. NMR studies of the phosphorylated KID-KIX complex shows that KID undergoes a transition from a largely unfolded to a helical conformation and binds to a shallow hydrophobic groove on one surface of KIX (Radhakrishnan *et al.*, 1997). Other activation domains have been proposed to recognize the same hydrophobic groove of KIX that is occupied by CREB (Radhakrishnan *et al.*, 1997; Van Orden *et al.*, 1999b).

The human transcriptional activator c-Jun is involved in a diverse array of protein-protein interactions and cellular process such as differentiation and apoptosis as a component of AP-1 (Chinenov & Kerppola, 2001; Shaulian & Karin, 2001; Vogt, 2001). The N-terminal activation domain of c-Jun binds the

KIX domain of CBP (Arias *et al.*, 1994; Bannister *et al.*, 1995; Van Orden *et al.*, 1999a), and the interaction between full-length c-Jun and CBP stimulates transcription *in vivo* (Bannister *et al.*, 1995). Phosphorylated c-Jun binds CBP (Arias *et al.*, 1994), although c-Jun phosphorylation is not required for the formation of the c-Jun-CBP complex (Bannister *et al.*, 1995; Van Orden *et al.*, 1999b).

Here we present the first structural study of the Jun-KIX complex. Deletion studies refine the region of c-Jun that binds KIX. Strikingly, the c-Jun activation domain binds at a distinctly different surface of KIX than KID, and the KID and c-Jun activation domains can simultaneously bind KIX. Our results illustrate a molecular basis for KIX binding that is different to the mechanism employed by CREB, and provide insight into the molecular basis of cooperative recruitment of CBP by multiple activation domains.

6.3. METHODS

6.3.A. Expression and Purification of JunAD and Jun(1-57)

JunAD corresponds to residues 1-89 of human c-Jun with an additional N-terminal Gly-Ser-His derived from the pET-15b expression vector (Figure 6.1). JunAD was expressed as a His-tag fusion protein using a pET15b vector harboring a PCR product encoding residues 1-89 of human c-Jun (called pET15b-JunAD) amplified from a plasmid encoding full-length c-Jun (gift of M. Karin). The coding sequence of pET15b-JunAD was confirmed with

dRhodamine automated sequencing, by the Colorado State University Macromolecular Resource Facility .

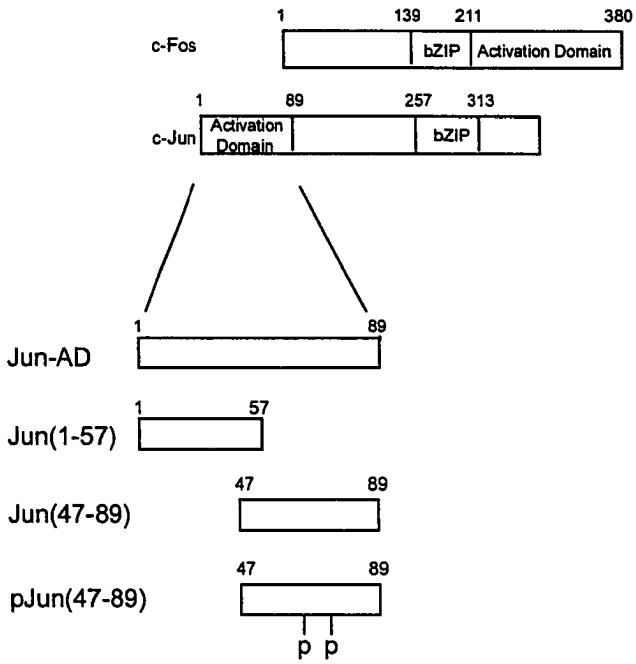

Figure 6.1. Schematic of c-Fos, c-Jun and the c-Jun deletion mutants. The leucine zipper of the bZIP domain of c-Jun mediates dimerization with c-Fos and the basic region of the bZIP domain binds DNA (Curran & Vogt, 1992) and the N-terminal domain activates transcription (Abate *et al.*, 1991). JunAD spans the human N-terminal activation domain (residues 1-89), Jun(1-57) spans the residues 1-57, Jun(47-89) spans residues 47-89 and pJun(47-89) spans residues 47-89 with Ser 63 and Ser 73 phosphorylated.

JunAD was expressed, using the T7 system (Studier et al., 1990), in Eshcherichia coli strain BL21 (DE3) grown in LB medium at 37 °C to an optical density of 0.6 and induced with 0.5 mM IPTG at 37 °C for 3 hours. The cells were harvested by centrifugation, resuspended in 50 ml His-bind buffer (5 mM

imidazole, 500 mM NaCl, 1 mM PMSF, 20 mM Tris-HCl, pH 7.9) and lysed by sonication. The cell lysate was centrifuged. The soluble fraction was filtered (0.45 (M filter) and loaded onto 10 ml His-bind resin (Novagen 70666) charged with 50 mM NiSO4 and equilibrated in His-bind buffer (5 mM imidazole, 500 mM NaCl, 20 mM Tris-HCl, pH 7.9). The column was washed with 100 ml His-bind buffer and 50 ml His-wash buffer (60 mM imidazole, 500 mM NaCl, 20 mM Tris-HCl, pH 7.9). JunAD was eluted from the column with 1 M imidazole, 500 mM NaCl, 20 mM Tris-HCl, pH 7.9. The eluted fraction was dialysed for 4 hours against 4 L of thrombin-cleavage buffer (150 mM NaCl, 2.5 mM CaCl2, 20 mM Tris-HCl, pH 8.4). The His-tag sequence was cleaved with 15 units of thrombin (Novagen 69671) for 16 hours at 25 °C. Digestion of JunAD with thrombin produced both JunAD and an additional product Jun (1-57), since JunAD has an cryptic thrombin site. Jun (1-57) corresponds to residues 1-57 of human c-Jun (Figure 6.1). The proteolysed products were passed over a 10 ml His-bind column to remove uncleaved fusion protein and the His-tag. 1 mM EDTA and 10 mM DTT was added and JunAD and Jun (1-57) were separated and further purified by reverse-phase C_{18} HPLC using 0.1%/minute linear acetonitrile/water gradients containing 0.1% v/v trifluoroaceticacid. JunAD and Jun (1-57) have three additional N-terminal amino acids, Gly-Ser-His derived from the His-tag.

6.3.B. Manual Boc Synthesis of Jun(47-89)

A synthetic peptide corresponding to residues 47-89 of human c-Jun (Figure 6.1) with an acetylated N-terminus and an amidated C-terminus was prepared with

manual Boc chemistry at the 0.25 mmol scale using MBHA resin (0.373 g) (Schnolzer et al., 1992). The following protecting groups were used: Thr(Bzl), His(DNP), Asn(Xan), Ser(Bzl), Gln(Xan), Arg(Tos), Glu(Bzl), Lys(ClZ), Asp(Bzl) and His(DNP) (Nova Biochem).

1 mmol of the first (C-terminal) Boc-amino acid was mixed with 0.359 g HBTU, 2.5 ml DMF and 0.3 ml DIEA in a test tube. The mixture was sonicated until clear. After waiting two minutes, the amino acid was added to the resin and the solution was mixed with shaking for 40 minutes (12 minutes for subsequent amino acids). The resin was rinsed with DMF. Coupling was confirmed by the Kaiser ninhydrin test (Kaiser *et al.*, 1970) or chloranil test for proline (Christensen *et al.*, 1979). A negative Kaiser test indicates that coupling is complete, whereas a positive Kaiser test results in a blue product and indicates the presence of a free amine. If the test was positive, coupling of the same amino acid was repeated. If the test was negative then the Boc group was removed with TFA (2 rounds of 3 ml TFA for 1 minute), the resin rinsed with DMF and the next amino acid was coupled. After coupling of the final amino acid, the N-terminus was acetylated with 3 ml acetic anhydride, 2 ml DMF and 2 ml DIEA and shaking for 12 minutes. The resin was then rinsed with DMF.

When synthesis was complete, the His(DNP) residue was deprotected by treating the resin with 5 ml thiophenol for approximately 12 hours. The resin was rinsed with DMF, CH_2Cl_2 and diethyl ether and desiccated under vacuum

overnight to remove residual solvents. The peptide was cleaved from the resin and the remaining protecting groups were removed by HF cleavage, for two hours, in an HF reaction apparatus (Stewart & Young, 1984) using 10 ml HF per g of dried resin and 1 ml anisole per g of dried resin. After the HF evaporated, the resin was resuspended with diethyl ether, rinsed with ether and the peptide was eluted from the resin with water. Purification of Jun(47-89) was by reversed-phase C_{18} HPLC using a linear 0.1%/minute acetonitrile/water gradient containing 0.1% TFA.

6.3.C. Manual Fmoc Synthesis of pJun(47-89)

pJun(47-89) is equivalent to Jun(47-89) except Ser 63 and Ser 73 are phosphorylated (Figure 6.1). pJun(47-89) was prepared with manual Fmoc chemistry (0.25 mmol scale) to avoid potential side reactions of the phosphate group during HF cleavage. The following protecting groups were used: Thr(tBu), His(Trt), Ser(tBu), pSer(OBzl), Tyr(tBu), Arg(Pbf), Gln(Trt), Asp(OtBu), Glu(OtBu), Lys(Boc) and Asn(Trt) (Nova Biochem).

1 mmol of the first (C-terminal) Fmoc-protected amino acid was mixed with 0.359 g HBTU, 2.5 ml DMF and 0.3 ml DIEA in a test tube. The mixture was sonicated until clear. After two minutes the amino acid was added to 0.373 g of Rink Amide Resin (Nova Biochem 01-64-0013) and the mixture was shaken for 1.5 hours (30 minutes for subsequent amino acids). The resin was rinsed with DMF. Coupling was confirmed by Kaiser ninhydrin test (Kaiser *et al.*, 1970) or chloranil test for

proline (Christensen *et al.*, 1979). A negative Kaiser test indicates that coupling is complete, whereas a positive Kaiser test results in a blue product and indicates the presence of a free amine. If the test was positive, coupling of the same amino acid was repeated. If the test was negative then the Fmoc group was removed by adding 5 ml of 20% (v/v) piperidine in DMF to the resin and shaking for 20 min. The resin was then rinsed with DMF, and the next amino acid was added. After coupling the final amino acid, the N-terminal was acetylated by adding 3 ml acetic anhydride, 2 ml DMF and 2 ml DIEA and shaking for 12 minutes.

When synthesis was complete, the resin was rinsed with DMF, CH_2Cl_2 and diethyl ether, and desiccated under vacuum overnight to remove residual solvents. The peptide was cleaved from the resin and the remaining protecting groups were removed by adding 14.2 ml TFA, 0.375 ml H_20, 0.375 ml ethanedithiol and 0.15 ml triisopropylsiliane to the resin and stirring for 2 hours. The solution was filtered to remove the resin and the filter was rinsed with TFA. Cold diethyl ether was added to the filtrate until the peptide precipitated. The solution was then filtered to separate the precipitate. The precipitate was washed with ether and the peptide was eluted with water. Purification of pJun(47-89) was by reverse-phase C_{18} HPLC using a linear 0.1%/minute acetonitrile/water gradient containing 0.1% TFA.

6.3.D. Expression and Purification of Human KIX

KIX (corresponding to residues 586-679 of human CBP) was prepared as described previously using a pET3a expression vector (Mestas & Lumb, 1999).

KIX was expressed in *Escherichia coli* strain BL21 (DE3) plysS grown in LB medium at 37 °C to an optical density at 600 nm of 1.0 and induced with 1 mM IPTG for 3 hours at 37 °C. Cells were harvested by centrifugation and resuspended in buffer A (10 mM Tris-HCl, 1 mM EDTA, pH adjusted to 7.5) containing 1 mM PMSF. Cells were lysed by sonication, the cell lysate was centrifuged and the soluble fraction dialyzed for 4 hours at 4 °C in buffer A containing 1 mM PMSF. After dialysis, the soluble fraction was filtered (0.45 μM) and loaded on a 5 ml HiTrap Q column (Pharmacia) equilibrated in buffer A. KIX flowed through the Q column and was loaded on a 5 ml HiTrap SP column (Pharmacia) equilibrated with buffer A. KIX eluted at about 300 mM NaCl from the SP column with a linear NaCl gradient in buffer A. The fraction containing KIX was further purified by reversed-phase C_{18} HPLC using a linear 0.1%/minute acetonitrile/water gradient containing 0.1% TFA.

^{15}N-labeled and ^{15}N/^{13}C-labeled KIX were prepared in the same way as unlabeled KIX except cells were grown in M9 minimal media supplemented with thiamine (McIntosh & Dahlquist, 1990) containing 1 g/L $(^{15}NH_4)_2SO_4$ and/or 3 g/L ^{13}C-glucose as the sole nitrogen and carbon sources.

6.3.E. Purification of pKID

pKID corresponds to residues 115-148 of human CREB, with Ser 133 phosphorylated. pKID was synthesized by Fmoc synthesis by the Colorado State University Macro-molecular Resource Facility (Mestas & Lumb, 1999). pKID was purified by reversed-phase C_{18} HPLC using a linear 0.1%/minute acetonitrile/water gradient containing 0.1% TFA.

The identity of all proteins was confirmed with electrospray mass spectrometry. In all cases the expected and observed masses agreed to within 1 Da.

6.3.F. Concentration Determination of Protein Solutions

Protein concentrations were determined by absorbance in 6 M GuHCl, 10 mM sodium phosphate, pH 6.5 at 25 °C using extinction coefficients at 276 nm of 12650 M^{-1} cm^{-1} for KIX, 4350 M^{-1} cm^{-1} for JunAD and Jun(1-57), and 1450 M^{-1} cm^{-1} for Jun(47-89), pJun(47-89) and pKID (Edelhoch, 1967).

6.3.G. Circular Dichroism

CD spectroscopy was performed with a Jasco J720 spectrometer. Spectra were collected at 10 °C on samples containing 20 μM of each protein in 10 mM sodium phosphate, 150 mM NaCl, pH 7.0.

6.3.H. Sedimentation Equilibrium

Sedimentation equilibrium was performed with a Beckman XL-I analytical

ultracentrifuge. Data for Jun(47-89) were collected in a six-sector cell at concentrations of 275 μM and 137 μM. Data for pJun(47-89) were collected in a six-sector cell at concentrations of 700 μM, 400 μM, 280 μM. Data for the KIX-pJun(47-89) and KIX-jun(47-89) complexes were collected in two-sector cells using interference optics on samples containing equimolar (450 μM) KIX and pJun(47-89) or equimolar (450 μM) KIX and Jun(47-89). Partial specific volumes (υ) of 0.738, 0.74, 0.752 and 0.752 ml g^{-1} were used for KIX, JunAD, pJun(47-89) and Jun(47-89), respectively, and were calculated as described elsewhere (Laue, 1995). The solvent density of 1.008 g ml^{-1} was measured directly. Masses are reported as the mean mass ± standard error of the masses obtained from single-species fits of data collected at 15 and 20 krpm for the complex and 40 and 48 krpm for pJun(47-89) and Jun(47-89).

6.3.I. NMR Spectroscopy

NMR spectroscopy was performed with a Varian Unity Inova spectrometer operating at 500.13 MHz for ^{1}H. All data were collected using spectral widths of 6000, 1800, 3773, and 4000 Hz for ^{1}H, ^{15}N, ^{13}C and ^{31}P, respectively. Mulitidimensional data sets were processed with NMRPipe and analyzed with NMRView (Johnson & Blevins, 1994; Delaglio *et al.*, 1995). ^{1}H and ^{31}P spectra were referenced to zero ppm with internal DSS and trimethylphosphate, respectively (Wishart *et al.*, 1995).

^{31}P NMR Titration of pJun(47-89)

The dissociation constant (K_d) for the pJun(47-89)-KIX complex was estimated at 10 °C from the change in ^{31}P chemical shift for samples containing 150 μM pJun(47-89) and 0-400 μM KIX in 10 mM sodium phosphate, 150 mM NaCl, pH 7.0. Data were analyzed by plotting the total concentration of KIX versus the chemical shift, assuming a 1:1 stoichiometry (determined by sedimentation equilibrium). Data were fit to the equation $\delta=(K_a \bullet [L]_t)/((1+K_a \bullet [L]_t)(\delta_F-\delta_B)+\delta_B)$ to estimate δ_F (the free chemical shift of pJun(47-89)) and δ_B (the bound chemical shift of pJun(47-89)). A plot of fraction bound (v) versus the concentration of free KIX, where $v=\delta_F-\delta/\delta_F-\delta_B$ and $[KIX]_{Free}=[KIX]_{Total}-v[pKID]_{Total}$, was then fit to the equation $\delta=(K_a \bullet \delta)/((1+K_a \bullet \delta)(\delta_F-\delta_B)+\delta_B)$ to estimate the association constant K_a. K_d is given by $1/K_a$.

NMR Assignment of the Resonances of KIX

Assignments for the resonances of unbound KIX at pH 5.5 were obtained from sensitivity-enhanced HNCA and HN(CO)CA spectra with minimal water excitation (Ikura *et al.*, 1990; Bax & Ikura, 1991; Kay *et al.*, 1994; Muhandiram & Kay, 1994) as implemented in Protein Pack suite of pulse programs (Varian). Assignments were consistent at three different temperatures (10, 25 and 35 °C). HNCA and HN(CO)CA spectra consisted of 32 complex increments in the ^{15}N dimension and 64 complex increments in the ^{13}C dimension defined by 16 transients and 1024 complex points. The sample contained 600 μM ^{15}N, ^{13}C-KIX in 10 mM sodium phosphate and 150 mM NaCl.

Assignments for KIX at 10 °C and pH 7.0 were obtained by following resonances in gradient ^{1}H-^{15}N HSQC spectra (Kay *et al.*, 1992) as the pH was changed from 5.5 to 7.0 at 10 °C. The samples contained 600 μM ^{15}N-KIX in 10 mM sodium phosphate, 150 mM NaCl.

Assignment of the KIX resonances in the pJun(47-89)-KIX complex at 10 °C were obtained using sensitivity enhanced gradient HNCA and HN(CO)CA spectra (Ikura *et al.*, 1990; Bax & Ikura, 1991; Kay *et al.*, 1994; Muhandiram & Kay, 1994). Spectra consisted of 32 complex increments in the ^{15}N dimension and 64 complex increments in the ^{13}C dimension defined by 32 transients and 1024 complex points. The sample contained 600 μM ^{15}N, ^{13}C-KIX and 1 mM unlabeled pJun(57-89) in 10 mM sodium phosphate, 150 mM NaCl, pH 7.0. Assignments for KIX in the KIX-pKID complex at 10 °C were obtained from a gradient ^{1}H-^{15}N HSQC spectrum (Kay *et al.*, 1992) of 225 μM ^{15}N KIX and 550 μM pKID in 10 mM sodium phosphate, 150 mM NaCl, pH 7.0 by transferring assignments of a different KID-KIX complex (Radhakrishnan *et al.*, 1999).

Chemical-Shift Mapping

Changes in KIX chemical shifts upon binding pJun(47-89) were measured from gradient HSQC spectra (Kay *et al.*, 1992) that were collected with higher digital resolution than the triple-resonance data. Spectra consisted of 256 complex increments defined by 112 transients and 1024 complex points. Samples

contained 225 μM ^{15}N KIX, or 225 μM ^{15}N KIX and 550 μM pJun(57-89), or 225 μM ^{15}N KIX and 550 μM pKID, or 225 μM ^{15}N KIX and 550 μM pKID and 550 μM pJun(57-89), in 10 mM citrate, 150 mM NaCl, pH 7.0. The Δδ (normalized change in chemical shift) was calculated using $\Delta\delta=[(\Delta H^N)^2+(\Delta N/5)^2]^{0.5}$.

Analysis of Ternary Complex Formation

^{31}P NMR studies of binary and ternary complex formation were performed at 10 °C on samples containing 225 μM of each protein in 10 mM citrate, 150 mM NaCl, pH 7.0.

Changes in H^N and ^{15}N KIX chemical shifts at 10 °C were measured by HSQC NMR spectroscopy as described above upon addition of 550 μM pJun(47-89) to the preformed pKID-KIX complex (225 μM ^{15}N KIX, 550 μM pKID) in 10 mM sodium citrate, 150 mM NaCl, pH 7.0.

6.4. RESULTS

6.4.A. Intrinsic Structural Disorder of the c-Jun Activation Domain

JunAD (Figure 6.1) corresponds to the N-terminal activation domain of human c-Jun (residues 1-89 of human c-Jun). The CD spectrum of JunAD is reminiscent of an unfolded protein, with a minimum at 199 nm and a lack of spectral features above 210 nm that are characteristic of α-helix or β-sheet formation (Figure 6.2). The H^N chemical shifts obtained from the HSQC spectrum of JunAD at 10 °C and pH 7.0 span 7.7-8.55 ppm (Figure 6.3), as expected for an unfolded protein

(Wishart & Sykes, 1994). These results indicate that the full-length N-terminal activation domain of c-Jun is intrinsically disordered or largely unfolded at neutral pH, a property shared with other full-length activation domains (O'Hare & Williams, 1992; Schmitz *et al.*, 1994; Chang *et al.*, 1995; McEwan *et al.*, 1996; Campbell *et al.*, 2000).

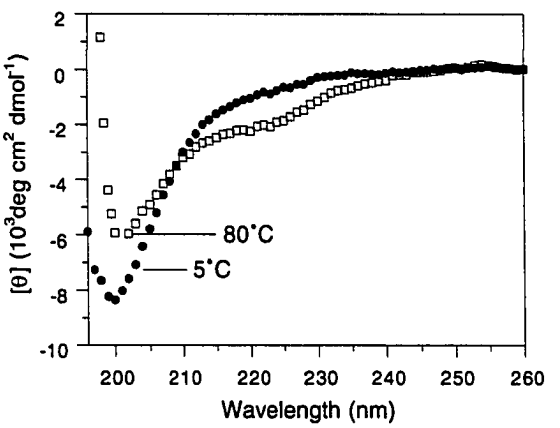

Figure 6.2. CD Spectra of Jun-AD at 5 and 80 °C. The spectra contains a negative band at 200 nm and an increase in negative ellipticity at 222 nm, with increasing temperature, which is indicative of a disordered conformation.

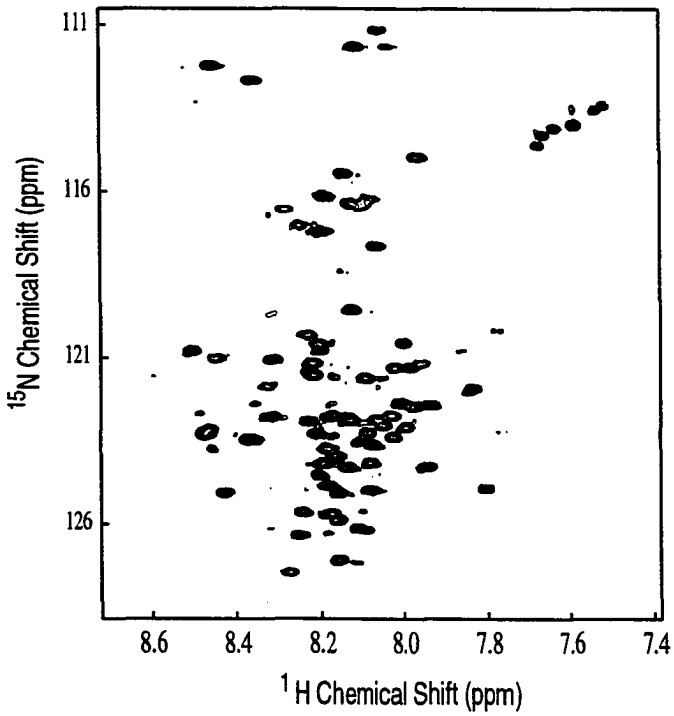

Figure 6.3. HSQC Spectra of ^{15}N Jun-AD. HSQC spectra at pH 7 and 10°C, lacks chemical shift dispersion, the H^N chemical shifts span 7.7-8.5 ppm, as expected for an unfolded protein (Wishart & Sykes, 1994).

6.4.B. CD Indicates that the Jun Activation Domain Binds KIX

The Interaction Between JunAD and KIX

CD spectroscopy shows that unphosphorylated JunAD binds to KIX (residues 586-679 of human CBP). The CD spectrum of free KIX is indicative of a helical protein (Figure 6.4), in accord with the NMR structure of the KIX domain *(Radhakrishnan et al., 1997)*. Addition of JunAD results in a slight increase in helicity at 222 nm over the spectrum that would be expected if the two proteins do not interact (Figure 6.4). This result suggests that the unphosphorylated Jun

activation domain binds KIX, in accord with previous molecular biology studies *(Bannister et al., 1995; Van Orden et al., 1999b).* In addition, the CD data suggest that a conformational change occurs that induces helix formation upon formation of the complex. Further biophysical characterization of the JunAD-KIX complex was precluded by precipitation at neutral pH (CD spectroscopy indicates that the formation of the JunAD-KIX complex is much less favorable at lower pH values, and does not occur at pH 5).

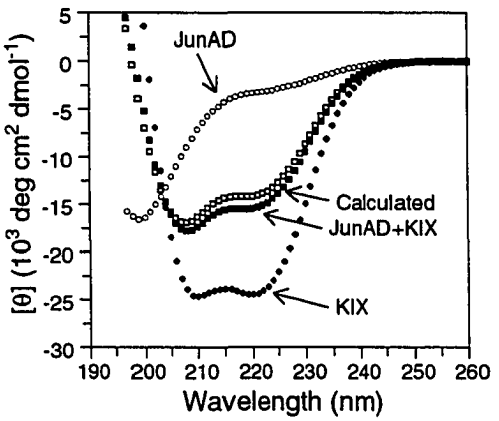

Figure 6.4. CD spectra of JunAD and KIX. Mixing of KIX with JunAD results in a spectrum with greater ellipticity at 208 and 222 nm than calculated from the sum of the two isolated proteins, suggesting that KIX forms a complex with JunAD, with a small increase in helix content.

Residues 1-57 of c-Jun are not Sufficient to Bind KIX

Jun(1-57) corresponds to residues 1-57 of c-Jun (Figure 6.1). The CD spectrum of Jun(1-57) is reminiscent of an unfolded protein (Figure 6.5), as expected since the full-length domain is also unfolded (Figure 6.4). Addition of Jun(1-57) to KIX results in a CD spectrum that is identical to the average spectra of Jun(1-57) and KIX, suggesting that Jun(1-57) does not bind KIX (Figure 6.5).

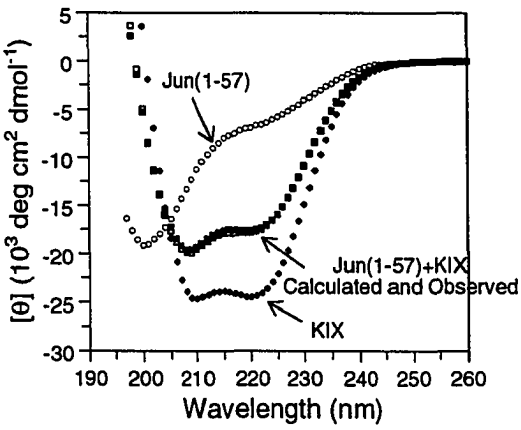

Figure 6.5. CD spectra of Jun(1-57) and KIX. Mixing of KIX with Jun(1-57) results in a spectrum identical to that calculated for the sum of the spectra of the two isolated proteins, suggesting that KIX does not form a complex with Jun(1-57).

Residues 47-89 of c-Jun Bind KIX and Phosphorylation is not Required

Jun(47-89) corresponds to residues 47-89 of human c-Jun (Figure 6.1). The CD spectrum of Jun(47-89) is characteristic of a largely unfolded protein, and addition of KIX results in an observed spectrum of significantly higher helix content than expected if Jun(47-89) and KIX do not interact (Figure 6.6). Essentially identical changes in the CD spectrum are observed for KIX and pJun(47-89), corresponding to Jun(47-89) with Ser 63 and 73 phosphorylated (Figure 6.7). These results indicate that residues 47-89 are sufficient for KIX binding and suggesting that phosphorylation is not required for binding.

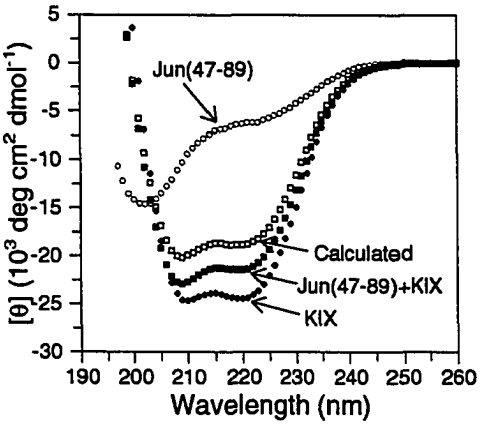

Figure 6.6. CD spectra of Jun(47-89) and KIX. Mixing of KIX with Jun(47-89) results in a spectrum with greater ellipticity at 208 and 222 nm than calculated from the sum of the spectra of the two isolated proteins, suggesting that KIX forms a complex with Jun(47-89), with an increase in helix content.

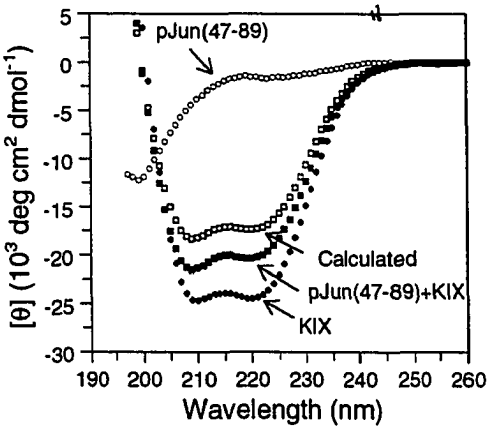

Figure 6.7. CD spectra of pJun(47-89) and KIX. Mixing of KIX with pJun(47-89) results in a spectrum with greater ellipticity at 208 and 222 nm than calculated from the sum of the spectra of the two isolated proteins, suggesting that KIX forms a complex with pJun(47-89), with an increase in helix content.

6.4.C. Changes in the Chemical Shifts of JunAD in the Presence of KIX

The HSQC spectrum of ^{15}N JunAD is characteristic of an unfolded protein (Figure 6.3) and addition of KIX results in chemical shift changes, as expected upon complex formation (Figure 6.8). Since the resonances of Jun-AD have not been assigned, it is not clear which amino acids of Jun-AD are affected by binding. However, the HSQC data provides further evidence for complex formation.

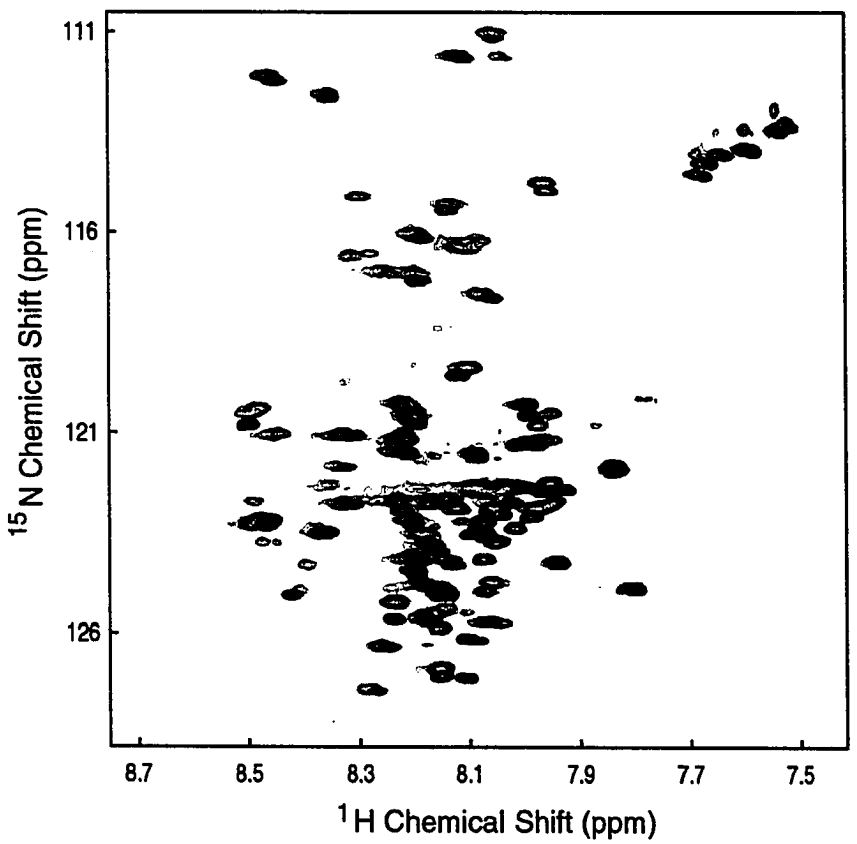

Figure 6.8. HSQC spectra of ^{15}N JunAD and the ^{15}N JunAD-KIX complex. The ^{15}N JunAD spectrum is shown in black and ^{15}N JunAD-KIX spectrum is shown in red.

6.4.D. Sedimentation Equilibrium

Sedimentation equilibrium was used to determine the stoichiometry of the fully bound complex, using high concentrations of total protein (900 μM), which required the use of interference optics. The observed molecular mass for the pJun(47-89)-KIX complex is 15.9 ± 0.2 kDa, whereas the expected value for the 1:1 complex is 16.1 kDa. The observed molecular mass for the Jun(47-89)-KIX complex is 15.4 ± 0.4 kDa, whereas the expected value for the 1:1 complex is 16.0 kDa. KIX was previously shown to be monomeric (S.P. Mestas & K.J. Lumb, unpublished results) and pJun(47-89) and Jun(47-89) are both monomeric by sedimentation equilibrium, with masses of 5600 ± 400 Da (expected: 4984.5 Da) and 4900 ± 500 Da (expected: 4824.5) respectively. This indicates that the observed masses of the complexes do not reflect self-association of the proteins as opposed to complex formation and the the KIX-Jun complex associates with a 1:1 stoichiometry (Figure 6.9).

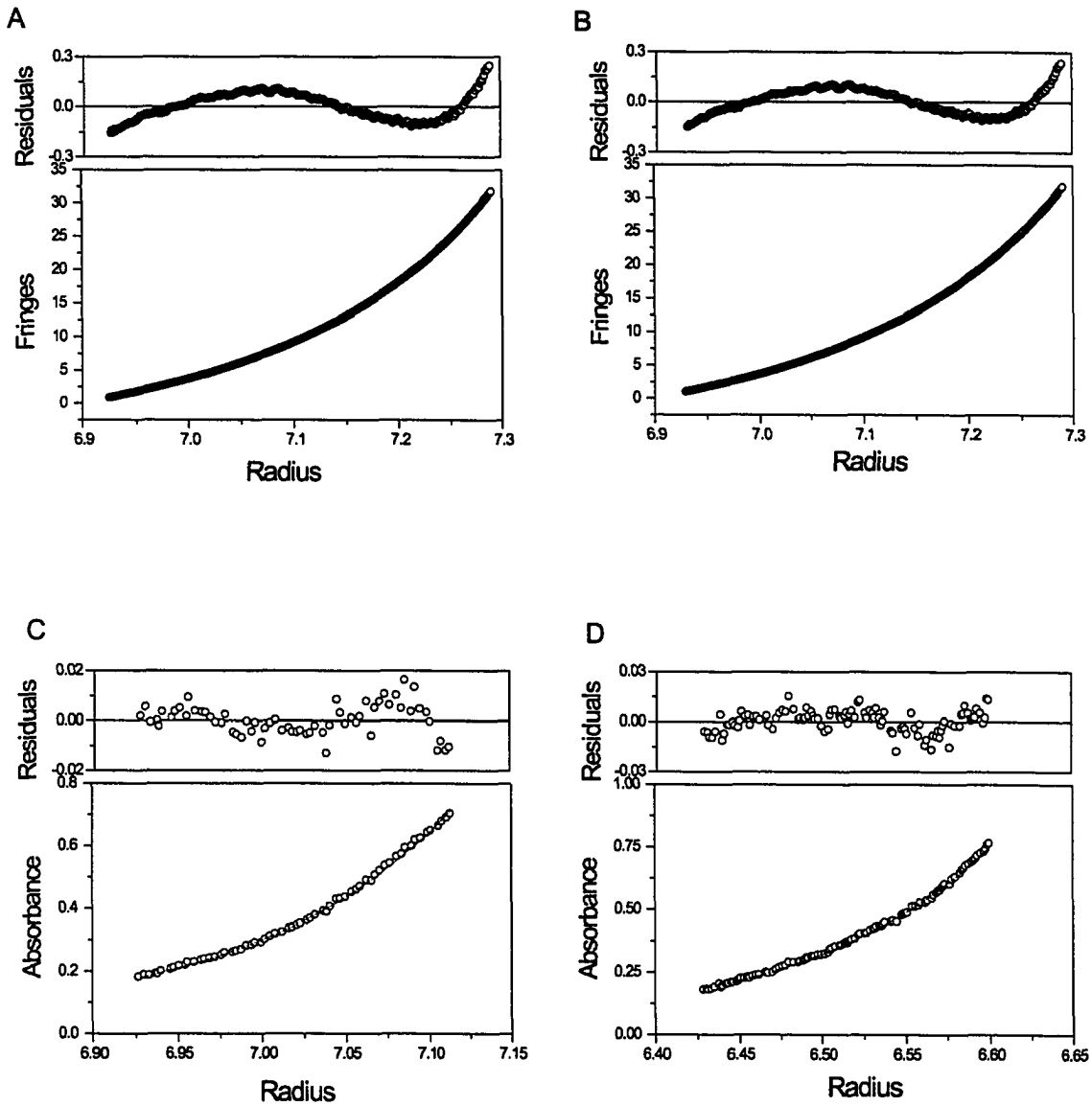

Figure 6.9. Sedimentation equilibrium data for (A) the pJun(47-89)-KIX complex, (B) the Jun(47-89)-KIX complex, (C) pJun(47-89) and (D) Jun(47-89). Residuals for interference data are an instrumental artifact and do not reflect fit quality.

6.4.E. K_d Measurement for the Jun-KIX Complex

K_d measurements for complexes of KIX and the various Jun deletions by either CD or fluorescence spectroscopy were hindered by the small spectroscopic changes seen upon binding. An estimated K_d of 31 μM for the pJun(47-89)-KIX complex, however, was measured with ^{31}P NMR spectroscopy (Figure 6.10). The ^{31}P chemical shifts of pJun(47-89) are in fast exchange between the free and KIX-bound forms, and the changes in the ^{31}P chemical shifts upon titration with KIX are hyperbolic as expected for a specific binding event. Data were fit for 1:1 complex formation, confirmed by sedimentation equilibrium.

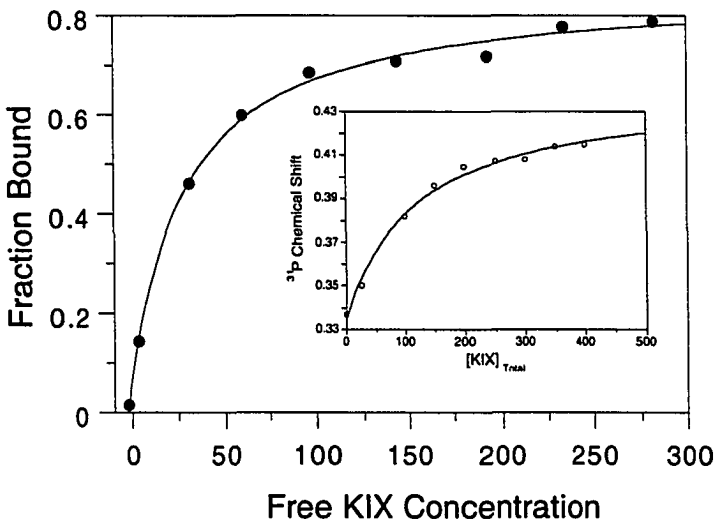

Figure 6.10. K_d determination for the KIX-pJun(47-89) complex by ^{31}P NMR. ^{31}P chemical shifts of pJun(47-89) were monitored with an increasing concentration of KIX. Only one pJun(47-89) ^{31}P resonance is shown for clarity.

6.4.F. Resonance Assignments of KIX at pH 5.5 and 10 °C

Unambiguous assignments were made for 73 of 93 residues of KIX at pH 5.5 and 10 °C, using connectivities between HNCA and HN(CO)CA experiments (Figure 6.11 and Table 6.1).

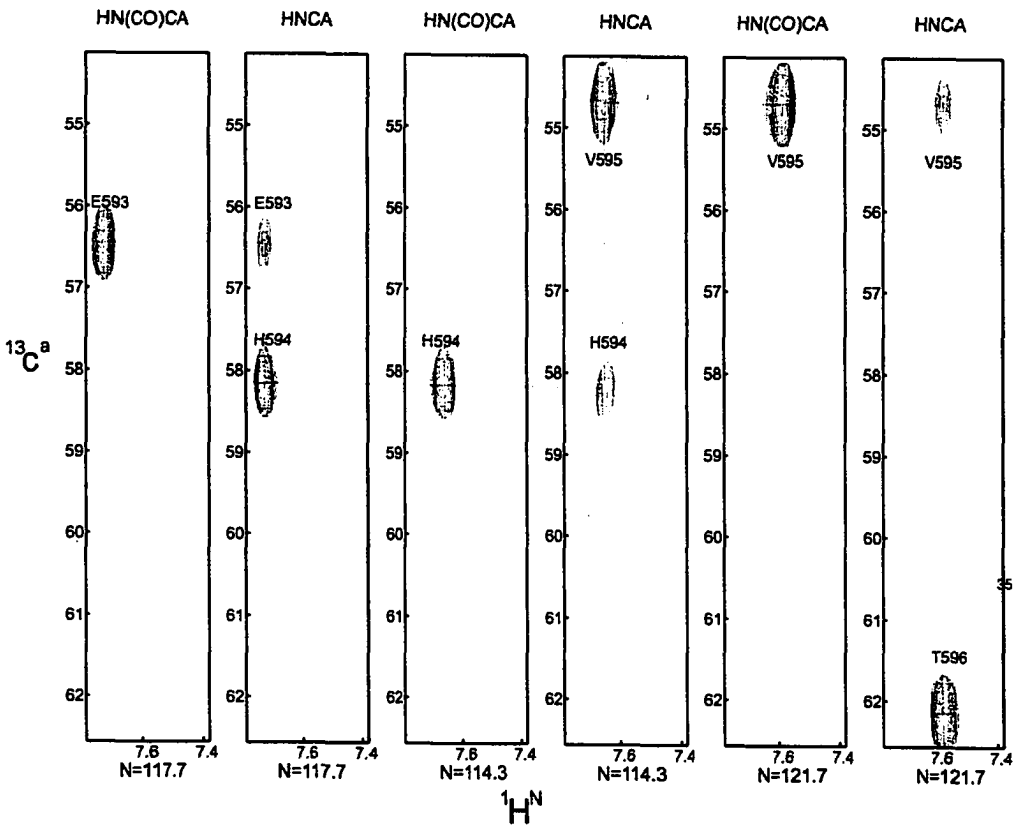

Figure 6.11. Example of sequential and intraresidue connectivities in HNCA and HN(CO)CA spectra of KIX.

Table 6.1. Assignments for KIX (10 °C, pH 5.5), chemical shifts are in ppm.

Residue	H^N	C^α	N	Residue	H^N	C^α	N
V587	8.772	62.14	125.71	P613			
R588	8.739	56.07	127.95	T614	7.994		115.37
K589	8.253	54.86	123.02	P615			
G590	8.861	47.11	114.11	D616			
W591	8.126	58.11	120.49	P617			
H592	7.192	56.19	120.64	A618	8.302	57.69	121.60
E593	7.780	57.99	117.72	A619	7.843	52.88	122.28
H594	7.688	54.37	114.31	L620	7.837	55.78	119.60
V595	7.602	61.98	121.90	K621	8.006	56.43	120.43
T596	7.664	59.99	116.76	D622	8.050	54.10	121.60
Q597	9.059	58.58	121.66	R623	8.456		121.83
D598	8.545	56.99	119.04	R624			
L599	7.772	58.30	124.12	M625			
R600	7.890	60.21	119.58	E626	8.486	59.67	120.57
S601	8.634	61.42	113.88	N627	8.328	55.47	119.16
H602	8.152	58.99	122.90	L628	8.057	57.86	124.82
L603	8.262	58.27	123.30	V629	8.552	66.77	121.16
V604	8.497	67.62	121.14	A630	7.869	55.55	121.60
H605	8.065		117.72	Y631	8.002	60.71	121.14
K606				A632	8.716	55.07	123.51
L607				K633	8.764	59.55	117.14
V608	8.194		120.01	K634	7.829	59.11	124.53
Q609	8.127	58.93	117.10	V635	8.107	65.66	120.00
A610	7.595	67.28	120.50	E636	8.614	61.17	121.52
I611	7.669	57.83	115.55	G637	8.254	47.27	108.36
F612	8.182	53.77	121.71	D638	8.269	56.89	123.55

Residue	H^N	C^α	N	Residue	H^N	C^α	N
M639	8.106	58.80	122.37	E665	8.419	56.8	120.36
Y640	9.404	61.85	122.23	E666	8.449	56.01	121.64
E641	8.159	57.55	116.13	K667	8.420	45.164	111.07
S642	8.100	60.09	114.04	R668	8.090	61.20	121.06
A643	8.260	52.69	125.32	R669	8.379	54.80	126.51
N644	9.178	53.29	118.10	S670	7.997		116.87
S645	6.944	56.37	112.40	R671			
R646	8.800	58.97	123.22	L672			
D647	8.350	57.19	118.34	H673			
E648	7.894	59.25	122.32	K674			
Y649	7.449	60.74	122.83	Q675			
Y650	8.306	60.57	117.01	G676			
H651	8.413	59.09	119.93	I677			
L652	9.121	57.69	122.18	L678			
L653	7.843	52.88	122.28	G679			
A654	7.837	55.19	119.60				
E655	8.368	59.04	119.07				
K656	7.933	57.79	122.26				
I657	8.332	66.05	120.33				
Y658	8.049	60.77	120.37				
K659	8.259	59.70	120.55				
I660	8.490	64.90	122.18				
Q661	8.436		120.08				
K662							
E663							
L664							

6.4.G. The Jun-Binding Surface of KIX

Unambiguous assignments for 73 of 93 residues of KIX were made at pH 7.0 and 10 °C (figure 6.12), by transferring assignments from KIX pH 5.5 and 10 °C (methods section 6.3.I.). The binding site on KIX was mapped with NMR spectroscopy from the changes in ^{15}N-labeled KIX chemical shifts upon binding unlabeled pJun(47-89). NMR chemical-shift perturbations are sensitive probes of protein-protein interaction surfaces (Zuiderweg, 2002). Resonances from the unlabeled pKID and pJun(47-89) domains are not seen in ^{1}H-^{15}N HSQC spectra of the complexes.

Addition of pJun(47-89) to ^{15}N-labelled KIX at neutral pH causes progressive changes in the ^{1}H and ^{15}N chemical shifts of ^{1}H-^{15}N HSQC spectra, indicating that the free and bound forms of KIX are in fast exchange on the H^N and ^{15}N chemical shift time scales. The average change in chemical shift upon formation of the fully bound KIX-pJun(47-89) complex is 0.02 ppm. The largest changes in chemical shift (>0.1 ppm) are seen for Leu 620, Lys 621, Asp 622, Glu 626 and Arg 669. Smaller but still significant changes (>0.05 ppm) seen for Val 604, Gln 609, Ile 611, Phe 612, Thr 614, Asn 627, Val 629, Ala 630, Ala 632, Lys 659, Ile 661, and Arg 668 (Figure 6.13 and 6.15). These residues form a contiguous surface of KIX containing solvent-exposed hydrophobic residues (Figure 6.16).

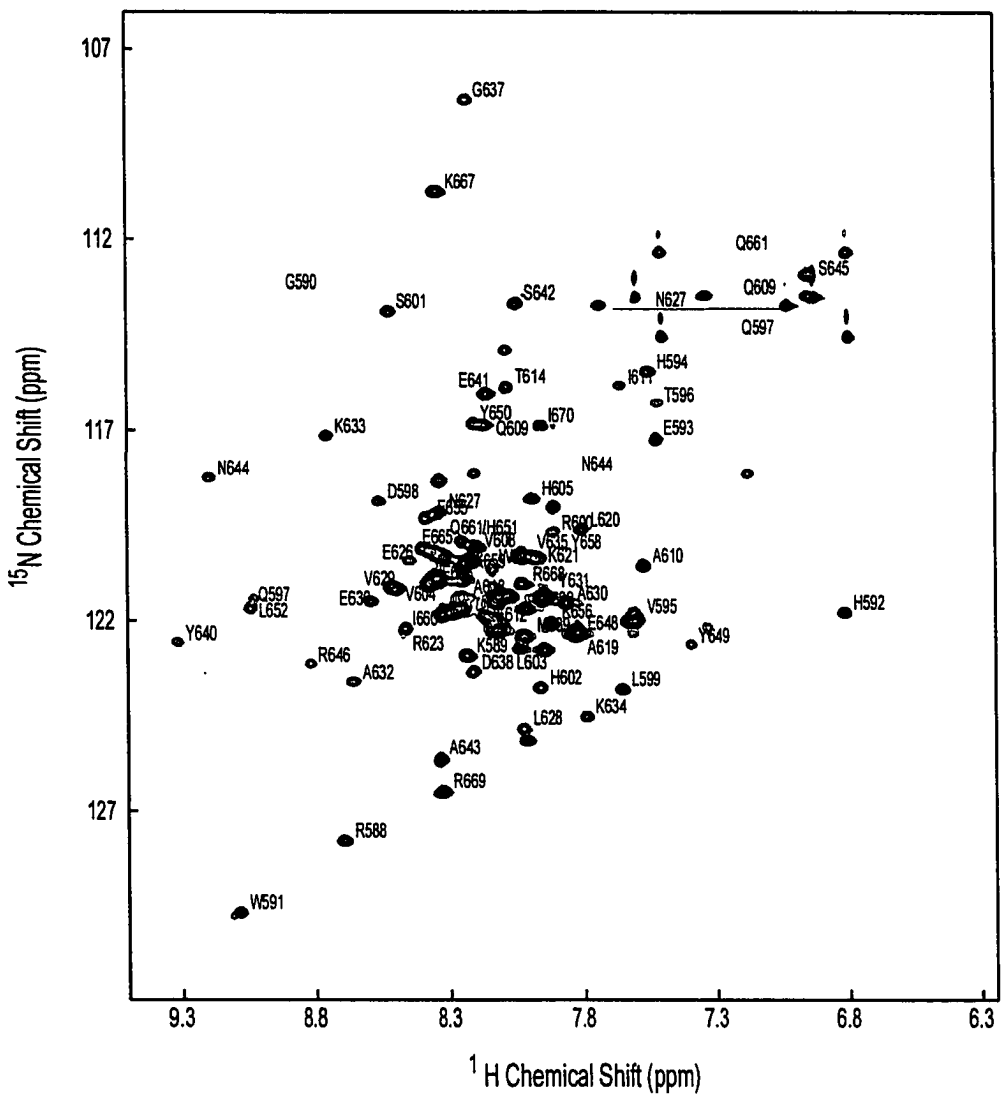

Figure 6.12. HSQC spectrum of ^{15}N KIX at pH7 and 10°C. The assigned resonances are labled.

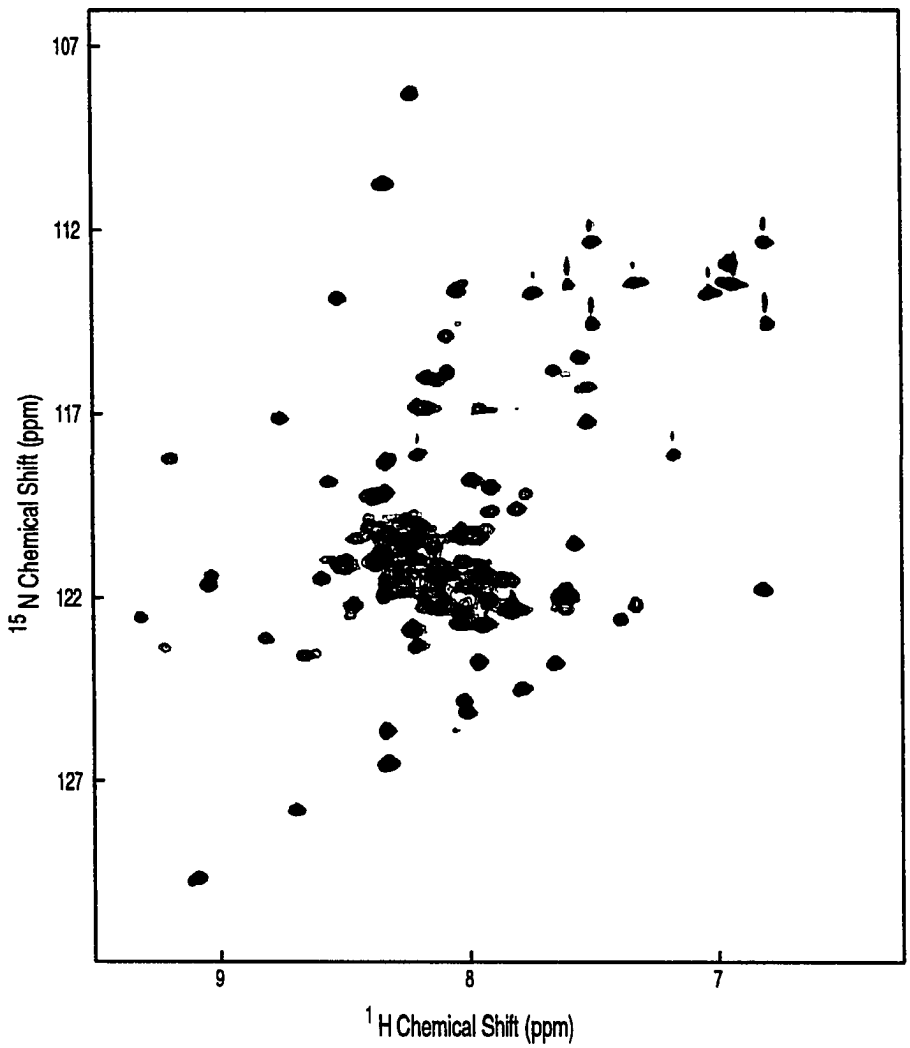

Figure 6.13. HSQC spectra of ^{15}N KIX and ^{15}N KIX-pJun(47-89). The KIX spectrum is shown in black and the KIX-pJun(47-89) spectrum is shown in red.

6.4.H. The pKID Binding Site of KIX

Changes in the ^{15}N-KIX chemical shifts were measured upon binding unlabeled pKID (residues 115-148 of human CREB phosphorylated at Ser 133) at 10 °C and pH 7.0. Unambiguous assignments for 56 of 93 residues of KIX in the pKID-KIX complex were obtained by transferring assignments of the mouse KIX-rat KID complex (Radhakrishnan *et al.*, 1999). The average change in KIX chemical shifts upon binding pKID is 0.08 ppm, with the largest changes (> 0.2 ppm) observed for Glu 655, Lys 656, Lys 659 and Gln 661 (Figure 6.14 and 6.15). The changes in KIX chemical shifts upon binding pKID agree qualitatively with those reported previously for the rat KID-mouse KIX complex at pH 5.5 and 27°C. (Radhakrishnan *et al.*, 1999), indicating consistency between the KID binding sites obtained by chemical-shift mapping methods and the structure of the pKID-KIX complex.

The surface recognized by pKID is different to the region of KIX that interacts with pJun(47-89) (Figure 6.15 and Figure 6.16), indicating that c-Jun and CREB bind KIX at different sites.

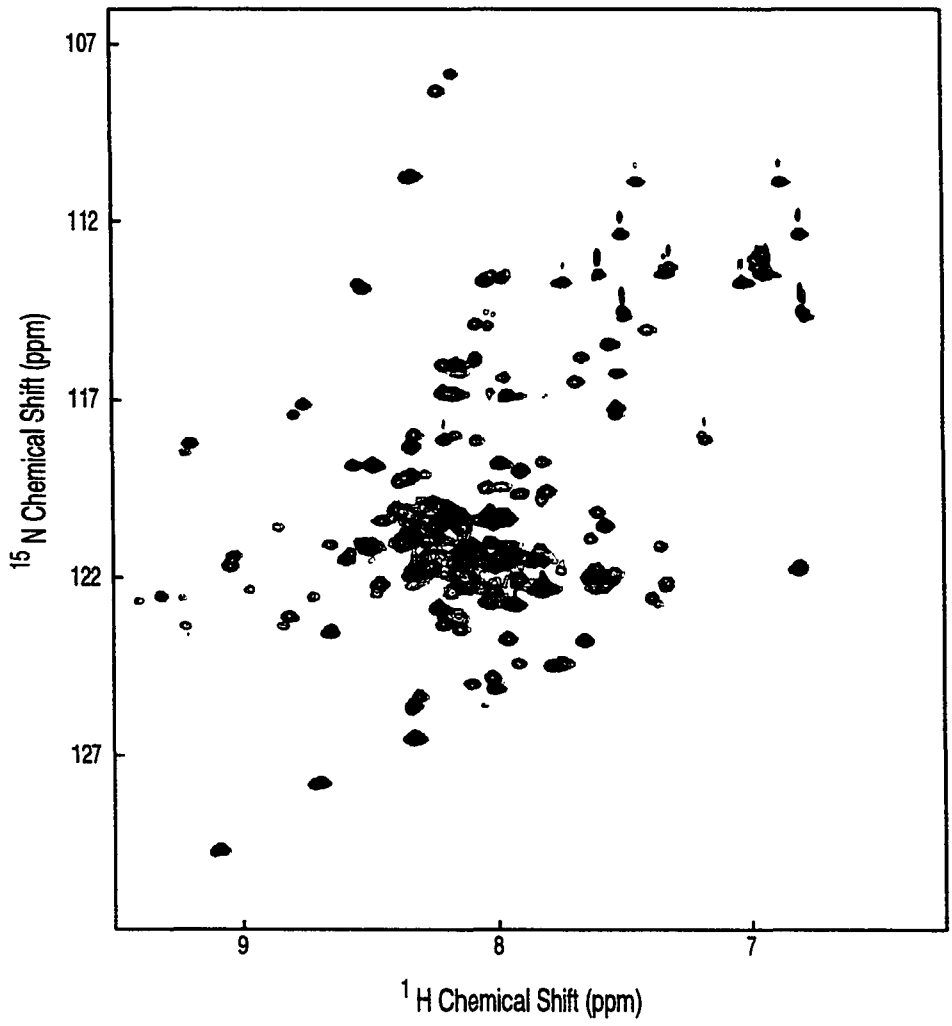

Figure 6.14. HSQC spectra of ^{15}N KIX and ^{15}N KIX-pKID. The ^{15}N KIX spectrum is shown in black and the ^{15}N KIX-pKID spectrum is shown in red.

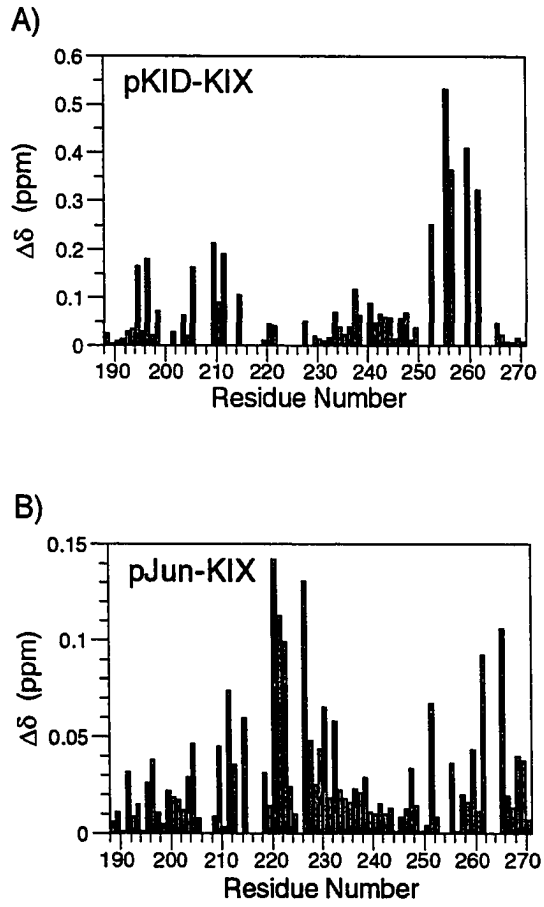

Figure 6.15. Chemical-shift changes (Δδ) induced in KIX by (A) pKID and (B) pJun(47-89). Changes are normalized averages from the amide ^{1}H and N chemical-shift changes as described in Section 6.3.I.

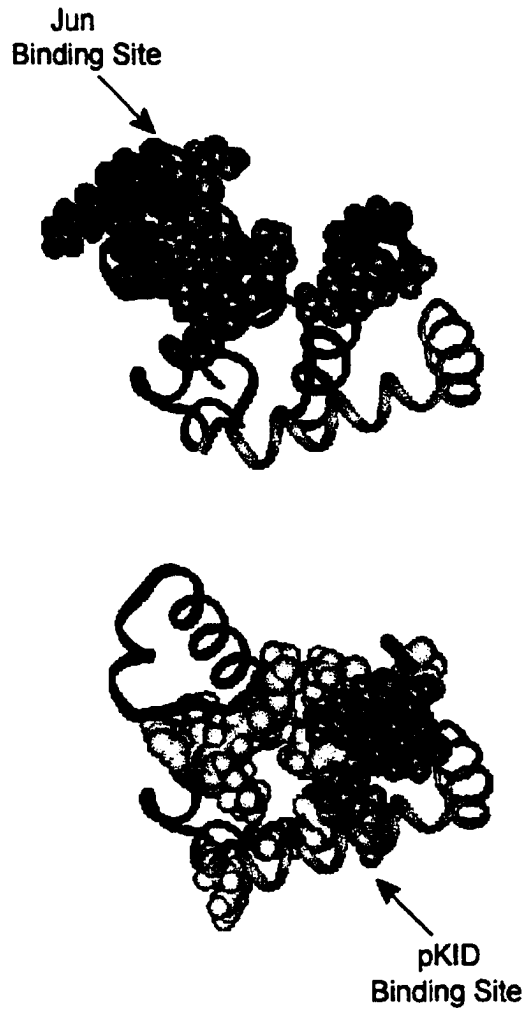

Figure 6.16. pJun(47-89) and pKID recognize different surfaces of KIX.
The amino acids of KIX which have the largest chemical-shift changes induced by pJun(47-89) and pKID are shown as Van der Waals surfaces. (A.) Chemical shift changes greater than 0.1 induced by pJun(47-89) are shown in dark blue and changes between 0.05-0.1 are shown in light blue. (B.) Chemical shift changes greater than 0.2 ppm induced by pKID are shown in green and changes between 0.1-0.2 ppm are shown in yellow. In addition to the chemical shift changes described in Section 6.3.I, the changes observed by Radhakrishnan, *et. al* (1997), which are unresolved in our data set, are also shown. Both pKID and pJun(47-89) cause chemical-shift changes on a contiguous surface of KIX. However, the two surfaces are different, indicating that the two activation domains recognize different regions of KIX.

6.4.I. pJun(47-89) and KID Simultaneously Bind KIX

The different KIX-binding surfaces utilized by pKID and the c-Jun activation domain suggest that the CREB and c-Jun domains can bind KIX simultaneously. Formation of KIX binary and ternary complexes was monitored with solution ^{31}P NMR experiments (Figure 6.17). The Ser 133 ^{31}P resonances of pKID in the free and KIX-bound pKID are in slow exchange, such that dissociation of pKID is detected by the presence of a ^{31}P resonance at the chemical shift of free KID. The Ser 63 and Ser 73 ^{31}P resonances of pJun(47-89) in free and KIX-bound states are in fast exchange, such that complete dissociation of pJun(47-89) is detected as a resonance at the chemical shift of unbound pJun(47-89).

Addition of equimolar KIX to either pKID or pJun(47-89) causes changes in the chemical shifts of the ^{31}P resonances that reflect essentially complete formation of the complex (Figure 6.17). The resonances of an equimolar solution of KIX, pKID and pJun(47-89) fall at the values seen for the binary KIX-pKID and KIX-pJun(47-89) complexes, suggesting that the three proteins form a ternary complex with pKID and pJun(47-89) occupying the same binding sites of KIX as in the bimolecular complexes. No evidence is seen for unbound pKID or pJun(47-89) in the equimolar solution. The ^{31}P chemical shifts of pKID and pJun(47-89) are not changed upon mixing the two domains in the absence of KIX, indicating that pKID and pJun(47-89) do not form a binary complex.

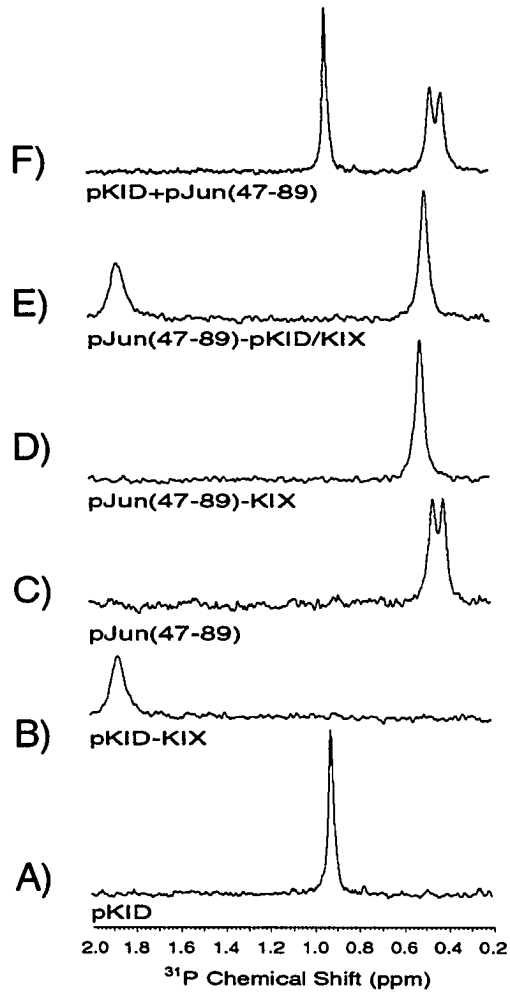

Figure 6.17. KIX can simultaneously bind pKID and pJun(47-89). ^{31}P chemical shifts of the pSer resonances were used as probes of the free and bound states of pKID and pJun(47-89). Formation of the binary KIX complexes cause changes in the ^{31}P resonances of pKID (spectra A and B) and pJun(47-89) (spectra C and D). These same changes are also induced when the three proteins are mixed together, suggesting formation of the ternary KIX-pKID-pJun(47-89) complex (spectrum E). Mixing of pKID and pJun(47-89) in the absence of KIX does not result in any chemical-shift changes (spectrum F). All proteins are present in equimolar amounts with no indication of either unbound pKID or pJun(47-89) in the presence of KIX.

In addition to the ^{31}P NMR results, many of the H^N and N chemical shift changes observed in ^{1}H-^{15}N HSQC spectra of KIX upon binding pKID or pJun(47-89) individually are also seen when both pKID and pJun(47-89) are present, again suggesting formation of a ternary complex with pKID and pJun(47-89) occupying the same binding sites of KIX as in the bimolecular complexes (Figure 6.18). The ^{31}P and HSQC chemical-shift data indicate that KIX, pKID and pJun(47-89) form a ternary complex.

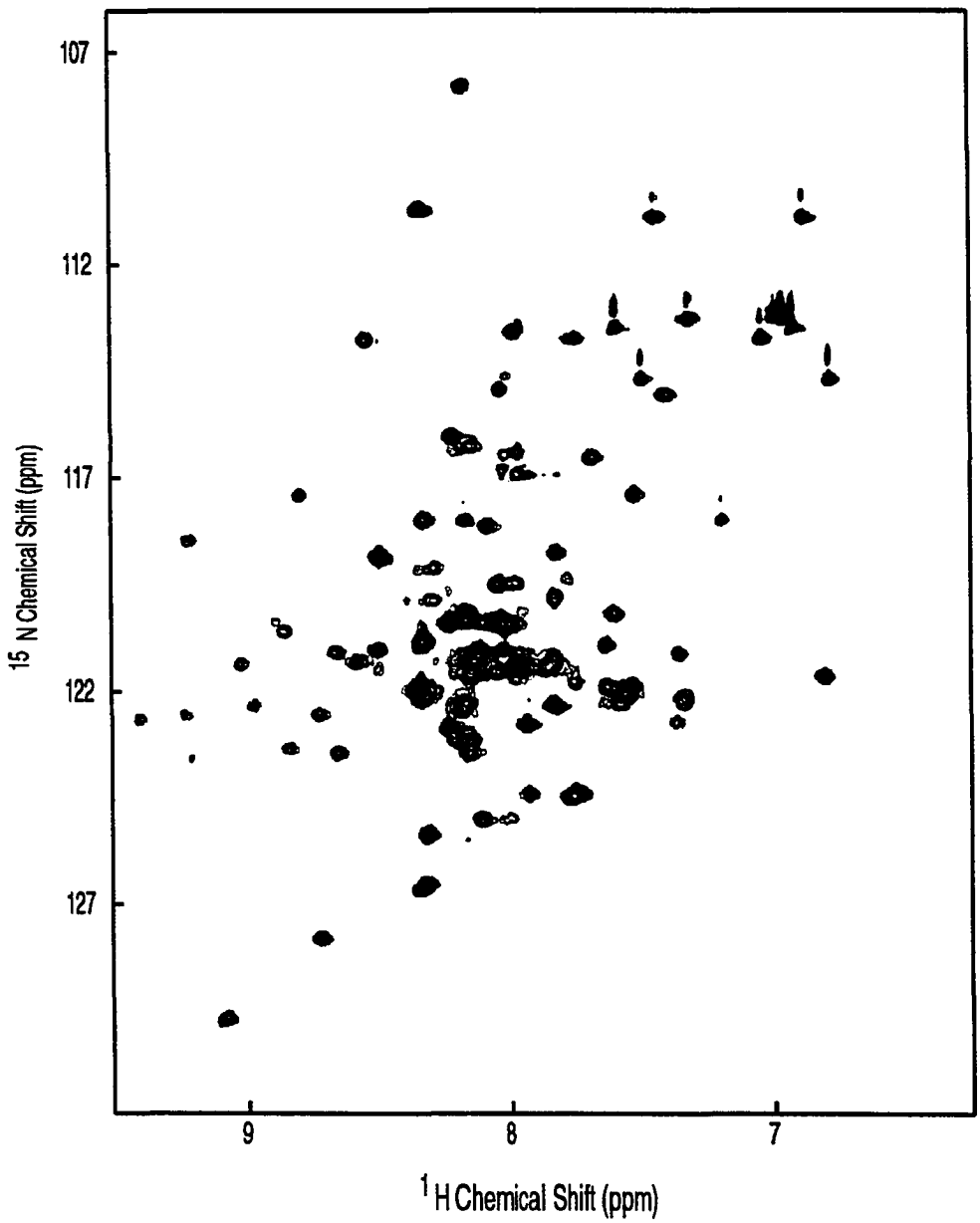

Figure 6.18. HSQC spectra of ^{15}N KIX-pKID and ^{15}N KIX-pKID-pJun(47-89). The ^{15}N KIX-pKID spectrum is shown in black and the ^{15}N KIX-pKID-pJun(47-89) spectrum is shown in red.

6.5. DISCUSSION

Formation of protein-protein complexes involving transcriptional activators and other factors such as the coactivator CBP form a central component to the regulation of gene expression (1-4). The KIX domain of CBP can bind numerous activation domains (Goodman & Smolik, 2000; Chan & Thangue, 2001). Formation of the CREB complex with KIX is inducible upon Ser 133 phosphorylation of the KID region of CREB (Kwok *et al.*, 1994; Parker *et al.*, 1996). In contrast, other activators bind constitutively to KIX without a requirement for post-translational modification. Examples of constitutive KIX-binding activators include the mammalian activators BRCA1, c-Jun, c-Myb, p53, Sap1a, SREBP, and the viral activators papillomavirus E2 and HTLV-1 Tax (Bannister *et al.*, 1994; Dai *et al.*, 1996; Janknecht & Nordheim, 1996; Oelgeschlager *et al.*, 1996; Oliner *et al.*, 1996; Van Orden *et al.*, 1999a; Van Orden *et al.*, 1999b; Lee *et al.*, 2000; Pao *et al.*, 2000).

The KID region of CREB binds to a shallow, hydrophobic groove of KIX (Radhakrishnan *et al.*, 1997). KID is largely unfolded in isolation and folds to form two helices upon binding KIX (Radhakrishnan *et al.*, 1997). The coupled folding and binding event introduces a significant entropy barrier to binding (Parker *et al.*, 1999), which is compensated for upon KID phosphorylation at Ser 133 by the unusually strong electrostatic contribution of the phosphate group to the binding free energy (Mestas & Lumb, 1999; Parker *et al.*, 1999). Inducible formation of the CREB-CBP complex is thus under thermodynamic control by

phosphorylation. A mechanism of constitutive activation is exemplified by c-Myb, which binds KIX without post-translational modification (Dai *et al.*, 1996; Oelgeschlager *et al.*, 1996). In contrast to KID, the c-Myb activation domain is partially folded (helical) prior to binding, which reduces the entropy penalty relative to that experienced by KID so that binding is constitutive (Parker *et al.*, 1999).

The results presented here show that c-Jun utilizes a distinctly different mode of KIX binding than employed by the KID region of CREB. Like KID, the N-terminal activation domain of c-Jun is devoid of significant preformed helical structure. Formation of the Jun-KIX complex results in an increase in helical structure formation, and so Jun binding to KIX is coupled with folding as seen in the formation of the pKID-KIX complex (Radhakrishnan *et al.*, 1997) and other activation-domain complexes (Kussie *et al.*, 1996; Uesugi *et al.*, 1997). Unlike KID, the results presented here and elsewhere (Bannister *et al.*, 1995; Van Orden *et al.*, 1999b) show that c-Jun phosphorylation is not a prerequisite for binding KIX. Therefore c-Jun phosphorylation does not contribute significantly to the binding enthalpy to overcome the entropy penalty associated with folding upon binding. Instead, chemical-shift mapping shows that c-Jun binds to a different surface of KIX than KID, and in doing so must form protein-protein interactions that make a more favorable enthalpic contribution to binding than realized by KID.

Other transcriptional activators may employ the c-Jun-binding site of KIX. For example, HTLV-1 Tax competes with c-Jun but not with CREB for binding KIX (Van Orden *et al.*, 1999b), suggesting that Tax binds to a similar surface of KIX to that observed here for c-Jun. Tax also competes with p53 and c-Myb for binding the KIX domain of CBP (Colgin & Nyborg, 1998; Van Orden *et al.*, 1999a), and with MyoD for binding the p300 KIX domain (Riou *et al.*, 2000), suggesting indirectly that p53, c-Myb and MyoD utilize the c-Jun binding site on KIX. In addition, the MLL (mixed-lineage leukemia) gene product can also bind KIX simultaneously with CREB (Ernst *et al.*, 2001), and possibly binds the same site on KIX as c-Jun.

Multiple contacts between transcription factors contribute greatly to transcriptional synergy and assembly of the enhancesome (Ptashne & Gann, 1997; Carey, 1998). Upstream regulatory sequences typically contain binding sites for multiple activators. For example, the tyrosine hydroxylase gene contains both AP-1 and CREB sites (Ghee *et al.*, 1998). The results presented here show that activation domains from c-Jun and CREB can bind KIX simultaneously, allowing combinatorial targeting of the KIX domain at genes that contain both AP-1 and CREB sites. Given that CBP may be present at limiting levels *in vivo*, simultaneous binding of CBP by two different transcriptional activators that target the c-Jun and CREB binding sites of KIX is likely to contribute greatly to the specificity and synergy of gene expression by resulting in the enhanced recruitment of CBP to target promoters.

REFERENCES

Abate, C., Luk, D. & Curran, T. (1991). Transcriptional regulation by Fos and Jun in vitro: Interaction among multiple activator and regulatory domains. *Molecular and Cellular Biology, 11*, 3624-3632.

Akey, D. L., Malashkevich, V. N. & Kim, P. S. (2001). Buried polar residues in coiled-coil interfaces. *Biochemistry, 40*, 6352-6360.

Arias, j., Alberts, A., Brindle, P., Claret, F., Smeal, T., Karin, M., Feramisco, J. & Montminy, M. (1994). Activation of cAMP amd mitogen responsive genes relies on a common nuclear factor. *Nature, 370.*

Bai, Y., Milne, J. S., Mayne, L. & Englander, S. W. (1994). Protein stability parameters measured by hydrogen exchange. *Proteins: Structure, Function and Genetics, 20*, 4-14.

Bannister, A. J., Brown, H. J., Sutherland, J. A. & Kouzarides, T. (1994). Phosphorylation of the c-Fos and c-Jun HOB1 motif stimulates its activation capacity. *Nucleic Acids Research,* 22, 5173-5176.

Bannister, A. J. & Kouzarides, T. (1995). CBP-induced stimulation of c-Fos activity is abrogated by E1A. *European Molecular Biology Organization Journal, 14*, 4758-4762.

Bannister, A. J., Oehler, T. W., D., Angel, P. & Kouzarides, T. (1995). Stimulation of c-Jun activity by CBP: c-Jun residues Ser63/73 are required for CBP induced stimulation *in vivo* and CBP binding *in vitro*. *Oncogene, 11*, 2509-2514.

Barlow, D. J. & Thornton, J. M. (1983). Ion-pairs in proteins. *Journal of Molecular Biology, 168*, 867-885.

Bax, A. & Ikura, M. (1991). An efficient 3D NMR technique for correlating the proton and ^{15}N backbone amide resonances with the alpha-carbon of the preceding residue in uniformly $^{15}N/^{13}C$ proteins. *Journal of Biomolecular NMR, 1*, 99-104.

Behrens, A., Sibilia, M. & Wagner, E. (1999). Amino-terminal phosphorylation of c-Jun regulates stress-induced apoptosis and cellular proliferation. *National Geneics., 21*, 326-329.

Berger, B., Wilson, D. B., Tonchev, T., Milla, M. & Kim, P. S. (1995). Predicting coiled coils using pairwise-residue correlations. *Proceedings of the National Academy of Sciences, U.S.A., 92*, 8259-8263.

Betz, S., Fairman, R., O'Neil, K., Lear, J. & DeGrado, W. (1995). Design of two-stranded and three-stranded coiled coil peptides. *Phil. Tran. Roy. Soc. Lond. B, 348*, 81-88.

Betz, S. F., Raleigh, D. P. & DeGrado, W. F. (1993). *De novo* protein design: From molten globules to native-like states. *Current Opinion in Structural Biology, 3*, 601-610.

Bienkiewicz, E. A., Adkins, J. N. & Lumb, K. J. (2002). Role of local helix formation in the intrinsically disordered cell-cycle inhibitor $p27^{Kip1}$. *Biochemistry, 41*, 752-759.

Bohmann, S. L. a. D. (1999). Diverse functions of JNK signaling and c-Jun in stress response and apoptosis. *Oncogene,*, 6158-6162.

Bolon, D. N. & Mayo, S. L. (2001). Polar residues in the protein core of *Escherichia coil* thioredoxin are important for fold specificity. *Biochemistry, 40*, 10047-10053.

Burkhard, P., Stetefeld, J. & Strelkov, S. V. (2001). Coiled coils: a highly versatile protein folding motif. *Trends in Cell Biology, 11*, 82-88.

Burley, S. K. & Roeder, R. G. (1996). Biochemistry and structural biology of transcription factor IID (TFIID). *Annual Review of Biochemistry, 65*, 769-799.

Campbell, K. M., Terrell, A. R., Laybourn, P. J. & Lumb, K. J. (2000). Intrinsic structural disorder of the C-terminal activation domain from the bZIP transcription factor Fos. *Biochemistry, 39*, 2708-2713.

Campbell, K.M., Ranallo, R.T., Stargell, L..A., Lumb, K.J. (2000b). Reevaluation of transcriptional regulation by TATA binding protein: Predominance of monomers. *Biochemistry*, 39, 2633-2638.

Campbell. K.M., Sholders, A.J., Lumb, K.J. (2002). Contribution of buried lysine residues to the oligomerization specificity and stability of the Fos coiled coil. in press *Biochemistry*.

Campbell, K.M. & Lumb, K. J. (2002a). Complementation of buried lysine and surface polar residues in a designed heterodimeric coiled coil. accepted for publication in *Biochemistry*.

Campbell, K.M. & Lumb, K. J. (2002b). Structurally distinct modes of recognition of the KIX domain of CBP by Jun and CREB. submitted to *Proceedings of the National Academy of Sciences.*

Cantor, C. R. & Schimmel, P. R. (1980). *Biophysical Chemistry*, Freeman, New York.

Carey, M. (1998). The enhanceosome and transcriptional synergy. *Cell, 92*, 5-8.

Chan, H. & Thangue, N. L. (2001). p300/CBP proteins: HATs for transcriptional bridges and scaffolds. *Journal of Cellular Science., 114*, 2363-2373.

Chang, J., Kim, D., Lee, S. W., Choi, K. Y. & Sung, Y. C. (1995). Transactivation ability of p53 transcriptional activation domain is directly related to the binding affinity to TATA-binding protein. *Journal of Biological Chemistry, 270*, 25014-25019.

Chasman, D. I., Flaherty, K. M., Sharp, P. A. & Kornberg, R. A. (1993). Crystal structure of yeast TATA-binding protein and model for interaction with DNA. *Proceedings of the National Academy of Sciences. 90*, 8174-8178.

Chen, R.-H., Juo, P. C.-H., Curran, T. & Blenis, J. (1996). Phosphorylation of c-Fos at the C-terminus Enhances Its Transforming Activity. *Oncogene, 12*, 1493-1502.

Chen, Y.-H., Yang, J. T. & Martinez, H. M. (1972). Determination of the secondary structure of proteins by circular dichroism and optical rotatory dispersion. *Biochemistry, 11*, 4120-4131.

Chinenov, Y. & Kerppola, T. (2001). Close encounters of many kinds: Fos-Jun interactions that mediate transcription regulatory specificity. *Oncogene, 20*, 2438-2452.

Cho, H. S., Liu, C. W., Damberger, F., Pelton, J., Nelson, H. & Wemmer, D. (1996). Yeast heat shock transcription factor N-terminal activation domains are unstructured as probed by heteronuclear NMR spectroscopy. *Protein Science, 5*, 262-269.

Christensen, T., Gross, E. & Meienhofer, J. (1979). Peptides, structure and biological function. *Pierce Chemical Company,* 385-8.

Chrivia, J. C., Kwok, R. P. S., Lamb, N., Hagiwara, M., Montminy, M. R. & Goodman, R. H. (1993). Phosphorylated CREB binds specifically to the nuclear protein CBP. *Nature, 365*, 855-859.

Coleman, R. A. & Pugh, B. F. (1997). Slow dimer dissociation of the TATA binding protein dictates the kinetics of DNA binding. *Proceedings of the National Academy of Sciences, 94*, 7221-7226.

Coleman, R. A., Taggart, A. K. P., Benjamin, L. R. & Pugh, B. F. (1995). Dimerization of the TATA binding protein. *Journal of Biological Chemistry, 270*, 13842-13849.

Colgan, J. & Manley, J. L. (1992). TFIID can be rate limiting in vivo for TATA-containing, but not TATA-lacking, RNA polymerase II promoters. *Genes and Development, 6*, 304-315.

Colgin, M. A. & Nyborg, J. K. (1998). The human T-cell leukemia virus type 1 oncoprotein Tax inhibits the transcriptional activity of c-Myb through competition for the CREB binding protein. *Journal of Virology, 72*, 9396-9399.

Conway, J. F. & Parry, D. A. D. (1990). Structural features in the heptad substructure and longer range repeats of two-stranded alpha-fibrous proteins. *International Journal of Biological Macromolecules, 12*, 328-334.

Creighton, T. E. (1993). *Proteins: Structures and Molecular Properties*. 2nd edit, W. H. Freeman and Company, New York, NY.

Curran, T. & Morgan, J. I. (1995). Fos: An immediate-early transcription factor in neurons. *J. Neurobiology, 26*, 403-412.

Curran, T. & Vogt, P. K. (1992). Dangerous liaisons: Fos and Jun, oncogenic transcription factors. In *Transcriptional Regulation*, pp. 797-831. Cold Spring Harbor Laboratory Press.

Cusack, S., Berthet-Colominas, C., Härtlein, M., Nassar, N. & Leberman, R. (1990). A second class of synthetase structure revealed by X-ray analysis of *Escherichia coil* seryl-tRNA synthetase at 2.5 Å. *Nature, 347*, 249-255.

Dahlman-Wright, K., Baumann, H., McEwan, I., Almlof, T., Wright, A., Gustafsson, J.-A. & Hard, T. (1995). Structural characterization of a minimal functional transactivation domain from the human glucocorticoid receptor. *Proceedings of the National Academy of Sciences, 92*, 1699-1703.

Dai, P., Akimaru, H., Tanaka, Y., Hou, D. X., Yasukawa, T., Kanei-Ishii, C., Takahashi, T. & Ishii, S. (1996). CBP as a Transcriptional Coactivator of c-Myb. *Genes and Development, 10*, 528-540.

Daugherty, M. A., Brenowitz, M. & Fried, M. G. (1999). The TATA-binding protein from *Saccharomyces cerevisiae* oligomerizes in solution at micromolar concentrations to form tetramers and octomers. *Journal of Molecular Biology, 285*, 1389-1399.

Delaglio, F., Grzesiek, S., Vuister, G. W., Zhu, G., Pfeifer, J. & Bax, A. (1995). NMRPipe: A multidimensional spectral processing system based on UNIX pipes. *Journal of Biomolecular NMR, 6*, 277-293.

Donaldson, L. & Capone, J. P. (1992). Purification and characterization of the carboxyl-terminal transactivation domain of Vmw65 from herpes simplex virus type 1. *Journal of Biological Chemistry, 267*, 1411-1414.

Donne, D. G., Viles, J. H., Groth, D., Mehlhorn, I., James, T. L., Cohen, F. E., Prusiner, S. B., Wright, P. E. & Dyson, H. J. (1997). Structure of the recombinant full-length hamster prion protein PrP(29-231): The N terminus is highly flexible. *Proceedings of the National Academy of Sciences, 94*, 13452-13457.

Dyson, H. J. & Wright, P. E. (1996). Insights into Protein Folding from NMR. *Annual Review of Physical Chemistry, 47*, 369-395.

Eckert, D. M., Malashkevich, V. N. & Kim, P. S. (1998). Crystal structure of GCN4-pI_QI, a trimeric coiled coil with buried polar residues. *Journal of Molecular Biology, 284*, 859-865.

Edelhoch, H. (1967). Spectroscopic determination of tryptophan and tyrosine in proteins. *Biochemistry, 6*, 1948-1954.

Emili, A. & Ingles, C. (1995). Promoter-dependent Photocross-linking of the Acidic Transcriptional Activator E2F-1 to the TATA-binding Protein. *The Journal of Biological Chemistry, 270*, 13674-13680.

Englander, S. W., Downer, N. W. & Teitelbaum, H. (1972). Hydrogen exchange. *Annual Review of Biochemistry, 41*, 903-924.

Ernst, P., Wang, J., Huang, M., Goodman, R. H. & Korsmeyer, S. J. (2001). MLL and CREB bind cooperatively to the nuclear coactivator CREB-binding protein. *Molecular and Cellular Biology, 21*, 2249-2258.

Farrow, N. A., Muhandiram, R., Singer, A. U., Pascal, S. M., Kay, C. M., Gisg, G., Shoelson, S. E., Pawson, T., Forman-Kay, J. D. & Kay, L. E. (1994). Backbone dynamics of a free and phosphopeptide-complexed Src homology 2 domain studied by ^{15}N NMR relaxation. *Biochemistry, 33*, 5984-6003.

Farrow, N. A., Zhang, O., Forman-Kay, J. D. & Kay, L. E. (1997). Characterization of the backbone dynamics of folded and denatured states of an SH3 domain. *Biochemistry, 36*, 2390-2402.

Forrest, D. & Curran, T. (1992). Crossed signals: Oncogenic transcription factors. *Current Opinion in Genetics and Development, 2*, 19-27.

Frankel, A. D. & Kim, P. S. (1991). Modular structure of transcription factors: Implications for gene regulation. *Cell, 65*, 717-719.

Frankel, A. D. & Smith, C. A. (1998). Induced folding in RNA-protein recognition: More than a simple molecular handshake. *Cell, 92*, 149-151.

Franklin, C., McCulloch, A. & Craft, A. (1995). In vitro association between the Jun protein family and the general transcription factors, TBP and TFIIB. *Journal of Biochemistry, 3305*, 967-74.

Funk, M., Poensgen, B., Graulich, W., Jerôme, V. & Müller, R. (1997). A novel, transformation-relevant activation domain in Fos proteins. *Molecular and Cellular Biology, 17*, 537-544.

Geisberg, J., Lee, W., Berk, A. & Ricciardi, R. (1994). The zinc finger region of the adenovirus E1A transactivaating domain complexes with the TATA box binding protein. *Proceedings of the National Academy of Science, 29*, 2488-92.

Ghee, M., Baker, H., Miller, J. & Jiff, E. (1998). AP-1, CREB and CBP transcription factors differentially regulate the tryrosine hydroxylase gene. *Brain Research Molecular Brain Research., 55*, 101-114.

Giles, R. H., Peters, D. J. M. & Breuning, M. H. (1998). Conjunction dysfunction: CBP/p300 in human disease. *Trends in Biochemical Sciences, 14*, 178-183.

Glover, J. N. M. & Harrison, S. C. (1995). Crystal structure of the heterodimeric bZIP transcription factor c-Fos-c-Jun bound to DNA. *Nature, 373*, 257-261.

Goldman, P. S., Tran, V. K. & Goodman, R. H. (1997). The multifunctional role of the co-activator CBP in transcriptional regulation. *Recent Prog. Horm. Res., 52*, 103-119.

Gonzalez, L., Brown, R. A., Richardson, D. & Alber, T. (1996a). Crystal structures of a single coiled-coil peptide in two oligomeric states reveal the basis for structural polymorphism. *Nature Structural Biology, 3*, 1002-1009.

Gonzalez, L., Woolfson, D. N. & Alber, T. (1996b). Buried polar residues and structural specificity in the GCN4 leucine zipper. *Nature Structural Biology, 3*, 1011-1018.

Goodman, R. H. & Smolik, S. (2000). CBP/p300 in cell growth, transformation and development. *Genes and Development, 14*, 1553-1577.

Goto, Y. & Fink, A. L. (1989). Conformational states of β-lactamase: Molten globule states at acidic and alkaline pH with high salt. *Biochemistry, 28*, 945-952.

Guzman, R., Liu, H., Martinez-Yamout, M., Dyson, H. & Wright, P. (2000). Solution Structure of the TAZ2(CH3) Doamin of the Transcriptional Adaptor Protein CBP. *Journal of Molecular Biology, 303*, 243-253.

Handel, T. M., Williams, S. A. & DeGrado, W. F. (1993). Metal ion-dependent modulation of the dynamics of a designed protein. *Science, 261*, 879-885.

Harbury, P. B., Kim, P. S. & Alber, T. (1994). Crystal structure of an isoleucine-zipper trimer. *Nature, 371*, 80-83.

Harbury, P. B., Zhang, T., Kim, P. S. & Alber, T. (1993). A switch between two-, three-, and four stranded coiled coils in GCN4 leucine zipper mutants. *Science, 262*, 1401-1407.

Hendsch, Z. S. & Tidor, B. (1994). Do salt bridges stabilize proteins? A continuum electrostatic analysis. *Protein Science, 3*, 211-226.

Hensley, P. (1996). Defining the structure and stability of macromolecular assemblies in solution: The re-emergence of analytical ultracentrifugation as a practical tool. *Structure, 4*, 367-373.

Hermann, S., Berndt, K. & Wright, A. (2001). How Transcriptional Activators Bind Target Proteins. *The Journal of Biological Chemistry, 276*, 40127-40132.

Hill, R. B., Raleigh, D. P., Lombardi, A. & DeGrado, W. F. (2000). De novo design of helical bundles as models for protein folding and function. *Accounts of Chemical Research, 33*, 745-754.

Hua, Q., Jia, W., Bullock, B. P., Habener, J. F. & Weiss, M. A. (1998). Transcriptional activator-coactivator recognition: Nascent folding of a kinase-inducible transactivation domain predicts its structure on coactivator binding. *Biochemistry, 37*, 5858-5866.

Ikura, M., Kay, L. & Bax, A. (1990). A novel approach for sequential assignment of ^{1}H, ^{13}C, and ^{15}N spectra of proteins: heteronuclear triple resonance three-dimensional NMR spectroscopy. Application to calmodulin. *Biochemistry, 15*, 4659-67.

Jackson-Fisher, A. J., Burma, S., Portnoy, M., Schneeweis, L. A., Coleman, R. A., Mitra, M., Chitikila, C. & Pugh, B. F. (1999a). Dimer dissociation and thermosensitivity kinetics of the *Saccharomyces cerevisiae* and human TATA binding proteins. *Biochemistry, 38*, 11340-11348.

Jackson-Fisher, A. J., Chitikila, C., Mitra, M. & Pugh, B. F. (1999b). A role for TBP dimerization in preventing unregulated gene expression. *Molecular Cell, 3*, 717-727.

Janknecht, R. & Nordheim, A. (1996). Regulation of the c-fos promoter by the ternary complex factor Sapla and its coactivator CBP. *Oncogene, 12*, 1961-1969.

Jochum, W., Passegué, E. & Wagner, E. F. (2001). AP-1 in mouse development and tumorigenesis. *Oncogene, 20*, 2401-2412.

John, M., Briand, J., Granger-Schnarr, M. & Schnarr, M. (1994). Two pairs of oppositely charged amino acids fron jun and fos confer heterodimerization to the GCN4 leucine zipper. *Journal of Biological Chemistry, 269*, 16247-16253.

Johnson, B. A. & Blevins, R. A. (1994). NMRView: A computer program for the visualization and analysis of NMR data. *Journal of Biomolecular NMR, 4*, 603-614.

Junius, F. K., Mackay, J. P., Bubb, W. A., Jensen, S. A., Weiss, A. S. & King, G. F. (1995). Nuclear magnetic resonance characterization of the Jun leucine zipper domain: Unusual properties of coiled-coil interfacial polar residues. *Biochemistry, 34*, 6164-6174.

Kaiser, E., Bossinger, R. & Cook, C. (1970). Color test for detection of free amino groups groups in the solid- phase synthesis of peptides. *Analytical Biochemistry, 267*, 4213-21.

Karin, M., Liu, Z. & Zandi, E. (1997). AP-1 Function and Regulation. *Current Opinion in Cell Biology, 9*, 240-246.

Kato, K., Makino, Y., Kishimoto, T., Yamauchi, J., Kato, S., Muramatsu, M. & Tamura, T. (1994). Multimerization of the mouse TATA-binding protein (TBP) driven by its C-terminal conserved domain. *Nucleic Acids Research, 22*, 1179-1185.

Kay, L., Keifer, P. & Saarinen, T. (1992). Pure absorption gradient enhanced heteronuclear single quantum correlation spectroscopy with improved sensitivity. *Journal of the American Chemical Society, 114*, 10663-10665.

Kay, L., Xu, G. & Yamazaki, T. (1994). Enhanced-Sensitivity Triple-Resonance Spectroscopy with Minimal H_20 Saturation. *Journal of Magnetic Resonance, 109*, 129-133.

Kerppolla, T. K. & Curran, T. (1991). Transcription factor interactions: basics on zippers. *Current Opinion in Structural Biology, 1*, 71-79.

Kim, Y., Geiger, J. H., Hahn, S. & Sigler, P. B. (1993). Crystal structure of a yeast TBP/TATA-box complex. *Nature, 365*, 512-520.

Kohn, W. D. & Hodges, R. S. (1998). *De novo* design of α-helical coiled coils and bundles: models for the development of protein-design principles. *Trends in Biotechnology, 16*, 379-389.

Kriwacki, R. W., Hengst, L., Tennant, L., Reed, S. I. & Wright, P. E. (1996). Structural studies of $p21^{Waf1/Cip1/Sdi1}$ in the free and Cdk2-bound state: Conformational disorder mediates binding diversity. *Proceedings of the National Academy of Sciences, 93*, 11504-11509.

Kuras, L. & Struhl, K. (1999). Binding of TBP to promoters *in vivo* is stimulated by activators and requires Pol II holoenzyme. *Nature, 399*, 609-613.

Kussie, P. H., Gorina, S., Marechal, V., Elenbaas, B., Moreau, J., Levine, A. J. & Pavletich, N. P. (1996). Structure of the MDM2 oncoprotein bound to the p53 tumor suppressor transactivation domain. *Science, 274*, 948-953.

Kuwajima, K. (1989). The molten globule state as a clue for understanding the folding and cooperativity of globular-protein structure. *Proteins: Structure, Function and Genetics, 6*, 87-103.

Kwok, R. P. S., Lundblad, J. R., Chrivia, J. C., Richards, J. P., Bachinger, H. P., Brennan, R. G., Roberts, S. G. E., Green, M. R. & Goodman, R. H. (1994). Nuclear protein CBP is a coactivator for the transcription factor CREB. *Nature, 370*, 223-226.

Laue, T. M. (1995). Sedimentation equilibrium as thermodynamic tool. *Methods in Enzymology, 259*, 427-452.

Laue, T. M., Shah, B. D., Ridgeway, T. M. & Pelletier, S. L. (1992). Computer-aided interpretation of analytical sedimentation data for proteins. In *Analytical Ultracentrifugation in Biochemistry and Polymer Science* (Harding, S. E., Rowe, A. J. & Horton, J. C., eds.), pp. 90-125. The Royal Society of Chemistry, Cambridge.

Lech, K., Anderson, K. & Brent, R. (1988). DNA-Bound Fos Proteins Activate Transcription in Yeast. *Cell, 52*, 179-184.

Lee, D. K., Dejong, J., Hashimoto, S., Horikoshi, M. & Roeder, R. G. (1992). TFIIA induces conformational changes in TFIID via interactions with the basic repeat. *Molecular and Cellular Biology, 12*, 5189-5196.

Lee, H., Mok, K. H., Muhandiram, R., Park, K., Suk, J., Kim, D., Chang, J., Sung, Y. C., Choi, K. Y. & Han, K. (2000). Local structural elements in the mostly

unstructured transcriptional activation domain of human p53. *Journal of Biological Chemistry, 275*, 29426-29432.

Lemon, B. & Tjian, R. (2000). Orchestrated response: a symphony of transcription factors for gene control. *Genes and Development, 14*, 2551-2569.

Li, X., Virbasius, A., Zhu, X. & Green, M. R. (1999). Enhancement of TBP binding by activators and general transcription factors. *Nature, 399*, 605-609.

Lieberman, P. M., Schmidt, M. C., Kao, C. C. & Berk, A. J. (1991). Two distinct domains in the yeast transcription factor IID and evidence for a TATA box-induced conformational change. *Molecular and Cellular Biology, 11*, 63-74.

Lin, C., Hare, B., Wagner, G., Harrison, S., Maniatis, T. & Fraenkel, E. (2001). A Solution Domain of CBP/p300 Binds Diverse Proteins: Solution Structure and Functional Studies. *Molecular Cell, 8*, 581-590.

Liu, Y. & Schepartz, A. (2001). Kinetic Preference for Oriented Binding by the Yeast TATA-Binding Protein TBP. *Biochemistry, 40*, 6257-6266.

Lumb, K. J., Carr, C. M. & Kim, P. S. (1994). Subdomain folding of the coiled coil leucine zipper from the bZIP transcriptional activator GCN4. *Biochemistry, 33*, 7361-7367.

Lumb, K. J. & Kim, P. S. (1994). Formation of a hydrophobic cluster in denatured bovine pancreatic trypsin inhibitor. *J. Mol. Biol., 236*, 412-420.

Lumb, K. J. & Kim, P. S. (1995). A buried polar interaction imparts structural uniqueness in a designed heterodimeric coiled coil. *Biochemistry, 34*, 8642-8648.

Lumb, K. J. & Kim, P. S. (1996). Interhelical salt bridges, coiled coil stability, and specificity of dimerization. *Science, 271*, 1137-1138.

Lupas, A. (1996). Coiled coils: new structures and new functions. *Trends in Biological Sciences, 21*, 375-382.

Lupas, L., Van Dyke, M. & Stock, J. (1991). Predicting coiled coils from protein sequences. *Science, 252*, 1162-1164.

Martínez-Balbás, M. A., Bannister, A. J., Martin, K., Haus-Seuffert, P., Meisterernst, M. & Kouzarides, T. (1998). The acetyltransferase activity of CBP stimulates transcription. *EMBO Journal, 17*, 2886-2893.

Matthias, J., Briand, J. & Schnarr, M. (1996). A c-Jun activation domain peptide and its corresponding phosphopeptide have potential to adopt alpha-helical conformation. *Peptide Research,*.

Maxwell, K. L. & Davidson, A. R. (1998). Mutagenesis of a buried polar interaction in an SH3 domain: Sequence conservation provides the best prediction of stability effects. *Biochemistry, 37*, 16172-16182.

McBride, K. & Nemer, M. (1998). The C-Terminal Domain of c-Fos is Required for Activation of an AP-1 Site Specific for Jun-Fos Heterodimers. *Molecular and Cellular Biology, 18*, 5073-5081.

McEwan, I. J., Dahlman-Wright, K., Ford, J. & Wright, A. P. H. (1996). Functional interaction of the c-Myc transactivation domain with the TATA binding protein: Evidence for an induced fit model of transactivation domain folding. *Biochemistry, 35*, 9584-9593.

McIntosh, L. P. & Dahlquist, F. W. (1990). Biosynthetic incorporation of ^{15}N and ^{13}C for assignment and interpretation of nuclear magnetic resonance spectra of proteins. *Quarterly Review of Biophysics, 23*, 1-38.

McLachlan, A. D. & Stewart, M. (1975). Tropomyosin coiled-coil interactions: Evidence for an unstaggered structure. *Journal of Molecular Biology, 98*, 293-304.

McRorie, D. K. & Voelker, P. J. (1993). *Self-associating Systems in the Analytical Ultracentrifuge*, Beckman Instruments, Inc., Fullerton, CA.

Mestas, S. P. & Lumb, K. J. (1999). Electrostatic contribution of phosphorylation to the stability of the CREB-CBP activator-coactivator complex. *Nature Structural Biology, 6*, 613-614.

Metz, R., Bannister, A. J., Sutherland, J. A., Hagemeier, C., O'Rourke, E. C., Cook, A., Bravo, R. & Kouzarides, T. (1994). c-Fos-Induced Activation of a TATA-Box-Containing Promoter Involves Direct Contact with TATA-Box Binding Protein. *Molecular and Cellular Biology,* September, 6021-6029.

Micklatcher, C. & Chmielewski, J. (1999). Helical peptide and protein design. *Current Opinion in Chemical Biology, 3*, 724-729.

Moffet, D. A. & Hecht, M. H. (2001). De novo proteins from combinatorial libraries. *Chemical Reviews, 101*, 3191-3203.

Montminy, M. (1997). Transcriptional Regulation by Cyclic AMP. *Annual Review of Biochemistry, 66*, 807-822.

Muhandiram, D. & Kay, L. (1994). Gradient-Enhanced Triple Resonance Three-Dimensional NMR Experiments with Improved Sensitivity. *Journal of Magnetic Resonance, 103.*

Musti, A. M., Treier, M. & Bohmann, D. (1997). Reduced ubiquitin-dependent degradation of c-Jun after phosphorylation by MAP kinases. *Science, 275*, 400-402.

Näär, A., Lemon, B. & Tjian, R. (2001). Transcriptional Coactivator Complexes. *Annual Review of Biochemistry, 70*, 475-501.

Neri, D., Billeter, M., Wider, G. & Wuthrich, K. (1992). NMR determination of residual structure in a urea-denatured protein, the 434-repressor. *Science, 257*, 1559-1563.

Newman, J. R. S., Wolf, E. & Kim, P. S. (2000). A computationally directed screen identifying interacting coiled coils from *Saccharomyces cerevisiae*. *Proceedings of the National Academy of Sciences, U.S.A., 97*, 13203-13208.

Nicklin, M. J. H. & Casari, G. (1991). A single site mutation in a truncated Fos protein allows it to interact with TRE *in vitro*. *Oncogene, 6*, 173-179.

Nishikawa, J.-I., Kokubo, T., Horikoshi, M., Roeder, R. G. & Nakatani, Y. (1997). *Drosophila* $TAF_{II}230$ and the Transcriptional Activator VP16 Bind Competitively to the TATA Box-Binding Domain of the TATA Box-binding Protein. *Proceedings of the National Academy of Sciences, 94*, 85-90.

Nozaki, Y. (1972). The preparation of guanidine hydrochloride. *Methods in Enzymology, 26*, 43-50.

O'Hare, P. & Williams, G. (1992). Structural studies of the acidic transactivation domain of the Vmw65 protein of herpes simplex virus using ^1H NMR. *Biochemistry, 31*, 4150-4156.

O'Shea, E. K., Lumb, K. J. & Kim, P. S. (1993). Peptide "Velcro": Design of a heterodimeric coiled coil. *Current Biology, 3*, 658-667.

O'Shea, E. K., Rutkowski, R. & Kim, P. S. (1992). Mechanism of specificity in the Fos-Jun oncoprotein heterodimer. *Cell, 66*, 699-708.

O'Shea, E. K., Klemm, J. D., Kim, P. S. & Alber, T. A. (1991). X-ray structure of the GCN4 leucine zipper, a two-stranded, parallel coiled coil. *Science, 254*, 539-544.

O'Shea, E. K., Rutkowski, R. & Kim, P. S. (1989a). Evidence that the leucine zipper is a coiled coil. *Science, 243*, 538-542.

O'Shea, E. K., Rutkowski, R., Stafford, W. F. & Kim, P. S. (1989b). Preferential heterodimer formation by isolated leucine zippers from Fos and Jun. *Science, 245*, 646-648.

Oakley, M. G. & Hollenneck, J. J. (2001). The design of antiparallel coiled coils. *Current Opinion in Structural Biology, 11*, 450-457.

Oakley, M. G. & Kim, P. S. (1998). A buried polar interaction can direct the relative orientation of helices in a coiled coil. *Biochemistry, 37*, 12603-12610.

Oelgeschlager, M., Janknecht, R., Kreig, J., Schreek, S. & Luscher, B. (1996). Interaction of the co-activator CBP with Myb proteins effects on Myb-specific transcativation and on the coopertivity with NF-M. *European Molecular Biology Organization, 15*, 2771-2780.

Ofir, R., Dwarki, V. J., Rashid, D. & Verma, I. M. (1990). Phosphorylation of the C terminus of Fos protein is required for transcriptional transrepression of the *c-fos* Promotor. *Nature, 348*, 80-82.

Oliner, J., Anderson, J., Hansen, S., Zhou, S. & Tjian, R. (1996). SREBP transcriptional activity is mediated through an interaction with the CREB-binding protein. *Genes and Development, 10*, 2903-2911.

Orphanides, G., Lagrange, T. & Reinberg, D. (1996). The general transcription factors of RNA polymerase II. *Genes and Development, 10*, 2657-2683.

Pace, C. N. (1986). Determination and analysis of urea and guanidine hydrochloride denaturation curves. *Methods in Enzymology, 131*, 266-280.

Pao, G., Janknecht, R., Ruffner, H., Hunter, T. & Verma, I. (2000). CBP/p300 interact with and function as transcriptional coactivators of BRAC1. *Proceedings of the National Academy of Sciences, 97*, 1020-1025.

Parker, D., Ferreri, K., Nakajima, T., LaMorte, V. J., Evans, R., Koerber, S. C., Hoeger, C. & Montminy, M. R. (1996). Phosphorylation of CREB at Ser-133 induces complex formation with CREB-Binding Protein via a direct mechanism. *Molecular and Cellular Biology, 16*, 694-703.

Parker, D., Rivera, M., Zor, T., Henrion-Caude, A., Radhakrishnan, I., Kumar, A., Shapiro, L. H., Wright, P. E., Montminy, M. & Brindle, P. K. (1999). Role of secondary structure in discrimination between constitutive and inducible activators. *Molecular and Cellular Biology, 19*, 5601-5607.

Parry, D. A. D. (1982). Coiled-coils in alpha-helix-containing proteins: analysis of the residue types within the heptad repeat and the use of these data in the prediction of coiled-coils in other proteins. *Bioscience Reports, 2*, 1017-1024.

Penkett, C. J., Redfield, C., Dodd, I., Hubbard, J., McBay, D. L., Mossakowska, D. E., Smith, R. A. G., Dobson, C. M. & Smith, L. J. (1997). NMR analysis of main-chain conformational preferences in an unfolded fibronectin-binding protein. *Journal of Molecular Biology, 274*, 152-159.

Penkett, C. J., Redfield, C., Jones, J. A., Dodd, I., Hubbard, J., Smith, R. A. G., Smith, L. J. & Dobson, C. M. (1998). Structural and dynamic characterization of a biologically active unfolded fibronectin-binding protein from *Staphylococcus aureus*. *Biochemistry, 37*, 17054-17067.

Perez-Howard, G. M., Weil, P. A. & Beecham, J. M. (1995). Yeast TATA binding protein interaction with DNA: Fluorescence determinantion of oligomeric state, equilibrium binding, on-rate and dissociation kinetics. *Biochemistry, 34*, 8005-8017.

Piechaczk, M. & Blanchard, J. (1994). c-fos protoncogene regulation and function. *Critical Revue of Oncology and Hematology, 17*, 91-131.

Plaxco, K. W. & Gross, M. (1997). The Importance of Being Unfolded. *Nature, 386*, 657-659.

Porte, D., Oertel-Buchheit, P., Granger-Schnarr, M. & Schnarr, M. (1995). Fos leucine zipper variants with increased association capacity. *Journal of Biological Chemistry, 270*, 22721-22730.

Potekhin, S. A., Medvedkin, V. N., Kashparov, I. A. & Venyaminov, S. U. (1994). Synthesis and properties of the peptide corresponding to the mutant form of the leucine zipper of the transcriptional activator GCN4 from yeast. *Protein Engineering, 7*, 1097-1101.

Ptashne, M. (1988). How eukaryotic transcriptional activators work. *Nature, 335*, 683-689.

Ptashne, M. & Gann, A. (1997). Transcriptional activation by recruitment. *Nature, 386*, 569-577.

Radhakrishnan, I., Pérez-Alvarado, G. C., Parker, D., Dyson, H. J., Montminy, M. & Wright, P. E. (1999). Structural analysis of CREB-CBP transcriptional activator-coactivator complexes by NMR spectroscopy: Implications for mapping the boundaries of structural domains. *Journal of Molecular Biology, 287*, 859-865.

Radhakrishnan, I., Pérez-Alvarado, G. C., Parker, D., Dyson, H. J., Montminy, M. R. & Wright, P. E. (1997). Solution structure of the KIX domain of CBP bound to the transactivation domain of CREB: A model for activator:coactivator interactions. *Cell, 91*, 741-752.

Raleigh, D. P., Betz, S. F. & DeGrado, W. F. (1995). A *de novo* designed protein mimics the native state of natural proteins. *Journal of the American Chemical Society,* 7558-7559.

Ranallo, R.T., Struhl, K., Stargell, L.A. (1999). A TATA-binding protein mutant defective for TFIID complex formation *in vivo*. *Molecular and Cellular Biology*. 19, 3951-3957.

Ransone, L. J. & Verma, I. M. (1990). Nuclear Proto-oncogenes *fos* and *jun*. *Annual Review of Cell Biology, 6*, 539-557.

Rashin, A. A. & Honig, B. (1984). On the environment of ionizable groups in globular proteins. *Journal of Molecular Biology, 173*, 515-521.

Richardson, J. S., Richardson, D. C., Tweedy, N. B., Gernet, K. M., Quinn, T. P., Hecht, M. H., Erickson, B. W., Yan, Y., McClain, R. D., Donlan, M. E. & Surles,

M. C. (1992). Biophysical Society National Lecture. *Biophysical Journal, 63*, 1186-1209.

Riou, P., Bex, F. & Gazzolo, L. (2000). The human T cell leukimaia virus type 1represses MyoD-dependent trancription by inhibiting the KIX domain of p300. *Journal of Biological Science,* 10551-10560.

Roeder, R. (1996). The role of general initiation factors in transcription by RNA polymerase II. *TIBS, 21*, 327-335.

Schmidt, M. C., Kao, C. C., Pei, R. & Berk, A. J. (1989). Yeast TATA-Box Transcription Factor Gene. *Proceedings of the National Academy of Sciences, 86*, 7785-7789.

Schmitz, M. L., Silva, M. A. S., Altmann, H., Czisch, M., Holak, T. A. & Baeuerle, P. A. (1994). Structural and functional analysis of the NF-κB p65 C terminus. *Journal of Biological Chemistry, 269*, 25613-25620.

Schneider, J. P., Lear, J. D. & DeGrado, W. F. (1997). A designed buried salt bridge in a heterodimeric coiled coil. *Journal of the American Chemical Society, 119*, 5742-5743.

Schneider, J. P., Lombardi, A. & DeGrado, W. F. (1998). Analysis and design of three-stranded coiled coils and three-helix bundles. *Folding and Design, 3*, R29-R40.

Schnölzer, M., Alewood, P., Jones, A., Alewood, D. & Kent, S. B. H. (1992). *In situ* neutralization in Boc-chemistry solid phase peptide synthesis. *International Journal of Peptide and Protein Research, 40*, 180-193.

Schreiber, M., Kolbus, A., Piu, F., Szabowski, A., Möhle-Steinlein, U., Tian, J., Karin, M., Angel, P. & Wagner, E. F. (1999). Control of cell cycle progression by c-Jun is p53 dependent. *Genes and Development, 13*, 607-619.

Sem, D. S., Casiniro, D. R., Kliewer, S. A., Provencal, J., Evans, R. M. & Wright, P. E. (1997). NMR spectroscopic studies of the DNA-binding domain of the monomer-binding nuclear orphan receptor, human estrogen related receptor-2. *Journal of Biological Chemistry, 272*, 18038-18043.

Semisotnov, G. V., Rodionova, N. A., Razgulyaev, O. I., Uversky, V. N., Gripas, A. F. & Gilmanshin, R. I. (1991). Study of the "molten globule" intermediate state in protein folding by a hydrophobic fluorescent probe. *Biopolymers, 31*, 119-128.

Seto, E., Usheva, A., Zambetti, G., Momand, J., Horikoshi, N., Weinmann, T., Levine, A. & Shenk, T. (1992). Wild-type p53 binds to the TATA-binding protein

and represses transcription. *Proceedings from the National Academy of Science, 15*, 12028-32.

Shaulian, E. & Karin, M. (2001). AP-1 in cell proliferation and survival. *Oncogene, 20*, 2390-2400.

Shikama, N., Lyon, J. & La Thangue, N. B. (1997). The p300/CBP family: Integrating signals with transcription factors and chromatin. *Trends in Cell Biology, 7*, 230-236.

Shoemaker, B. A., Portman, J. J. & Wolynes, P. G. (2001). Speeding molecular recognition by using the folding funnel: The fly-casting mechanism. *Proceedings of the National Academy of Sciences, 97*, 8868-8873.

Sia, S. K. & Kim, P. S. (2001). A designed protein with packing between left-handed and right-handed helices. *Biochemistry, 40*, 8981-8989.

Siegel, L. M. & Monty, K. J. (1966). Determination of molecular weights and frictional ratios of proteins in impure systems by use of gel filtration and density gradient centrifugation. Application to crude preparations of sulfite and hydroxylamine reductases. *Biochim. Biophys. Acta, 112*, 346-362.

Sigler, P. B. (1988). Acid blobs and negative noodles. *Nature, 333*, 210-212.

Spolar, R. S. & Record, M. T. (1994). Coupling of local folding to site-specific binding of proteins to DNA. *Science, 263*, 777-784.

Stargell, L.A. & Struhl, K. (1996). A new class of activation-defective TATA-binding protein mutants: Evidence for two steps of transcriptional activation *in vivo. Molecular and Cellular Biology.* 16, 4456-4464.

Stebbins, C., Borukhov, S., Orlova, M., Polyakov, A., Goldfarb, A. & Darst, S. (1995). Crystal structure of the GreA transcript cleavage factor from Escherichia coli. *Nature, 16*, 636-40.

Stewart, J. & Young, J. (1984). Solid phase peptide synthesis. *New York Pierce Chemical Coompany,*.

Stone, D., Sodek, J., Johnson, P. & Smillie, L. B. (1975). Tropomyosin: Correlation of amino acid sequence and structure. In *Proteins of Contractile Systems* (Biro, E. N. A., ed.), pp. 125-136. North-Holland, Amsterdam.

Stringer, K., Ingles, C. & Greenblatt, J. (1990). Direct and selective binding of an acidic transcriptional activation domain to the TATA-box factor TFIID. *Nature, 345*, 783-786.

Stryer, L. (1965). The interaction of a naphthalene dye with apomyoglobin and apohemoglobin. A fluorescent probe of non-polar binding sites. *Journal of Molecular Biology, 13*, 482-495.

Studier, F. W., Rosenberg, A. H., Dunn, J. J. & Dubendorff, J. W. (1990). Use of T7 RNA polymerase to direct expression of cloned genes. *Methods in Enzymology, 185*, 60-89.

Sutherland, J. A., Cook, A., Bannister, A. J. & Kouzarides, T. (1992). Conserved Motifs in Fos and Jun Define a New Class of Activation Domain. *Genes and Development, 6*, 1810-1819.

Suzuki, K., Yamada, T. & Tanaka, T. (1999). Role of the buried glutamate in the α-helical coiled coil domain of the macrophage scavenger receptor. *Biochemistry, 38*, 1751-1756.

Taggart, A. K. P. & Pugh, B. F. (1996). Dimerization of TFIID when not bound to DNA. *Science, 272*, 1331-1333.

Tjian, R. & Maniatis, T. (1994). Transcriptional activation: A complex puzzle with few easy pieces. *Cell, 77*, 5-8.

Triezenberg, S. J. (1995). Structure and function of transcriptional activation domains. *Current Opinion in Genetics and Development, 5*, 190-196.

Tripet, B., Wagschal, K., Lavigne, P., Mant, C. T. & Hodges, R. S. (2000). Effects of side-chain characteristics on stability and oligomerization state of a *de novo*-designed model coiled-coil: 20 amino acid substitutions in position "d". *Journal of Molecular Biology, 300*, 377-402.

Uesugi, M., Nyanguile, O., Lu, H., Levine, A. J. & Verdine, G. L. (1997). Induced α helix in the VP16 activation domain upon binding to a human TAF. *Science, 277*, 1310-1313.

Utley, R. T., Ikeda, K., Grant, P. A., Cote, J., Steger, D. J., Eberharter, A., John, S. & Workma, J. L. (1998). Transcriptional activators direct histone acetyltransferase complexes to nucleosomes. *nature, 394*, 498-502.

Van Hoy, M., Hansen, A. & Kodadek, T. (1992). Spectroscopic studies of a transcriptional activation peptide. *Journal of the American Chemical Society, 114*, 362-363.

Van Hoy, M., Leuther, K. K., Kodadek, T. & Johnston, S. A. (1993). The acidic activation domains of the GCN4 and GAL4 proteins are not α-helical but form β-sheets. *Cell, 72*, 587-594.

Van Orden, K., Giebler, H. A., Lemasson, I., Gonzales, M. & Nyborg, J. K. (1999a). Binding of p53 to the KIX domain of CREB binding protein. *Journal of Biological Chemistry, 274*, 26321-26328.

Van Orden, K., Yan, J.-P., Ulloa, A. & Nyborg, J. K. (1999b). Binding of the human T-cell leukemia virus Tax protein to the coactivator CBP interferes with CBP-mediated transcriptional control. *Oncogene, 18*, 3766-3772.

van Straaten, F., Muller, R., Curran, T., van Beveren, C. & Verma, I. M. (1983). Complete Nucleotide Sequence of a Human *c-onc* Gene: Deduced Amino Acid Sequence of the Human *c-fos* protein. *Proceedings of the National Academy of Sciences, U.S.A., 80*, 3183-3187.

van Zijl, P. C. M., Johnson, M. O., Mori, S. & Hurd, R. E. (1995). Magic-angle-gradient double-quantum filtered COSY. *Journal of Magnetic Resonance, A113*, 265-270.

Vinson, C. R., Hai, T. & Boyd, S. M. (1993). Dimerization specificty of the leucine zipper-containing bZIP motif on DNA binding: prediction and rational design. *Genes and Development, 7*, 1047-1058.

Vogt, P. (2001). Jun, the oncoprotein. *Oncogene, 20*, 2365-2377.

Wagschal, K., Tripet, B. & Hodges, R. S. (1999a). De novo design of a model peptide sequence to examine the effects of single amino acid substitutions in the hydrophobic core on both stability and oligomerization of coiled coils. *Journal of Molecular Biology, 285*, 785-803.

Wagschal, K., Tripet, B., Lavigne, P., Mant, C. & Hodges, R. S. (1999b). The role of position a in determining the stability and oligomerization state of alpha-helical coiled coils: 20 amino acid stability coefficients in the hydrophobic core of proteins. *Protein Science, 8*, 2312-2329.

Waldburger, C., Schildbach, J. & Sauer, R. (1995). Are buried salt bridges important for protein stability and conformational specificity? *Nature Structural Biology, 2*, 122-128.

Walshaw, J. & Woolfson, D. N. (2001). SOCKET: A program for identifying and analysing coiled-coil motifs within protein structures. *Journal of Molecular Biology, 307*, 1427-1450.

Wendt, H., Berger, C., Baici, A., Thomas, R. M. & Bosshard, H. R. (1995). Kinetics of folding of leucine zipper domains. *Biochemistry, 34*, 4097-4107.

Wilson, T. & Treisman, R. (1988). Fos C-Terminal mutations block down-regulation of c-fos transcription following serum stimulation. *European Molecular Biology Organization Journal,* 8, 4193-4202.

Wisdom, R., Johnson, R. & Moore, C. (1999). c-Jun regulates cell cycle progression and apoptosis by distinct mechanisms. *European Molecular Biology Organization Journal*, 18, 188-197.

Wisdom, R. & Verma, I. M. (1993). Transformation by Fos Proteins Requires a C-terminal Transactivation Domain. *Molecular and Cellular Biology*, 13, 7429-7438.

Wishart, D. S., Bigam, C. G., Yao, J., Abildgaard, F., Dyson, H. J., Oldfield, E., Markley, J. L. & Sykes, B. D. (1995). ^{1}H, ^{13}C and ^{15}N chemical shift referencing in biomolecular NMR. *Journal of Biomolecular NMR*, 6, 135-140.

Wishart, D. S. & Sykes, B. D. (1994). Chemical shifts as a tool for structure determination. *Methods in Enzymology*, 239, 363-392.

Wolf, E., Kim, P. S. & Berger, B. (1997). MultiCoil: A program for prediciting two- and three-stranded coiled coils. *Protein Science*, 6, 1179-1189.

Woody, R. (1992). Circular dichroism and conformation of unordered polypeptides. *Advances in Biophysical Chemistry*, 2, 37-79.

Woody, R. & Dunker, A. (1996). . Circular Dicroism and the Conformational Analysis of Biomolecules (Fasman, G., Ed.), Plenum Press, New York.

Woolfson, D. N. & Alber, T. (1995). Predicting oligomerization states of coiled coils. *Protein Science*, 4, 1596-1607.

Wright, P. E. & Dyson, H. J. (1999). Intrinsically unstructured proteins: Re-assessing the protein structure-function paradigm. *Journal of Molecular Biology*, 293, 321-331.

Yphantis, D. A., Correia, J. J., Johnson, M. L. & Wu, G. (1978). Detection of heterogeneity in self-associating systems. In Physical Aspects of Protein Interactions (Catsimpoolas, N., ed.), pp. 275-303. Elsevier, Amsterdam.

Zeng, X., Herndon, A. M. & Hu, J. C. (1997). Buried asparagines determine the dimerization specificites of leucine zipper mutants. *Proceedings of the National Academy of Sciences*, 94, 3673-3678.

Zhang, Y., Feng, X.-H. & Derynck, R. (1998). Smad3 and Smad4 cooperate with c-Jun/c-Fos to mediate TGF-b-induced transcription. *Nature*, 394, 909-913.

Zhu, H., Celinski, S. A., Scholtz, J. M. & Hu, J. C. (2000). The contribution of buried polar groups to the conformational stability of the GCN4 coiled coil. *Journal of Molecular Biology*, 300, 1377-1387.

Zuiderweg. (2002). Mapping protein-protein interactions in solution by NMR spectroscopy. *Biochemistry*, 41, 1-7.□